Annu. Rev. Astron. Astrophys. 2020.58:257-312. Downloaded from www.annualreviews.org
Access provided by National Astronomical Observatories, Chinese Academy of Sciences on 09/05/23. For personal use only.

ANNUAL REVIEWS

Annual Review of Astronomy and Astrophysics

Intermediate-Mass Black Holes

Jenny E. Greene,[1] Jay Strader,[2] and Luis C. Ho[3]

[1]Department of Astrophysical Sciences, Princeton University, Princeton, New Jersey 08544, USA; email: jgreene@astro.princeton.edu

[2]Center for Data Intensive and Time Domain Astronomy, Department of Physics and Astronomy, Michigan State University, East Lansing, Michigan 48824, USA

[3]Kavli Institute for Astronomy and Astrophysics, and Department of Astronomy, School of Physics, Peking University, Beijing 100871, China

Annu. Rev. Astron. Astrophys. 2020. 58:257–312

First published as a Review in Advance on June 29, 2020

The *Annual Review of Astronomy and Astrophysics* is online at astro.annualreviews.org

https://doi.org/10.1146/annurev-astro-032620-021835

Copyright © 2020 by Annual Reviews. All rights reserved

ANNUAL REVIEWS CONNECT

www.annualreviews.org

- Download figures
- Navigate cited references
- Keyword search
- Explore related articles
- Share via email or social media

Keywords

active galactic nuclei, globular clusters, gravitational waves, tidal disruption, ultraluminous X-ray sources

Abstract

We describe ongoing searches for intermediate-mass black holes with $M_{BH} \approx 10$–10^5 $M_\odot$. We review a range of search mechanisms, both dynamical and those that rely on accretion signatures. We find the following conclusions:

- Dynamical and accretion signatures alike point to a high fraction of 10^9–10^{10} $M_\odot$ galaxies hosting black holes with $M_{BH} \sim 10^5$ $M_\odot$. In contrast, there are no solid detections of black holes in globular clusters.
- There are few observational constraints on black holes in any environment with $M_{BH} \approx 100$–10^4 $M_\odot$.
- Considering low-mass galaxies with dynamical black hole masses and constraining limits, we find that the M_{BH}–σ_* relation continues unbroken to $M_{BH} \sim 10^5$ $M_\odot$, albeit with large scatter. We believe the scatter is at least partially driven by a broad range in black hole masses, because the occupation fraction appears to be relatively high in these galaxies.
- We fold the observed scaling relations with our empirical limits on occupation fraction and the galaxy mass function to put observational bounds on the black hole mass function in galaxy nuclei.
- We are pessimistic that local demographic observations of galaxy nuclei alone could constrain seeding mechanisms, although either high-redshift luminosity functions or robust measurements of off-nuclear black holes could begin to discriminate models.

Annu. Rev. Astron. Astrophys. 2020.58:257-312. Downloaded from www.annualreviews.org
Access provided by National Astronomical Observatories, Chinese Academy of Sciences on 09/05/23. For personal use only.

Contents

1. INTRODUCTION 259
   1.1. Motivation 259
   1.2. Definition 259
   1.3. Historical Context 260
2. FORMATION PATHS: WHERE TO FIND IMBHs 261
   2.1. Seeding Models 261
   2.2. From Seeds to Local Predictions: Population III and Direct-Collapse Channels 263
   2.3. Number Densities of Early Seeding Models 264
   2.4. From Seeds to Local Predictions: Gravitational Runaway 265
   2.5. Number Densities of Gravitational Runaway Models 266
   2.6. From Seeds to Local Predictions: Wandering Black Holes 266
   2.7. Number Densities of Wandering Black Hole Models 267
   2.8. Tests of Seeding Mechanisms 268
3. STELLAR AND GAS DYNAMICAL SEARCHES FOR IMBHs 269
   3.1. Dynamics from Integrated Light Measurements 269
   3.2. Proper Motions 270
   3.3. IMBH Demographics in Galaxy Nuclei from Dynamics 271
   3.4. Dynamical Searches for IMBHs in the Milky Way 273
   3.5. IMBH Demographics in Globular Clusters from Stellar Dynamics 273
   3.6. Hypervelocity Stars 274
4. SEARCHES FOR ACCRETING IMBHs IN GALAXY NUCLEI 275
   4.1. Optical Spectroscopic Selection 276
   4.2. Multiwavelength Searches and Confusion with Star Formation 278
   4.3. Pushing Down the Luminosity Function with X-Ray or Radio Observations 279
   4.4. Going Further with the Fundamental Plane of Radio Activity 280
   4.5. The Promise of Variability Selection 281
   4.6. Moving to Higher Redshift 282
5. SEARCHES FOR ACCRETING BLACK HOLES OUTSIDE OF GALAXY NUCLEI 282
   5.1. Ultraluminous X-Ray Sources 282
   5.2. HLX-1 and Friends 283
   5.3. Fundamental Plane Searches in Globular Clusters 285
6. IMBH SEARCHES WITH TRANSIENT PHENOMENA 286
   6.1. Tidal Disruption Events 286
   6.2. Gravitational Waves 288
7. IMBH CANDIDATE TABLES 289
8. SCALING RELATIONS 292
   8.1. M_{BH}–σ_* 292
   8.2. M_{BH}–M_* 293
   8.3. Using Active Galactic Nuclei to Probe Scaling Relations 294
   8.4. Scaling with Nuclear Star Clusters 295
9. DEMOGRAPHICS 296

9.1. Existing Limits on the Occupation Fraction 296
9.2. Inferred Black Hole Mass Functions at Low Mass 298
10. THE FUTURE 300
11. SUMMARY 301

Annu. Rev. Astron. Astrophys. 2020.58:257-312. Downloaded from www.annualreviews.org
Access provided by National Astronomical Observatories, Chinese Academy of Sciences on 09/05/23. For personal use only.

1. INTRODUCTION

1.1. Motivation

Intermediate-mass black holes (IMBHs) are often introduced as what they are not. They are not stellar-mass black holes, which are formed in the deaths of massive stars, and are historically thought to be ∼10 $M_\odot$ (Remillard & McClintock 2006). They are not supermassive black holes, which are historically considered to have masses of 10^6–10^{10} $M_\odot$. The question is often framed thus: Are there black holes with masses between these two classes?

We frame the central question differently. At some point in cosmic time, black holes between 10 and 10^6 $M_\odot$ had to exist in order to make the 10^9 $M_\odot$ black holes that are seen only hundreds of millions of years after the Big Bang (e.g., Bañados et al. 2018). The central question of this review is whether we can find evidence for these IMBHs. The corollary is whether, based on the mass distributions and environments of the black holes, we can determine how these IMBHs were formed. Currently we have no concrete evidence for black holes with masses $\gtrsim$ 100–10^5 $M_\odot$, although there are some important candidates in this mass range that we discuss later. Finding objects, and characterizing the black hole mass function in this range, is of interest for many reasons.

Extending scaling relations to this regime may provide unique insight into the evolution of black holes (e.g., Kormendy & Ho 2013, Shankar et al. 2016, Pacucci et al. 2018), along with the possible importance of feedback for dwarf galaxies (Silk 2017, Bradford et al. 2018, Penny et al. 2018, Dickey et al. 2019). Demographics of black holes at lower masses should help elucidate the dynamical evolution of dense stellar systems (e.g., Miller & Hamilton 2002, Portegies Zwart & McMillan 2002, Gürkan et al. 2004, Antonini & Rasio 2016).

IMBHs will also be prime sources of gravitational radiation for upcoming gravitational wave detectors in space (*Laser Interferometer Space Antenna* or LISA; e.g., Amaro-Seoane et al. 2015). To determine the rates and interpret the gravitational wave signals, we need independent measurements of the black hole number densities (e.g., MacLeod et al. 2016a, Stone & Metzger 2016, Eracleous et al. 2019). Furthermore, ongoing and future time-domain surveys are detecting more and more tidal disruption events (TDEs). In principle, lower-mass black holes should be significant contributors to the detected TDEs, and they are starting to be detected (Maksym et al. 2013, Wevers et al. 2017, van Velzen 2018).

Finally, we do not know exactly how emission from accretion flows onto black holes will evolve with black hole mass: At lower masses the accretion disk gets hotter and the bolometric luminosity drops, perhaps leading the phenomenology to look more like X-ray binaries and less like accreting supermassive black holes (e.g., Cann et al. 2019). The emergent spectrum of such sources is of interest not only for understanding accretion but also in thinking about the impact of mini-quasars on the formation of the first galaxies and the reionization of the Universe (e.g., Madau & Haardt 2015). For all these reasons, the time is right to review the current state of our knowledge, and to prepare for the rich new upcoming data sets that will bear on these questions.

1.2. Definition

Observationally, we have compelling evidence for black holes with $M_{\rm BH} \lesssim 100$ $M_\odot$ and with $M_{\rm BH} \gtrsim 10^5$ $M_\odot$. Work over the past 25 years has clearly established that galaxy centers harbor

normal active galactic nuclei (AGNs) with masses $M_{BH} \approx 10^5$ $M_\odot$ and higher (Section 4). Existential discovery space lies in the mass range of $M_{BH} \approx 100$–10^5 $M_\odot$. Nevertheless, from the perspective of understanding the growth and demographics of black holes, we show that black holes in the range of $M_{BH} \approx 10^5$–10^6 $M_\odot$ also encode important (and poorly quantified) information. Thus, we cover them under the purview of this review as well.

1.3. Historical Context

The growth of supermassive black hole seeds and the existence of IMBHs have both long been discussed in the literature, even before we were completely sure of the existence of astrophysical black holes (e.g., Eardley & Press 1975). Quickly thereafter, the community developed theoretical ideas about how one might form non-stellar-mass black holes; the famous diagram from Rees (1978) includes all the formation mechanisms we consider today, including gravitational runaway (Bahcall & Ostriker 1975, Begelman & Rees 1978, Quinlan & Shapiro 1990, Lee 1993), the collapse of Population III (Pop III) stars (e.g., Bond et al. 1984, Madau & Rees 2001), and the idea of a direct collapse into a black hole (e.g., Haehnelt & Rees 1993, Loeb & Rasio 1994, Koushiappas et al. 2004). There was also early interest in IMBHs as a possible explanation for dark matter (e.g., Lacey & Ostriker 1985, Carr 1994), although there are now many limits on black holes as dark matter (e.g., Tisserand et al. 2007, Ali-Haïmoud et al. 2017, Zumalacárregui & Seljak 2018).

As observations of young quasars push to earlier and earlier times (e.g., Fan et al. 2006, Mortlock et al. 2011, Bañados et al. 2018), the community has recognized the significant challenge of creating such massive black holes so quickly (e.g., Haiman 2013); this has led researchers to search for a theoretical mechanism that makes massive black hole seeds, which further motivates searches for IMBHs. Accordingly, theoretical work identified that local observations of black holes in dwarf galaxies, which suffer fewer mergers and less accretion, may provide an additional key to understanding seeding processes (e.g., Volonteri et al. 2008).

In parallel, the Einstein Telescope enabled the discovery of the first ultraluminous X-ray sources (ULXs; e.g., Long et al. 1981, Fabbiano 1989), whose luminosities are nominally above the Eddington limit for compact stellar objects. One natural explanation for the high X-ray luminosities of these sources is that they are powered by more massive compact objects, namely IMBHs (e.g., Kaaret et al. 2017, and references therein; Section 4). The ULXs show association with young star clusters and this spurred continuing interest in the formation of IMBHs in dense stellar clusters through gravitational runaway (e.g., Ebisuzaki et al. 2001, Miller & Hamilton 2002, Portegies Zwart & McMillan 2002). Puzzling suggestions of abnormal numbers of young stars in the Galactic Center also sparked interest in a possible IMBH to carry in the stars (e.g., Ghez et al. 2003, Hansen & Milosavljević 2003).

Thanks to the successful detection of supermassive black holes in galaxy nuclei (e.g., Kormendy & Richstone 1995), dynamical searches for IMBHs at the centers of globular clusters like M15 were also underway, yielding conflicting results (e.g., Gebhardt et al. 2000, 2002; Gerssen et al. 2002; McNamara et al. 2003). Early dynamical searches for black holes in the nuclei of low-mass galaxies also reported nondetections (Gebhardt et al. 2001, Valluri et al. 2004). Comprehensive searches for AGN signatures in nearby galaxies likewise pointed to a low fraction of AGNs in late-type and low-mass galaxies (e.g., Ho et al. 1997, Kauffmann et al. 2003). These facts together led the community to conclude that black holes are rarely found in the nuclei of $<10^{10}$ $M_\odot$ galaxies (i.e., galaxies less massive than the Milky Way). Even today, there is a severe dearth of information about black hole demographics in sub-L_* galaxies.

Real progress in the past decade, based on both dynamical studies (Section 3) and accretion-based studies (Section 4), suggests instead that a high fraction (>50%) of 10^9–10^{10}-$M_\odot$ galaxies do harbor central black holes, likely with $M_{BH} > 10^5$ $M_\odot$ (Miller et al. 2015, Nguyen et al.

Annu. Rev. Astron. Astrophys. 2020.58:257-312. Downloaded from www.annualreviews.org
Access provided by National Astronomical Observatories, Chinese Academy of Sciences on 09/05/23. For personal use only.

Annu. Rev. Astron. Astrophys. 2020.58:257-312. Downloaded from www.annualreviews.org
Access provided by National Astronomical Observatories, Chinese Academy of Sciences on 09/05/23. For personal use only.

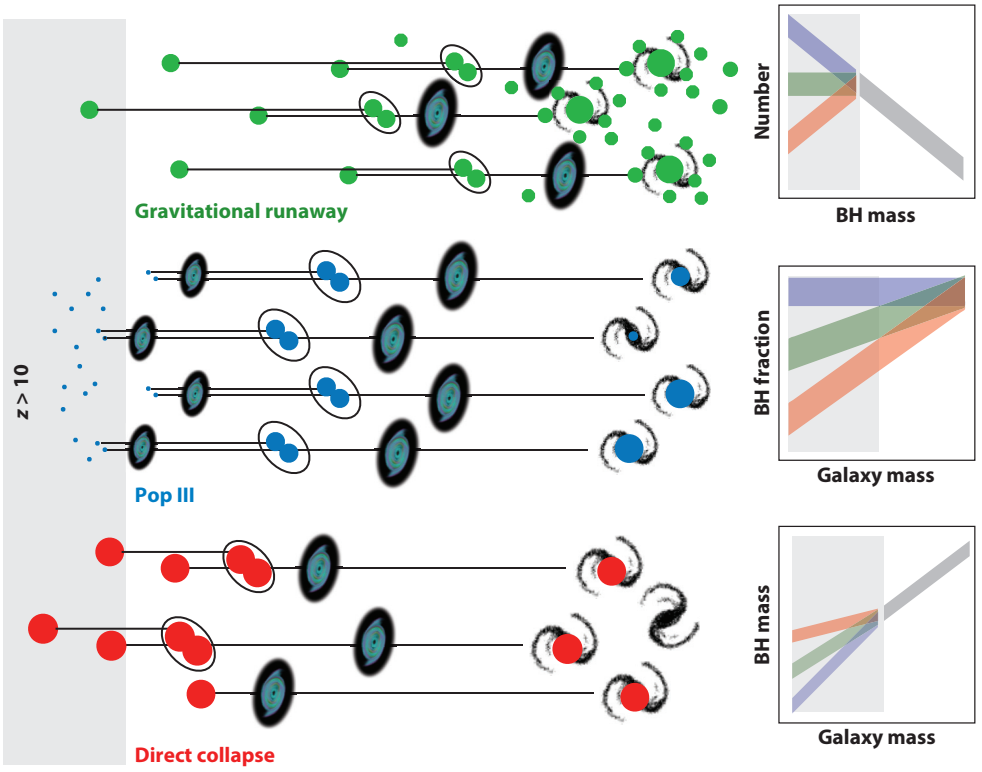


Figure 1

Possible observable differences between different seeding scenarios. Early formation through direct collapse (*red*) or Pop III stars (*blue*) occurs at $z > 10$, whereas gravitational runaway (*green*) can happen throughout cosmic time. As cosmic structures evolve, the seed black holes suffer mergers (*black ovals*), leading to the emission of gravitational waves, as well as accretion episodes (*blue disks*) that could be observed as active galactic nuclei. At the present day, differences in black hole mass functions, occupation fractions, and black hole–galaxy scaling relations may ensue from different seeding channels, for simplicity here shown only for nuclear black holes. Gray bars in these relations show where we do not yet have observational constraints. Abbreviation: BH, black hole; Pop III, Population III.

2019b; and Section 9). We use this recent progress as motivation to revisit both scaling relations (Section 8) and the allowed range of black hole mass functions for $M_{\rm BH} < 10^6$ $M_\odot$ (Section 9).

We are not the first to attempt a review of the linked subjects of IMBH searches and seeding mechanisms (Volonteri 2010, Greene 2012, Reines & Comastri 2016, Mezcua 2017). We also refer readers to a related review about seeding mechanisms by Inayoshi et al. (2020) in this volume.

2. FORMATION PATHS: WHERE TO FIND IMBHs

We briefly review the primary theoretical channels for seeding supermassive black holes (**Figure 1**). We then describe the predictions for local observations in terms of number densities and environments of IMBHs.

2.1. Seeding Models

We know that black holes are made in the deaths of massive stars. This process happens at the present day, but at early times we expect theoretically that the first (so-called Pop III) stars were

quite massive, due to the inability of molecular hydrogen gas to cool (Bromm & Larson 2004, Karlsson et al. 2013, and references therein). Such massive stars would likely end their lives as black holes with $M_{\rm BH} \sim 100\ M_\odot$ (e.g., Fryer et al. 2001), excepting first stars in the mass range of 140–260 $M_\odot$ that would explode as pair-instability supernovae and leave no remnant (Heger et al. 2003). As shown by Madau & Rees (2001), if these first massive stars are rare, such that only about one is made in each high-density peak at very high redshift, then the number density of black holes would be well matched to the number of supermassive black holes today. However, growing from $\sim$100 $M_\odot$ to a billion Suns in a fraction of a gigayear requires dramatic fueling (Haiman & Loeb 2001). Specifically, for a typical *e*-folding time of 45 million years, 14 such *e*-foldings are available at $z = 7$, but 17 are needed if the black hole grows at the Eddington limit (Madau et al. 2014, and references therein). Arranging this uninterrupted growth seems challenging even for these rare quasars (e.g., Johnson & Bromm 2007, Milosavljević et al. 2009). However, a few episodes of super-Eddington accretion could largely alleviate the tension, and super-Eddington accretion now appears to arise naturally in numerical experiments (e.g., Jiang et al. 2019).

A different channel, with no local analogs, is that of collapsing gas clouds forming a massive seed black hole without passing through all the phases of stellar evolution. These direct-collapse models form seed black holes with $M_{\rm BH} \sim 10^4$–$10^6\ M_\odot$ (e.g., Loeb & Rasio 1994, Bromm & Loeb 2003, Begelman et al. 2006, Lodato & Natarajan 2006), which perhaps pass through a quasi-star phase (e.g., Begelman 2010). This channel can only operate at very high redshift, because pristine gas is required to suppress cooling and fragmentation. Recent literature discusses in detail how rare the conditions may be to ensure that the gas does not cool and fragment into smaller units (e.g., Visbal et al. 2014, Habouzit et al. 2016), typically assuming that an elevated Lyman–Werner background is needed (e.g., Omukai 2001). Some works instead argue that additional photons from star formation in nearby halos (e.g., Dijkstra et al. 2008, Visbal et al. 2014), additional gas heating through mergers (Yoshida et al. 2003, Wise et al. 2019), or even star formation within individual halos (Dunn et al. 2018), may provide sufficient heating or ionizing photons to make this channel viable. We emphasize that the number density of halos that suffer direct collapse is very uncertain, with predictions differing on the halo gas accretion rates as a function of mass, the required elevation of the ionizing background, and the possible sources of ionizing photons. See the comprehensive review by Inayoshi et al. (2020, in this volume).

A final class of models generates $\sim 10^3$–$10^4\ M_\odot$ black holes in a gravitational runaway event within a dense stellar cluster. Modern discussion divides globular cluster IMBH formation scenarios into slow and fast versions, depending on whether the formation occurs over $\sim$100 Myr to 1 Gyr or less than around a few million years, respectively. Here, we focus specifically on the formation of the seed at the centers of dense clusters. In any scenario in which an IMBH does form, the present-day mass may well be higher due to accretion of gas and/or stars (e.g., Rosswog et al. 2009, MacLeod et al. 2016a, Sakurai et al. 2017; Section 9). We also note that though normal single stars are not expected to produce black holes $>100\ M_\odot$, it is plausible that repeated mergers in star clusters could occasionally produce IMBHs larger than 100 $M_\odot$ by this channel (Rodriguez et al. 2019).

The modern incarnation of the slow scenario (Miller & Hamilton 2002) envisions a black hole of mass $\gtrsim$50 $M_\odot$ forming as the remnant of a massive star, then growing through mergers of mass-segregated black holes, and leading to $\sim 10^3\ M_\odot$ IMBHs in a few $\times 10\%$ of massive globular clusters. In this scenario, the occupation fraction is set by considering the central densities observed in Galactic globular clusters. Lower-mass ($\sim$10–20 $M_\odot$) black hole seeds will not lead to a runaway because early stellar interactions tend to eject these lighter black holes from the cluster. A governing uncertainty in this scenario is whether even 50-$M_\odot$ seeds can form, as such remnants might be rare or absent in single-star evolution (Woosley 2017).

Annu. Rev. Astron. Astrophys. 2020.58:257-312. Downloaded from www.annualreviews.org
Access provided by National Astronomical Observatories, Chinese Academy of Sciences on 09/05/23. For personal use only.

The fast scenario was reintroduced in a contemporary form by Portegies Zwart & McMillan (2002), who used a combination of simulations and analytic calculations to argue that sufficiently dense star clusters undergo a collisional runaway of massive stars, the product of which could eventually lead to the formation of an IMBH. Such supermassive stars could potentially also produce enough ejected material with unusual abundances to explain the multiple stellar populations seen in globular clusters (Gieles et al. 2018b). Both this scenario and the direct-collapse scenario may be sensitive to metallicity: at high metallicity, stellar winds may remove so much mass that collapse to a black hole is uncertain (e.g., Mapelli 2016). In the context of very low metallicity and very high redshift, some models predict that very dense and massive clusters may form black holes at their centers (e.g., Devecchi & Volonteri 2009, Katz et al. 2015, Sakurai et al. 2017). Although clusters this dense are not found at lower redshift, hypothetical Pop III star clusters could optimistically be detectable with the *James Webb Space Telescope* (JWST).

2.2. From Seeds to Local Predictions: Population III and Direct-Collapse Channels

Currently it is challenging to compare predictions of local demographics based on the seeding mechanism. To that end, we gather approximate predicted number densities and mass distributions of present-day IMBH populations as a function of channel and modeling approach. Even with perfect knowledge of the number density and halo locations of black hole seeds at early times, there are many unknown factors at play as the seeds evolve toward the present day (e.g., Volonteri et al. 2008, Volonteri 2010, Mezcua 2017, Buchner et al. 2019, Mezcua et al. 2019). We outline some of these uncertainties and then compare the predictions from different types of models.

When galaxies merge, the central black holes may also merge, and any differences in the mass and angular momentum of the two black holes can translate into anisotropic gravitational wave emission during the merger, which in turn can impart a linear momentum kick to the merged remnant (e.g., Redmount & Rees 1989). A major uncertainty in going from initial seed models to local observations of black holes in galaxy nuclei comes from the unknown fraction of black holes that are ejected via gravitational recoil. These kicks may be more than sufficient to exceed the escape velocity of low-mass halos (e.g., Haiman 2004, Campanelli et al. 2007), but the most common mergers with much lower-mass black hole secondaries likely never lead to recoil (Volonteri & Rees 2006). In practice, the distribution of kick velocities depends on the mass ratios and relative spins of the incoming black holes, for which we do not have complete models. There are other dynamical uncertainties to consider. Such low-mass black holes in such shallow potentials may never settle at the centers of their galaxies (Bellovary et al. 2019). Away from the center of the potential, the black holes may not grow efficiently, and would likely be missed with current searches (although see Barrows et al. 2019, Reines et al. 2019).

Finally, tracking accretion in a physically motivated way requires prohibitively high spatial resolution for cosmological simulations. In particular, if super-Eddington accretion is possible, then the differences between the Pop III channel and the direct-collapse channel may be washed out at early times (e.g., Volonteri & Gnedin 2009, Alexander & Natarajan 2014). Thus, it is possible that the high-redshift luminosity function and number of gravitational wave detections from growing black holes may be more sensitive to seeding (e.g., Sesana et al. 2007, Tanaka & Haiman 2009). Furthermore, late-time growth contributes in an unconstrained way to the present-day black hole mass distribution. Nuclear star clusters, the hosts of at least some candidate IMBHs (Section 3), experience multiple bursts of star formation (e.g., Walcher et al. 2006, Carson et al. 2015, Kacharov et al. 2018). Such bursts may well feed the black hole, and additional accretion via stellar interactions may also occur (e.g., Alexander & Bar-Or 2017, Stone et al. 2017).

Annu. Rev. Astron. Astrophys. 2020.58:257-312. Downloaded from www.annualreviews.org
Access provided by National Astronomical Observatories, Chinese Academy of Sciences on 09/05/23. For personal use only.

Table 1 Seeds to local predictions[a]

Model	Redshift	Tooth fairies	F_{occ} 10^8	F_{occ} 10^9	# Mpc^{-3} nuclei	M_{BH} today	# Mpc^{-3} wander
Direct collapse	$z > 10$	UV background pristine gas	0.2–0.4	0.4–0.8	0.1–0.15	10^4–10^6	0.1–0.3
Population III	$z > 15$	Super-Eddington accretion	0.2–1.0	0.5–1.0	0.1–0.4	10^4–10^6	0.1–0.3
Fast runaway	All	BH retention high stellar density	0.1–0.7	0.1–1.0	0.02–0.25	10^3–10^5	>0.3
Slow runaway	All	BH retention high σ_*	0.1–0.7	0.1–1.0	0.02–0.25	10^3	>0.3

Abbreviations: BH, black hole; UV, ultraviolet.

[a]We show the range of occupation fractions and implied number densities for each seed formation channel. The direct-collapse numbers are based on Bellovary et al. (2019), and the Population III numbers are based on Ricarte & Natarajan (2018). For the gravitational runaway channel, we have relied on a number of sources described in Section 2.4.

2.3. Number Densities of Early Seeding Models

The Pop III and direct-collapse channels are distinguished from the dynamical runaway channels in that they happen exclusively at very high redshift and rely on the presence of metal-free gas, so we refer to them collectively as early seeding models. As described above, the direct-collapse scenario requires finely tuned conditions. For those theoretical works that consider direct collapse viable, then both channels are generally thought to make at most one IMBH per halo (although as emphasized above, direct-collapse black holes may be considerably rarer), and thus yield very similar number-density predictions (**Table 1**).

The hope for observable differences between these two seeding mechanisms has hinged on the idea that heavy seeding would leave lower numbers of more massive seeds, whereas Pop III remnants would be more common but of lower mass (e.g., van Wassenhove et al. 2010, Greene 2012). Two approaches have been taken to predict the observable signatures of seeding mechanisms on the black hole population today, semianalytic modeling and hydrodynamic simulations.

Semianalytic modeling (Volonteri et al. 2008) can quickly track the evolution of black holes using merger trees and explore the dependence on all the uncertain accretion and merging prescriptions (see also Volonteri & Natarajan 2009, van Wassenhove et al. 2010). Most of the semianalytic models in the literature that compare Pop III stars and heavy seeds adopt the heavy seeding model of Lodato & Natarajan (2006), which predicts a high number density of heavy seeds $\sim$0.1 Mpc^{-3} (Volonteri 2010), as compared to $\sim 10^{-4}$ Mpc^{-3} quoted by Inayoshi et al. (2020, in this volume). Thus, these are optimistic scenarios for heavy seeds and likely depend in detail on the assumed ionizing background (e.g., Valiante et al. 2016). Recently, Bellovary et al. (2019) also used zoom-in hydrodynamical simulations to track seeds to the present day as formed in high redshift via a direct-collapse scenario (Dunn et al. 2018). We take the recent work by Ricarte & Natarajan (2018) as representative of the semianalytic approach, because they consider a range of fueling mechanisms. The two have comparable predicted occupation fractions in the context of direct collapse. However, Ricarte & Natarajan find a very wide range of acceptable occupation fractions for the Pop III channel (see also Section 9). We note that according to predictions from both models, the occupation fraction starts to change dramatically below galaxy host masses of 10^9 $M_\odot$, a regime that is not yet empirically constrained.

We translate these occupation fractions into number densities for the two channels (**Table 1**). To convert the occupation fractions into number-density predictions, we take a galaxy stellar-mass

Annu. Rev. Astron. Astrophys. 2020.58:257-312. Downloaded from www.annualreviews.org
Access provided by National Astronomical Observatories, Chinese Academy of Sciences on 09/05/23. For personal use only.

function (Wright et al. 2017) and integrate from 10^7–10^{10} $M_\odot$, incorporating the range of occupation fractions presented in **Table 1**. Note that we have observational constraints only down to 10^9 $M_\odot$, and so these predictions represent a significant extrapolation but are consistent with existing observations in all cases. These numbers are also roughly consistent with the numbers quoted by Volonteri (2010), which again rely on the optimistic direct-collapse channel from Lodato & Natarajan (2006). Although mass distributions may differ between the two, the full range of predicted occupation fractions for the direct-collapse and Pop III channels are quite similar. We emphasize that the accretion history will be tracked eventually with active galaxy luminosity functions (e.g., Civano et al. 2019), which should provide additional constraints on the fueling models and may allow us to distinguish between seeding models more effectively (see Section 10).

Annu. Rev. Astron. Astrophys. 2020.58:257-312. Downloaded from www.annualreviews.org
Access provided by National Astronomical Observatories, Chinese Academy of Sciences on 09/05/23. For personal use only.

2.4. From Seeds to Local Predictions: Gravitational Runaway

We now attempt to translate theory on the different channels of gravitational runaway into predictions for the number density and mass distribution of IMBHs at present (**Table 1**). Unique to this channel is the expectation of $\gg 1$ massive black hole per galaxy, which will be quantifiable if we ever manage to detect or rule out nonnuclear black holes.

Recent work has revisited the slow-formation scenario described in Section 2.1 in the context of dynamical formation of black hole–black hole binaries observable as gravitational wave mergers (e.g., Rodriguez et al. 2018). Indeed, there is some prospect for useful observational constraints for this channel using gravitational wave observations from the current generation of detectors (Kovetz et al. 2018). The predictions for the slow scenario depend in essential ways on whether the dynamics of close encounters are treated in a relativistic manner. Although there is no simple expression for the gravitational recoil velocity as a function of the black hole masses, mergers with more extreme-mass ratios tend to have lower velocities. The predictions also depend strongly on the unknown initial spins of black holes, which can lead to enormous velocities that will eject nearly all systems from clusters (Campanelli et al. 2007). Even if the initial spins are low, postmerger products will have higher spins, suggesting that successive mergers are more likely to eject black holes. Holley-Bockelmann et al. (2008) found that in most cases the IMBH is ejected over a wide range of seed masses, unless all the encounters have mass ratios $M_{\rm low}/M_{\rm high} \lesssim 0.05$. To ensure that this condition is met would require that the initial seed be $\gtrsim$500 $M_\odot$ and that it is surrounded by a subcluster of $\lesssim$25 $M_\odot$ stellar-mass black holes. Seeds of lower mass would have a high likelihood of ejection if other black holes are present.

In the very densest clusters, the escape velocity might be high enough to allow merger products to remain bound (Antonini et al. 2019), which would limit IMBH retention to rare dense clusters that are more than about a few $\times 10^6$ $M_\odot$. Some other studies (e.g., Giersz et al. 2015) that advocate for slow IMBH formation in star clusters sometimes miss the crucial contribution of recoil in the dynamics of IMBH formation through this channel. Although the occupation fraction from the slow channel is uncertain, current simulations are consistent with a low or negligible value for typical globular clusters.

For the fast channel, Portegies Zwart & McMillan (2002) argue that fast runaway only applies to clusters with short initial relaxation times. A short relaxation time excludes most typical globular clusters, unless perhaps they are born with primordial mass segregation. Gürkan et al. (2004) find that runaway collisions should be common in dense clusters, but the final product of the runaway is uncertain, because a supermassive star formed by collisions will evolve on a timescale comparable with the collision rate (Freitag et al. 2006). The metallicity of the stars and the possible presence of gas in the core add additional complications. Hence, it is difficult to predict whether a supermassive star will form at all, its expected mass if it does form, and whether it would eventually collapse to an IMBH or instead destroy itself entirely as a pair-instability supernova (Spera & Mapelli 2017).

Annu. Rev. Astron. Astrophys. 2020.58:257-312. Downloaded from www.annualreviews.org
Access provided by National Astronomical Observatories, Chinese Academy of Sciences on 09/05/23. For personal use only.

Other papers have discussed the possibility of fast seeds selectively forming only at high redshift in star clusters at the centers of dense and relatively massive halos (e.g., Sakurai et al. 2017). If so, then most of these clusters will preferentially migrate to galaxy centers. However, there is voluminous evidence that most globular clusters of all metallicities formed in the same way that massive clusters still form today, rather than in a unique channel only operating in the early Universe (e.g., Brodie & Strader 2006, El-Badry et al. 2019).

Miller & Davies (2012) argue that all clusters above a central velocity dispersion of ∼40 km s^{-1} necessarily form an IMBH through some mechanism, because neither primordial nor dynamically formed binaries of stars or stellar remnants can prevent core collapse for these velocity dispersions. This analytic argument rests on efficient ejection of stellar-mass black holes. Breen & Heggie (2013) argue that black hole ejection is expected to be rather inefficient for typical globular clusters, and hence core collapse will usually occur only after many relaxation times. This result is generally borne out by numerical simulations (e.g., Kremer et al. 2019), though few simulations of $\gtrsim 10^6$-$M_\odot$ clusters have yet been published.

Overall, there is little theoretical support for the idea that IMBH formation is favored in typical globular clusters. By contrast, many nuclear star clusters have high velocity dispersions and a range of relaxation times, and may be plausible sites for the formation of IMBHs. We return to this idea in Section 5.

Although old globular clusters are currently too dynamically evolved to suffer recent gravitational runaway, young star clusters or growing nuclear star clusters should still be in a position to grow massive black holes if this channel is robust. To date, no such trustworthy sources have been found (although see Section 5 for some candidates). One way out of this constraint is to note that few sensitive optical, radio, or X-ray surveys for massive black holes are currently possible outside of the Milky Way, which itself has scarcely any young massive clusters (see Section 5). Another way out is that the channel may require low metallicities (Mapelli 2016), and then we would not expect it to operate in the local Universe. However, metal-poor and metal-rich clusters have no observed substantial structural or dynamical differences, so if IMBHs form commonly but only in low-metallicity clusters, they have not yet been found to affect the clusters in any noticeable way.

2.5. Number Densities of Gravitational Runaway Models

To translate these predictions into number densities, we first consider galaxy nuclei, and then the cluster population. If gravitational runaway happens, one would think that nuclear star clusters, the most massive and densest clusters, may be the most likely to form and retain IMBHs. However, not all nuclear star clusters may successfully form massive black holes by gravitational collapse (Breen & Heggie 2013; Section 5). We therefore assume that under this channel, there will be a wide range of occupation fractions in galaxy nuclei, between 10% and 100%. Adopting a measured range of nucleation fractions as a function of stellar mass from Sánchez-Janssen et al. (2019; see also Neumayer et al. 2020) we find a final number density of 0.02–0.25 Mpc^{-3} (**Table 1**). This number could be higher than that for early collapse models. We consider predictions for off-nuclear black holes below.

2.6. From Seeds to Local Predictions: Wandering Black Holes

In addition to black holes in galaxy centers, any seeding model will lead to a population of off-nuclear wandering black holes. We divide wandering black hole channels into those in which the black hole is made via gravitational runaway in star clusters and those in which the black hole is formed in the nucleus of a satellite galaxy.

If gravitational runaway operates, Holley-Bockelmann et al. (2008) show that any IMBH formation scenario within globular clusters would lead to the majority of IMBHs with $M_{\rm BH} <$ 3,000 $M_\odot$ being ejected. Fragione et al. (2018) use a semianalytic model and explore a range of $M_{\rm BH}/M_{\rm cluster}$ of 0.5–4% to find that only a small percentage (3%) of IMBHs would be retained in globular clusters today, whereas the majority of the ∼1,000 IMBHs in the Milky Way would either be ejected during black hole–black hole mergers (70–90%) or have their clusters dissolve around them (4–30%), leaving a large population of wandering black holes with a low-mass dense stellar cluster remaining bound.

To find these wanderers, consider that at the present day ∼20–40 stars are expected to remain surrounding the $M_{\rm BH} \sim 10^4$-$M_\odot$ IMBHs and perhaps $\sim 10^3$ stars surrounding rarer $M_{\rm BH} \sim 10^5\ M_\odot$ (see also Komossa & Merritt 2008). The expected half-light radii of these remnant clusters are small, $\lesssim$1 pc. Such clusters should be detectable as resolved stars in future wide-field surveys such as that to be conducted on the Large Synoptic Survey Telescope (LSST), because current observations are already discovering very low-mass globular clusters in the outer halo (e.g., HSC-1, with ∼250 stars; Homma et al. 2019). Follow-up spectroscopy of even a few stars in such objects could reveal their provenance via an unexpectedly large velocity dispersion. Closer to the Sun, remnant recoil clusters containing only a handful of stars could be identified using *Gaia* data as a population in a small patch of sky (less than about a few ×10 arcsec) with a net proper motion and a substantial dispersion around that value. These IMBHs could also pass through molecular clouds in the disk, sparking into detectability from the additional fuel as a faint radio source with high proper motion (Fender et al. 2013).

Even if there are no black holes in globular clusters, disrupted infalling satellite galaxies that harbor IMBHs will deposit their black holes somewhere outside the nucleus of the larger halo. If some infalling satellites harbor a massive black hole (which is likely for at least some of the massive satellites; Section 9), then we expect a population of wandering black holes (Governato et al. 1994, Schneider et al. 2002, Volonteri et al. 2003, Islam et al. 2004, Bellovary et al. 2010, Micic et al. 2011, Rashkov & Madau 2014). A related pathway comes from very early accretion of satellites. Mergers between satellites could have led to ejections of black holes that might still be wandering around the Milky Way. The recoiling black hole will likely take with it a tightly bound cluster of stars (O'Leary & Loeb 2009, 2012). O'Leary & Loeb estimate $\gtrsim$100 black holes with $M_{\rm BH} > 10^3\ M_\odot$ (and $\gtrsim$10 black holes with $M_{\rm BH} > 10^4\ M_\odot$) in the Milky Way. That massive black holes have been detected in the centers of ultracompact dwarf galaxies (Seth et al. 2014, Ahn et al. 2018), which are the dense remnants of tidally stripped galaxies, provides empirical evidence for this channel.

2.7. Number Densities of Wandering Black Hole Models

We make two different estimates for the number density of wanderers (nonnuclear IMBHs), first for those deposited by globular clusters, and second for those formed in satellites. We make our estimates as fully empirical as possible, by linking the number of wanderers from clusters directly to observed numbers of globular clusters per unit host stellar mass and number of wanderers from satellites to the number of ultracompact dwarf galaxies per unit host stellar mass, assuming these are tidally stripped galaxies.

We start by calculating the number of globular clusters per galaxy using the stellar mass to globular cluster number relation from Harris (2016). We assume a V-band mass-to-light ratio of two for galaxies with $M_* < 3 \times 10^{10}\ M_\odot$, and three for more massive galaxies. Not all globular clusters host black holes. We assume that 10% of massive globular clusters with $M_* > 10^6\ M_\odot$ can form and retain massive black holes (Holley-Bockelmann et al. 2008, Fragione et al. 2018). To estimate the fraction of globular clusters with $M_* > 10^6\ M_\odot$, we integrate the globular cluster

Annu. Rev. Astron. Astrophys. 2020.58:257-312. Downloaded from www.annualreviews.org
Access provided by National Astronomical Observatories, Chinese Academy of Sciences on 09/05/23. For personal use only.

luminosity functions from Jordán et al. (2007) for different galaxy masses. Integrating these luminosity functions, we find that ∼5% of the globular clusters around an $\sim 2 \times 10^{10}$-$M_\odot$ galaxy have $M_* > 10^6$ $M_\odot$, whereas ∼10% of the globular clusters around a 10^{11}-$M_\odot$ galaxy are of this mass or greater. Folding that in with the number of massive clusters per galaxy, we find a number density of 0.31 IMBH per cubic megaparsec (**Table 1**). Again, we emphasize that this is a lower limit, because it does not include black holes in dissolved clusters or those that may have been ejected from their cluster after a merger.

We further assume that massive clusters ($M_* > 10^6$ $M_\odot$) in a galaxy today comprise a mixture of a tail of truly massive objects that formed as clusters (∼80%) with the cores of stripped galaxies (∼20%) that we refer to as ultracompact dwarfs (e.g., Pfeffer et al. 2016). With the number of such clusters calculated in the prior paragraph, we then expect somewhere between zero and two ultracompact dwarfs for the Milky Way (e.g., M54 and perhaps ω Cen), and somewhere between 75 and 150 in a cluster like Virgo, as observed (Liu et al. 2015). Our assumption that ultracompact dwarfs do not dominate the globular cluster luminosity function even at high mass is also supported by the Jordán et al. luminosity functions, which do not change if all clusters with sizes greater than 5 pc (a proxy for stripped dwarf galaxies) are excluded.

To calculate the number of wandering black holes caused by disrupted satellites, we need to know both the number of disrupted satellites and how often the satellites host a black hole. This is mass dependent. Based on work summarized in Section 9, we take an occupation fraction between 10% and 50%; this leads to at most one wandering black hole in a Milky Way–mass galaxy according to this scaling. Our numbers are somewhat lower than predictions from some theoretical works (Bellovary et al. 2010, Rashkov & Madau 2014) but slightly higher than what is presented by Volonteri & Perna (2005). Integrating over the galaxy luminosity function (Wright et al. 2017), we find a comparable number density of IMBHs in wanderers in L_* galaxies as there are in dwarf nuclei, ∼0.06–0.3 per cubic megaparsec (**Table 1**).

A far more conservative number density is given by Voggel et al. (2019). They investigate the number density of black holes associated with ultracompact dwarf galaxies found in cluster environments and likely to host black holes detectable by current techniques. That number density is 2×10^{-3} supermassive black holes per cubic megaparsec. They then extend their methodology to include ultracompact dwarf galaxies around all elliptical galaxies to find $7–8 \times 10^{-3}$ supermassive black holes per cubic megaparsec. Our much higher numbers, in contrast, are dominated by so-far unknown lower-mass black holes ($<10^5$ $M_\odot$) that may be found in the halos of $\sim L_*$ galaxies because of stripping of low-mass satellites like Sagittarius and the Large Magellanic Cloud (LMC; e.g., Rashkov & Madau 2014).

2.8. Tests of Seeding Mechanisms

Clearly, number densities alone are too blunt a tool to distinguish different early seeding mechanisms. Other means have been discussed in the literature. The black hole mass function could encode seeding history, particularly if there is a mass cutoff corresponding to a heavy seeding mechanism (Section 9). Occupation fractions and black hole scaling relations (Section 8) might reflect differences in seeding mechanisms or depend more on fueling than seeding (e.g., Volonteri & Natarajan 2009, Ricarte & Natarajan 2018). Transients (tidal disruptions and gravitational waves; Section 6) may provide our best hope for finding wandering black holes along with direct evidence of early seeds from direct merger detections with LISA.

In summary, theoretical challenges continue to impede our ability to make definitive predictions for local IMBH populations based on the channel. It is still unclear from the theoretical literature whether enough gas can be in the prime condition for the direct-collapse channel to

Annu. Rev. Astron. Astrophys. 2020.58:257-312. Downloaded from www.annualreviews.org
Access provided by National Astronomical Observatories, Chinese Academy of Sciences on 09/05/23. For personal use only.

contribute a significant fraction of black holes. If yes, then the differences in local number density and mass distribution between direct-collapse and Pop III channels will likely be insufficient to distinguish between them. Likewise it is unclear whether Pop III seeds can grow efficiently in low-mass halos at early times (e.g., Pelupessy et al. 2007, Alvarez et al. 2009). Additional information on the early growth history of these black holes may come from active galaxy luminosity functions (e.g., Civano et al. 2019) and gravitational waves from black hole mergers at high redshift (Sesana et al. 2007).

Annu. Rev. Astron. Astrophys. 2020.58:257-312. Downloaded from www.annualreviews.org
Access provided by National Astronomical Observatories, Chinese Academy of Sciences on 09/05/23. For personal use only.

3. STELLAR AND GAS DYNAMICAL SEARCHES FOR IMBHs

3.1. Dynamics from Integrated Light Measurements

Dynamical modeling of supermassive black holes has a long history and has been reviewed elsewhere (e.g., Kormendy & Richstone 1995, Kormendy & Ho 2013). The kinematics can be measured from either stars or gas in the vicinity of the black hole. For stellar-dynamical modeling, state-of-the-art codes use Schwarzschild modeling (Schwarzschild 1979) to jointly model the mass density of the central black hole, stars, and dark matter by orbit superposition (e.g., Rix et al. 1997, Gebhardt et al. 2003). The stellar-mass profile is modeled from the light, which is then converted to a mass profile by solving for the stellar mass-to-light ratio (M/L), and if needed a dark matter halo component is also independently fitted (e.g., Gebhardt & Thomas 2009). The orbit families are weighted to match the spatially resolved stellar kinematical measurements. A major issue for all dynamical models is distinguishing between orbital anisotropy and mass (e.g., a black hole). This mass–anisotropy degeneracy is well known (e.g., Binney & Mamon 1982). Other (related) issues include: (*a*) degeneracy between the stellar M/L and the black hole mass, (*b*) incomplete stellar orbit libraries, and (*c*) the assumption of axisymmetry (van den Bosch & de Zeeuw 2010). The systematic uncertainties for black hole masses from gas dynamics are qualitatively different than they are for stellar dynamics, but given the large systematics for both kinds of analysis, we use them interchangeably in our discussion (although see a more complete discussion in Walsh et al. 2013).

Low-mass stellar systems (galaxies, nuclear star clusters, and globular clusters) present additional challenges. One is spatial resolution. To detect a black hole, the region within which the gravity of the black hole dominates the stellar motions must be resolved. This gravitational sphere of influence, roughly where the mass enclosed in stars equals that of the black hole, is given by: SOI (pc) $\approx 0.0043\ (M_{\rm BH}/{\rm M}_\odot)\ (\sigma/{\rm km\,s^{-1}})^{-2}$. If we consider black holes with $M_{\rm BH} \sim 10^5\ {\rm M}_\odot$, for typical $\sigma_* \approx 10$–$30\ {\rm km\ s^{-1}}$, then at the limiting distance of current samples (4 Mpc) the angular size is not more than ∼0.2 arcsec (e.g., Nguyen et al. 2018). Another challenge is M/L determinations, which are more complicated in low-mass galaxies due to ongoing star formation and dust. A third is nonaxisymmetric structures such as disks and bars, and other irregular star-forming features (e.g., Kormendy & Kennicutt 2004). A fourth is that individual bright stars can dominate the total light output, biasing the measured stellar dispersion (e.g., Lützgendorf et al. 2015). In galaxies with ongoing star formation, this issue is particularly important. In the Milky Way, Feldmeier et al. (2014) have shown that one blue supergiant could erase the signature of the black hole.

The issue of identifying a robust galaxy center is a fifth significant concern. For instance, center determinations for the LMC have an uncertainty that is greater than a square degree (van der Marel & Kallivayalil 2014). For more distant galaxies, the astronomical community has avoided issues of determining galactic centers by focusing on galaxies with known nuclear star clusters, which encompasses nearly all galaxies with $M_* \sim 10^9$–$10^{10}\ {\rm M}_\odot$ (Georgiev & Böker 2014, Sánchez-Janssen et al. 2019). At lower galaxy masses, as the nucleation fraction drops and galaxies appear more irregular, we will be fundamentally limited by centroid determinations.

Finally, one of the most challenging limitations to dynamical masses for $<10^4$-$M_\odot$ black holes in dense stellar systems is confusion between a putative IMBH and a central cluster of stellar-mass remnants. As dense stellar clusters evolve, the compact remnants sink to the center of the cluster and segregate in mass. Thus, the detailed assumptions made about the presence of stellar remnants (especially stellar-mass black holes) have a crucial impact on the relative evidence for an IMBH (e.g., Mann et al. 2019, and references therein). A related issue is that because of mass segregation and the desire to constrain IMBHs of modest mass, there may be very few luminous stars within the sphere of influence to provide dynamical constraints (see Section 3.2). Studies that do not carefully consider a range of predictions for stellar remnants will not reach robust conclusions about IMBHs. Observations in galaxy nuclei are already approaching this limit for the nearest sources (Nguyen et al. 2019b).

3.2. Proper Motions

When possible, stellar dynamics can be more precisely measured through proper motions of individual stars, which can break the mass–anisotropy degeneracy (e.g., Zocchi et al. 2017). Nevertheless, there are still challenges with these measurements, which generally are used to look for less massive black holes as well.

As a test case, consider the well-studied globular cluster 47 Tuc. The sphere of influence of an $\sim$1,000-$M_\odot$ black hole in 47 Tuc would only be $\sim$1 arcsec, and few stars will be observable within this radius. For example, studies of the central 1 arcsec with the *Hubble Space Telescope* (HST) have only produced precise proper motions for 11–12 stars (McLaughlin et al. 2006, Mann et al. 2019) down to a main-sequence mass of $\sim$0.65 $M_\odot$. Because the central mass function is relatively depleted of low-mass stars due to mass segregation, the total number of stars observable in the sphere of influence of such an IMBH, even down to the hydrogen-burning limit with next-generation extremely large telescopes, might still only be $\lesssim$50 stars. With this modest sample, it is not clear that the advantages in breaking the mass–anisotropy degeneracy gained from proper motions will be definitive in proving the presence of $\sim$1,000-$M_\odot$ IMBHs. By contrast, an $\sim$3,000–4,000-$M_\odot$ IMBH would have a factor of $\sim$10–15 more stars within the sphere of influence and hence be considerably easier to detect than a 1,000-$M_\odot$ IMBH.

The concerns about a misleading population of dense stellar remnants still apply to proper motion measurements. The current state of the art is to use *N*-body codes to model the possible signal from such a cluster of stellar-mass compact remnants (e.g., Baumgardt 2017), which still leaves ambiguous cases. A possible way to alleviate this degeneracy is to determine indirect tests of the presence of stellar-mass compact objects such as expected numbers of pulsars or X-ray binaries. Perhaps more promising is the finding by MacLeod et al. (2016a) that IMBHs should typically acquire companions with orbital periods of years, corresponding to semimajor axes of $\sim$5–10 mas for typical globular cluster distances and $\sim$1,000-$M_\odot$ IMBHs. In the models, the companions undergo frequent exchanges, but about half of the time these companions would be main-sequence stars or giants, most of which should be observable in data of sufficient depth with extremely large telescopes. The proper motion due to the orbit should be very high compared to other cluster members (more than about a few milliarcseconds per year), making such stars readily identifiable even in short-baseline observations, and distinguishable from foreground stars by their precise central location. The theoretical predictions by MacLeod et al. (2016a) cover a small range of parameter space, and it would be worthwhile to see extensions to a wider set of IMBH masses and core densities. This method could not prove the absence of an IMBH in any particular cluster, because a visible companion cannot be guaranteed. However, if a few hundred-$M_\odot$ black holes are common in clusters, companion studies could push down to lower masses than any other

Annu. Rev. Astron. Astrophys. 2020.58:257-312. Downloaded from www.annualreviews.org
Access provided by National Astronomical Observatories, Chinese Academy of Sciences on 09/05/23. For personal use only.

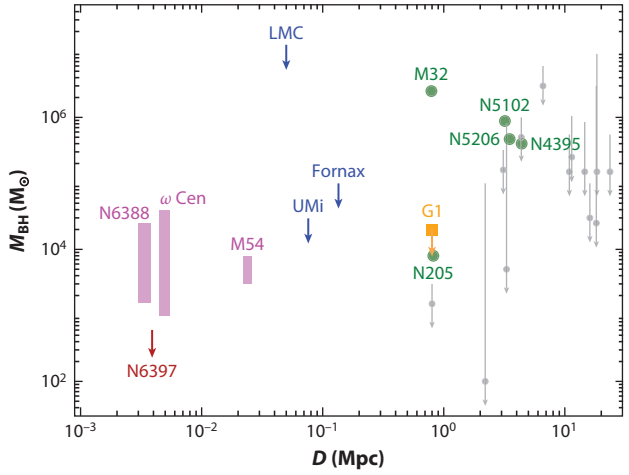


Figure 2

Summary of existing dynamical measurements or limits on black hole mass in low-mass stellar systems. Black hole masses in galactic nuclei (*green circles*) and limits (*gray arrows*) are from various sources (Neumayer & Walcher 2012, Nguyen et al. 2019b, and references therein). The upper-most extent of the gray arrows for the Neumayer & Walcher measurements represent their maximum allowed black hole mass, whereas the gray circles are their best measurement. In pink are Galactic globular clusters with controversial black hole mass measurements; the bottoms of the bars represent upper limits from radio observations (Tremou et al. 2018), whereas the tops are dynamical measurements (Lützgendorf et al. 2013). The similarly contested measurement in G1 is shown in orange (Gebhardt et al. 2005, van der Marel & Anderson 2010). The red upper limit for NGC 6397 (N6397) is representative of the best limits possible in the nearest systems (Kamann et al. 2016). Blue arrows are upper limits on three Milky Way satellite dwarf galaxies, the LMC (Boyce et al. 2017), Fornax (Jardel & Gebhardt 2012), and Ursa Minor (Lora et al. 2009). Abbreviation: LMC, Large Magellanic Cloud.

method. The timing of millisecond pulsars in even wider orbits could also reveal the presence of an IMBH, though the interpretation of these timing observations is not necessarily straightforward. We revisit some of these issues in Section 3.5.

3.3. IMBH Demographics in Galaxy Nuclei from Dynamics

The most definite existing dynamical measurements are for nucleated 10^9–10^{10}-$M_\odot$ galaxies within ∼4 Mpc of the Sun. Ten such galaxies have published black hole masses or limits from stellar and gas dynamics (see **Figure 2**). There are published detections in five of these galaxies: M32, NGC 5102, NGC 5206, NGC 205 (Nguyen et al. 2018, 2019b), and NGC 4395 (den Brok et al. 2015). There are published upper limits for five additional galaxies: NGC 300 and NGC 7793 (Neumayer & Walcher 2012), NGC 404 (Nguyen et al. 2018), the LMC (Boyce et al. 2017), and M33 (Gebhardt et al. 2001). Taking these ten objects and five detections at face value, we have a lower limit of >50% on the occupation fraction. This is a lower limit because the measurements are really only sensitive to black holes with $M_{BH} > 10^5\ M_\odot$ for galaxies outside of the Local Group.

It is worth commenting specifically on the case of the LMC. Later in this section, we discuss indirect evidence (from a hypervelocity star) for a massive black hole somewhere in the LMC. Because the LMC is so close to the Milky Way, we have high spatial resolution and thus sensitivity to even lower-mass black holes. However, the increased resolution is debilitating. No measurement of the center of the LMC is in good agreement with any other (van der Marel & Kallivayalil

Annu. Rev. Astron. Astrophys. 2020.58:257-312. Downloaded from www.annualreviews.org
Access provided by National Astronomical Observatories, Chinese Academy of Sciences on 09/05/23. For personal use only.

2014); thus it is very challenging to know where to search for a putative massive black hole. The best limit we have thus far was made with great effort by Boyce et al. (2017) using Very Large Telescope/MUSE observations, but their limit of $M_{\rm BH} < 10^7$ $M_\odot$ is not terribly constraining.

For galaxies with lower masses ($M_* < 10^9$ $M_\odot$) within the Local Group, there are three other interesting published upper limits to mention. In order of decreasing stellar mass, we have limits on putative black holes in the dwarf galaxies Sagittarius, Fornax, and Ursa Minor. In the case of Sagittarius, the nucleus is the globular cluster also known as M54. Because the galaxy is actively being disrupted, indirect means are needed to estimate the original mass of the galaxy. Summing of the light in the tidal features (Niederste-Ostholt et al. 2010) and modeling of the stream (Laporte et al. 2018) and stellar abundances and abundance ratios (de Boer et al. 2014) all suggest that the galaxy was one of the more massive satellites, comparable with the Small Magellanic Cloud, with a stellar mass of a few $\times 10^8$ $M_\odot$. Dynamical measurements of the center of M54 are reviewed below, but there is no consensus on the presence of a black hole in this cluster (Ibata et al. 2009, Baumgardt 2017).

Moving downward in mass to the Fornax dwarf galaxy, Jardel & Gebhardt (2012) present an orbit modeling limit of $M_{\rm BH} < 10^5$ $M_\odot$ (3σ limit) on any black hole. Finally, there is an interesting published limit on a massive black hole in the galaxy Ursa Minor. Lora et al. (2009) argue that any centrally located black hole with $M_{\rm BH} > 3 \times 10^4$ $M_\odot$ would dissolve observed stellar clumps. The major caveat here, also noted by the authors, is that the initial location of the black hole in the galaxy is unconstrained (e.g., Bellovary et al. 2019). To find any 10^3–10^4-$M_\odot$ black holes that may be lurking in Local Group dwarfs will likely require proper motions with an extremely large telescope (e.g., Greene et al. 2019).

Finally, Neumayer & Walcher (2012) perform Jeans modeling for a sample of nine nucleated spiral galaxies out to 10 Mpc in the $M_* = 10^9$–10^{10}-$M_\odot$ range. There are also published upper limits for NGC 3621 (Barth et al. 2009) and NGC 4474 (De Lorenzi et al. 2013). Together, these limits will prove crucial in measuring scaling relations in this mass range (Section 8).

In Section 9 below, we use the dynamical sample of ten galaxies with $10^9 < M_*/M_\odot < 10^{10}$ and $D < 4$ Mpc as one constraint on the occupation fraction. Although there is not a truly volume-complete sample of galaxies with dynamical measurements, there is no obvious bias in those galaxies that have been targeted. The searches have focused on galaxies with known nuclear star clusters, but the nucleation fraction among galaxies in this stellar-mass range is as high as ∼80–90% (Georgiev & Böker 2014, Sánchez-Janssen et al. 2019). Neumayer et al. (2020) do not see any differences between the nucleation fractions of red and blue galaxies. However, the nucleation fractions measured for blue galaxies in the $M_* = 10^9$–10^{10}-$M_\odot$ range may be biased against galaxies with ongoing vigorous star formation. A case in point is the LMC, which has no readily identified nuclear star cluster, although as discussed above, its center is unknown.

To explore these issues quantitatively, we rely on the nearby galaxy catalog of Karachentsev et al. (2013). This catalog includes *K*-band magnitudes, and we make the simplifying assumption that all galaxies have $M_K/M_\odot \approx 1$. There are 21 galaxies with $1.5 < D < 5$ Mpc and $10^9 < M_*/M_\odot < 10^{10}$ by this definition. Of these 21, 13 have known and well-studied nuclear star clusters, whereas 1 galaxy has none (NGC 55; Seth et al. 2006). Most of the remaining 7 galaxies have been imaged with HST; it is a high priority to examine these for the presence of nuclei (N. Hoyer, N. Neumayer, I.Y. Georgiev, and A.C. Seth, in preparation). In terms of mass and size, we do not see obvious biases in the nuclear star cluster properties in this sample relative to Georgiev & Böker (2014), nor is there evidence for differences between red and blue galaxies (see also Foord et al. 2017). Finally, it is worth noting again that dynamical measurements are particularly challenging in blue galaxies, owing to both their complicated nonaxisymmetric kinematics and the shot noise from individual young stars, which must be considered as more dynamical constraints become available.

Annu. Rev. Astron. Astrophys. 2020.58:257-312. Downloaded from www.annualreviews.org
Access provided by National Astronomical Observatories, Chinese Academy of Sciences on 09/05/23. For personal use only.

Annu. Rev. Astron. Astrophys. 2020.58:257-312. Downloaded from www.annualreviews.org
Access provided by National Astronomical Observatories, Chinese Academy of Sciences on 09/05/23. For personal use only.

3.4. Dynamical Searches for IMBHs in the Milky Way

Another special nucleus postulated to house an IMBH is the one within our own Galactic Center. The Milky Way may host a population of leftover IMBHs from past accretion of dwarf galaxies (e.g., Rashkov & Madau 2014, and Section 2.1). IMBHs have been invoked to explain several observational phenomena associated with the Galactic Center; however, to date, none of the evidence can be regarded as definitive. Rather strict constraints exist from the small residual proper motion of Sgr A* perpendicular to the plane of the Galaxy: No dark object larger than 10^4 $M_\odot$ is permitted within 10^3–10^5 AU from Sgr A* (Reid & Brunthaler 2004).

The paradox of youth of the stars within the central parsec of the Galactic Center (Ghez et al. 2003) has inspired mechanisms to shepherd stars into the Galactic Center with the aid of an IMBH (Hansen & Milosavljević 2003). The inward migration of an IMBH can also account for the origin of the kinematic distribution of these young stars (Yu et al. 2007). To this end, the bright IR source IRS 13E, at a projected distance of only 0.13 pc from Sgr A*, has been the subject of intense scrutiny. High spatial resolution observations by Maillard et al. (2004) resolve the source into a compact group of several comoving massive stars, prompting speculation that it constitutes the disrupted core of a young massive cluster in which an IMBH has coalesced by runaway growth (e.g., Portegies Zwart & McMillan 2002). The proper motion measurements by Schödel et al. (2005) would require a large black hole mass of $>10^4$ $M_\odot$, which is difficult to reconcile with the absence of clear nonthermal radio and X-ray emission. A dark object of this mass scale, however, would satisfy the ionized gas kinematics recently reported by Tsuboi et al. (2017).

Gas kinematics can be notoriously tricky to interpret. This challenge is well exemplified by the compact cloud CO-0.40-0.22, whose large line-of-sight velocity and large internal velocity dispersion ($\sim$100 km s^{-1}) prompted Oka et al. (2016) to suggest that it experienced a gravitational kick from a dark 10^5-$M_\odot$ object within 60 pc of the Galactic Center. The spectrum of its associated millimeter continuum and IR source, however, is more consistent with that of a protostellar disk instead of a scaled-down version of Sgr A* (Ravi et al. 2018), and its detailed kinematics are more consistent with cloud–cloud collisions (Tanaka 2018) or supernova-driven interactions (Yalinewich & Beniamini 2018). Interest in this topic continues unabated (Takekawa et al. 2019, Tsuboi et al. 2019).

3.5. IMBH Demographics in Globular Clusters from Stellar Dynamics

Many papers have presented dynamical evidence for IMBHs in globular clusters, but as of this writing there are no systems for which such evidence is unambiguous. Perhaps the best-studied system is ω Cen. There are claims of a massive IMBH ($\sim$4–5 $\times$ 10^4 $M_\odot$) in this star cluster based on isotropic modeling of the radial velocity dispersion and surface brightness profiles (Noyola et al. 2010, Jalali et al. 2012, Baumgardt 2017). However, the velocity dispersion signature of an IMBH is not found in the proper motions of central stars (van der Marel & Anderson 2010), and no resolution of this observational issue has been given in the literature. On the modeling side, anisotropy and the presence of dark remnants could account for most or all of the IMBH signature found in other studies (e.g., Zocchi et al. 2017, 2019; Baumgardt et al. 2019). Some papers have highlighted the need for more sophisticated modeling of the velocities and proper motions of individual stars (see Section 3.2) rather than a binned dispersion profile in the context of ω Cen and other clusters (Lützgendorf et al. 2012, Baumgardt et al. 2019, Mann et al. 2019). Additional observations and modeling are clearly needed for ω Cen, but in any case, the contrasting results highlight the challenges of this work. These challenges are only magnified as one considers IMBHs of lower mass.

Annu. Rev. Astron. Astrophys. 2020.58:257-312. Downloaded from www.annualreviews.org
Access provided by National Astronomical Observatories, Chinese Academy of Sciences on 09/05/23. For personal use only.

Claims of dynamical evidence for massive black holes have been made in multiple other clusters, including for NGC 6388 and M54. The case of NGC 6388 is similar to that of ω Cen, with contrasting results rooted partially in conflicting observational results (Lützgendorf et al. 2011, 2015; Lanzoni et al. 2013). Multiple studies working with similar data sets have found tentative evidence for an $\sim 10^4$-$M_\odot$ IMBH in M54, with the same interpretation caveats as that for ω Cen, and the additional complication that the cluster is embedded in the remnants of the Sagittarius dwarf galaxy (Ibata et al. 2009, Baumgardt 2017). There is no accretion evidence for an IMBH in any of these clusters (Tremou et al. 2018; Section 5). As a promising example of the dynamical limits possible using forefront instrumentation for nearby, dense globular clusters, Kamann et al. (2016) show that any IMBH in NGC 6397 must be $\lesssim$600 $M_\odot$ (**Figure 2**), which is consistent with the radio limit for this cluster (Tremou et al. 2018).

IMBH searches have been extended outside the Milky Way to the nearest massive galaxy with a large globular cluster population, M31. The best-studied globular cluster in M31 is G1. At this distance ($D = 0.8$ Mpc), the observational complication is that the putative sphere of influence of an $\sim 2 \times 10^4$-$M_\odot$ IMBH is barely resolved with HST spectroscopy and imaging. G1 was notable not solely for the contested interpretation of the central kinematics (Gebhardt et al. 2002, 2005; Baumgardt et al. 2003), which have the same issues already discussed, but also for the unique addition of X-ray and radio accretion evidence for a possible IMBH (Pooley & Rappaport 2006, Ulvestad et al. 2007, and Section 4). Unfortunately, this radio emission was not confirmed in deeper observations, and the multiwavelength data are consistent with a standard low-mass X-ray binary (Miller-Jones et al. 2012). Hence G1 belongs to a similar category as ω Cen and M54, with debated dynamical evidence for an IMBH.

Several recent papers have taken a new dynamical tack: using the timing properties of millisecond pulsars in the cores of globular clusters to constrain the presence of an IMBH. Kızıltan et al. (2017) modeled the properties of a subset of pulsars in the central regions of 47 Tuc, finding evidence that pulsar accelerations were best-explained by the presence of a central IMBH of mass $\sim$2,300 $M_\odot$. Subsequent analyses of similar pulsar data sets did not reproduce this result: They found no evidence for an IMBH, with a formal 99% upper limit of $<$4,000 $M_\odot$ (Freire et al. 2017, Abbate et al. 2018). This nondetection is consistent with the results of several studies that modeled the detailed proper motions of individual stars in the core of 47 Tuc (McLaughlin et al. 2006, Mann et al. 2019), or a combination of stars and pulsars (Hénault-Brunet et al. 2020), and found 1σ upper limits in the range of $\lesssim$1,000–1,500 $M_\odot$. These limits are also consistent with the 3σ radio upper limit of $<$1,040 $M_\odot$ (Tremou et al. 2018). We conclude that there is no compelling evidence for an IMBH in 47 Tuc based on available observations and modeling.

Perera et al. (2017) argue that a single pulsar in NGC 6624 has timing properties consistent with being in a long-period, eccentric, loosely bound orbit around an IMBH of mass $>$7,500 $M_\odot$. Other interpretations of these data are possible, and recent dynamical modeling of stars constrains an IMBH to be $\lesssim$1,000 $M_\odot$ (Baumgardt et al. 2019). Future observations and modeling will help distinguish among these possibilities. For a new and promising method, see the sidebar titled IMBH Demographics in Globular Clusters from Microlensing.

3.6. Hypervelocity Stars

Hypervelocity stars are those with galactocentric velocities in excess of the escape velocity at their present location. There is compelling evidence that some of the most extreme hypervelocity stars are due to interactions between stellar binaries and the supermassive black hole at the center of the Galaxy (Hills 1988; Brown et al. 2005, 2018; Zhang et al. 2013; Koposov et al. 2019). The remainder, including some of the stars with less extreme velocities, likely have a wide range of

Annu. Rev. Astron. Astrophys. 2020.58:257-312. Downloaded from www.annualreviews.org
Access provided by National Astronomical Observatories, Chinese Academy of Sciences on 09/05/23. For personal use only.

IMBH DEMOGRAPHICS IN GLOBULAR CLUSTERS FROM MICROLENSING

There is also a promising alternative method for IMBH searches in globular clusters. Typically, the microlensing effects discussed are photometric, resulting in magnification of the background source by the lens. However, the optical depth for photometric microlensing by IMBHs is very low (Safonova & Stalin 2010), and detections are unlikely for reasonable monitoring campaigns of Galactic globular clusters. Kains et al. (2016) instead suggest the possibility of using astrometric microlensing, which is much less sensitive to the angular separation of the source and lens than standard microlensing. The detectability of this astrometric microlensing signal is maximized for clusters close to the Sun that also have high background densities. This methodology was used to search for evidence of a central IMBH in M22 with HST by Kains et al. (2018). Owing to gaps in the astrometric time series, the resulting upper limit on an IMBH was not constraining compared to limits from other methods (Strader et al. 2012), but future observations with the JWST or the WFIRST should provide improved constraints to IMBH masses $\lesssim 10^4$ $M_\odot$ in a subset of nearby clusters, including M22, M4, and 47 Tuc.

origins, including close binaries disrupted by the death of one of the stars, dynamical encounters in star clusters, and even tidal material from accreted satellites (e.g., Hirsch et al. 2005, Abadi et al. 2009, Perets & Šubr 2012, Shen et al. 2018).

If star clusters or Galactic satellites host IMBHs, then extreme hypervelocity stars whose kinematics exclude a Galactic Center origin could provide evidence for IMBHs. Perhaps the best example of this is for the hypervelocity star HVS3, which may have been ejected from the LMC (Edelmann et al. 2005) by an interaction with an IMBH (Gualandris & Portegies Zwart 2007). The star is at most ∼35 Myr old, so the ejection must have been relatively recent and from a young stellar population (Edelmann et al. 2005). Erkal et al. (2019) add *Gaia* data to the analysis and show that an origin in the LMC is much more likely than an origin from the Galactic Center (see also Lennon et al. 2017). They argue that the relative velocity of HVS3 (∼870 km s^{-1}) could only have originated in an interaction with an $\sim 4 \times 10^3$–10^4-$M_\odot$ IMBH. This should intensify efforts to search for other evidence of an IMBH near the center of the LMC or in its young star clusters. We note that the confirmation of an IMBH in one of these clusters (which typically have $M_* \lesssim 10^5$ $M_\odot$) would be remarkable.

Hypervelocity stars may also prove to be the most robust probe of IMBHs in the Galactic Center (Yu & Tremaine 2003, Baumgardt et al. 2006). The observed spectrum of ejection velocities appears to be inconsistent with theoretical expectations for a supermassive black hole–IMBH binary, but the current data leave much room for improvement (Sesana et al. 2007). Even more powerful would be the eventual future detection of hypervelocity binary stars (Lu et al. 2007, Sesana et al. 2009).

Future missions such as LSST and *Wide Field Infrared Survey Telescope* (WFIRST) will improve the ability to search for hypervelocity stars as signposts to IMBHs in Galactic satellites or globular clusters, because they will be sensitive to more typical lower-mass stars. Because of the longer lifetimes of these stars, they may have more possible kinematic origins, and other information like chemical abundances and abundance ratios may be needed to interpret their origin.

4. SEARCHES FOR ACCRETING IMBHs IN GALAXY NUCLEI

Even with next-generation facilities, dynamical measurements will only reach ∼10 Mpc. Thus, to gain population statistics, we must rely on accretion signatures to identify the presence of a black hole. We discuss the physics of accretion signatures at different wavelengths and the samples that have resulted from searches so far.

Annu. Rev. Astron. Astrophys. 2020.58:257-312. Downloaded from www.annualreviews.org
Access provided by National Astronomical Observatories, Chinese Academy of Sciences on 09/05/23. For personal use only.

4.1. Optical Spectroscopic Selection

Optical spectroscopy was one of the first tools deployed to search for IMBHs in galactic nuclei. We discuss the power and shortcomings of these searches here, including temporal spectroscopic monitoring.

4.1.1. Single-epoch searches. The two prototype low-mass AGNs NGC 4395 (Filippenko & Sargent 1989, Filippenko & Ho 2003) and POX 52 (Kunth et al. 1987, Barth et al. 2004) were both originally identified based on optical spectroscopic signatures. In light of the apparent rarity of AGNs in late-type hosts (Ho et al. 1997, Ho 2008), large spectroscopic surveys are needed to tease out any significant statistical sample. Greene & Ho (2004) performed the first systematic search for AGNs powered by low-mass black holes using SDSS DR1 (Sloan Digital Sky Survey Data Release 1), producing 19 low-redshift ($z < 0.35$) broad-line AGNs with estimated black hole masses $\lesssim 10^6$ $M_\odot$, which was subsequently boosted to a sample of ∼200 using SDSS DR4 (Greene & Ho 2007b,c). Although the AGN-based masses are uncertain (see later in this section), follow-up shows that the ensemble of these objects is powered by low-mass black holes. The host galaxies are sub-L_*, disky galaxies (Greene et al. 2008, Jiang et al. 2011), with the low gas-phase metallicities expected at these masses (Ludwig et al. 2012). Subsequent efforts have adopted variants of this strategy to enlarge and refine the broad-line sample, which to date stands at ∼500 sources (Dong et al. 2012b, Chilingarian et al. 2018, Liu et al. 2018). These objects can only be detected in SDSS when they radiate at close to their Eddington limits, and as such they are rare, comprising only $f_{\rm AGN} \approx 0.1\%$ of the local galaxy population with $M_* < 10^{10}$ $M_\odot$.

In addition to selecting on broad-line properties, one can also preselect low-mass galaxies and look for those whose emission lines classify them as AGNs based on the Baldwin–Phillips–Terlevich (BPT) diagram (Baldwin et al. 1981), which classifies objects based on line ratios between strong ISM lines. AGNs have long been known to separate in these diagrams owing to their hard ionizing spectra (e.g., Ho et al. 1997). A number of groups have started with a stellar-mass-selected sample, $M_* < 10^{10}$ $M_\odot$ or less, to search for AGN signatures in dwarf galaxies (Barth et al. 2008, Reines et al. 2013, Moran et al. 2014, Sartori et al. 2015). Moran et al. focus on 28 sources within 80 Mpc ($f_{\rm AGN} = 2.7\%$), whereas Reines et al. present 151 AGN candidates from a parent sample of ∼25,000 emission-line galaxies ($f_{\rm AGN} \approx 0.5\%$). Most AGNs uncovered in this manner are narrow-line objects, but a subset have broad Hα emission indicating $M_{\rm BH} \approx 10^5$–10^6 $M_\odot$. The late-type spiral RGG118 (Baldassare et al. 2017) even has a black hole as small as 50,000 $M_\odot$ (Baldassare et al. 2015).

For the local AGNs selected from SDSS, there is substantial multiwavelength follow-up that can inform further searches. For instance, X-ray and mid-IR observations of the Barth et al. sample confirm their obscured AGN nature (Thornton et al. 2009, Hood et al. 2017). The AGNs selected based on broad emission lines behave like AGNs powered by more massive black holes. In the radio band, a small number of objects have deep follow-up observations but few are radio loud (Greene et al. 2006, Wrobel & Ho 2006, Wrobel et al. 2008). More attention has been devoted to the X-rays (Greene & Ho 2007a, Desroches et al. 2009, Dong et al. 2012a, Yuan et al. 2014, Plotkin et al. 2016), using *Chandra X-ray Observatory* and *X-ray Multi-Mirror Mission-Newton* (*XMM-Newton*) observations of sufficient depth to perform detailed spectral and timing analyses (Moran et al. 2005, Dewangan et al. 2008, Thornton et al. 2008, Miniutti et al. 2009, Ai et al. 2011, Kamizasa et al. 2012, Jin et al. 2016). The results from X-ray timing are particularly critical, as they help to lend confidence to and independently confirm the black hole mass estimates from broad Hα measurements. As a class, these objects are among the most rapidly variable extragalactic X-ray sources (Dewangan et al. 2008, Miniutti et al. 2009, Ai et al. 2011, Kamizasa et al. 2012), pointing to low-mass black holes.

In general, optically selected AGNs appear to be rare in dwarf galaxies. The AGN detection rate for low-mass galaxies using traditional optical tracers seems to hover around ∼1% (**Supplemental Table 1**). So far, correcting for the major incompleteness stemming from star-formation contamination, aperture dilution, and dust reddening in these samples has been prohibitive (e.g., Greene & Ho 2007b, Trump et al. 2015).

Supplemental Material >

Annu. Rev. Astron. Astrophys. 2020.58:257-312. Downloaded from www.annualreviews.org
Access provided by National Astronomical Observatories, Chinese Academy of Sciences on 09/05/23. For personal use only.

4.1.2. Reverberation mapping. For objects with broad emission lines, reverberation mapping yields information about the size scale of the broad-line region (BLR) by measuring the delay between the continuum and line light curve, emitted from the accretion disk and BLR, respectively (Peterson 2014). Combining the BLR radius r with the line width ΔV yields a virial-like mass $M_{\rm BH} = f_{\rm vir} r(\Delta V)^2/G$, with $f_{\rm vir}$ the virial constant. The low luminosities of low-mass AGNs suggest that their BLRs will be compact, and hence any attempt at reverberation mapping must have sufficiently high cadence to sample lags of less than a few days at most. We emphasize that the reverberation-mapping-based masses are currently calibrated with the dynamical samples through $f_{\rm vir}$. Because the structure and kinematics of the broad-line region are unknown, reverberation mapping yields a virial product, which is currently scaled by $f_{\rm vir}$ such that the AGN samples obey the same $M_{\rm BH}$–σ_* relations as those of inactive galaxies (although see Pancoast et al. 2014). This scaling has at least a factor of two ambiguity in it depending on what galaxy samples are used in the $M_{\rm BH}$–σ_* calibration sample (e.g., Ho & Kim 2014).

The initial effort to monitor the prototype low-mass AGN NGC 4395 gave only a marginally useful constraint on the lag for Hβ (Desroches et al. 2006), and preference has been given to the CIV λ1549 measurement by Peterson et al. (2005), which led to a black hole mass estimate of $M_{\rm BH} = (3.6 \pm 1.1) \times 10^5$ $M_\odot$. This mass is consistent, within the considerable tolerance of the uncertainties, with the direct dynamical estimate of $M_{\rm BH} = (4^{+8}_{-3}) \times 10^5$ $M_\odot$ by den Brok et al. (2015). Woo et al. (2019) recently advocated a markedly lower value of $M_{\rm BH} \approx 9{,}100$ $M_\odot$, based on a short, 80-min lag detected from a narrow-band Hα reverberation-mapping campaign with rapid sampling. The published mass adopts a virial constant $f_{\rm vir} = 4.5$. Using a value calibrated to lower-mass spiral galaxies ($f_{\rm vir} = 3.2$; Ho & Kim 2014), the mass formally drops to $M_{\rm BH} \approx 6{,}500$ $M_\odot$. The difference in black hole mass between Woo et al. and Peterson et al. is mainly due to differences between the line width of CIV and Hα, though the two works recover consistent lags. Very few studies have done intercomparisons of multiple lines in the context of reverberation mapping, and certainly not in this mass and luminosity range (e.g., Park et al. 2017).

Somewhat more massive but still in the neighborhood of 10^6 $M_\odot$ or less is UGC 6728, whose Hβ lag of $\tau = 1.5 \pm 0.8$ days yields $M_{\rm BH} = (5.2 \pm 2.9) \times 10^5$ $M_\odot$ (scaled to our preferred $f_{\rm vir} = 3.2$; Bentz et al. 2016). The published lag for SDSS J114008.71+030711.4 (i.e., the object named GH08 in Greene & Ho 2004) of $\tau = 1.5^{+4}_{-2}$ days is short and highly uncertain (Rafter et al. 2011), but it is likely less than 6 days, in which case $M_{\rm BH} < 3.9 \times 10^5$ $M_\odot$. Finally, we mention three Seyfert 1 nuclei with well-measured Hβ lags hosted in late-type spiral galaxies, as summarized by Ho & Kim (2014): NGC 4051 with $\tau = 2.5 \pm 0.1$ days and $\log(M_{\rm BH}/M_\odot) = 6.11 \pm 0.04$, NGC 4253 (Mrk 766) with $\tau = 5.4^{0.2}_{-0.8}$ days and $\log(M_{\rm BH}/M_\odot) = 5.98 \pm 0.29$, and Mrk 202 with $\tau = 3.5 \pm 0.1$ days and $\log(M_{\rm BH}/M_\odot) = 5.98 \pm 0.06$.

Reverberation mapping also provides a relationship (the so-called radius–luminosity relation) between the AGN luminosity and the typical size of the broad-line region (e.g., Bentz et al. 2013). Using the virial constant and the radius–luminosity relation, we can calculate single-epoch virial black hole masses for broad-line AGNs. It is hard to know what the systematic uncertainties are on these masses, particularly at low black hole mass where the radius–luminosity relation is not directly measured.

Annu. Rev. Astron. Astrophys. 2020.58:257-312. Downloaded from www.annualreviews.org
Access provided by National Astronomical Observatories, Chinese Academy of Sciences on 09/05/23. For personal use only.

4.2. Multiwavelength Searches and Confusion with Star Formation

Searching for concrete evidence of AGNs in low-mass galaxies poses a set of unique challenges. One of the major complications in applying the traditional optical BPT diagrams is that the AGNs become hopelessly intermingled with star-forming galaxies at low metallicity (Groves et al. 2006, Stasińska et al. 2006, Cann et al. 2019). Along with a BPT selection, Sartori et al. (2015) selected additional samples using both an HeII λ4686 diagnostic diagram and mid-IR color cuts that have proved effective in selecting luminous AGNs (Jarrett et al. 2011, Stern et al. 2012). Distressingly, almost none of the samples identified by the three methods overlap. Why?

As Hainline et al. (2016) emphasize, young starbursts in the low-metallicity environment of dwarf galaxies have red mid-IR colors that closely mimic those of AGNs. This, unfortunately, calls into question the usage of mid-IR color to select AGNs in late-type, low-mass galaxies (Satyapal et al. 2014, Marleau et al. 2017, Kaviraj et al. 2019). The lower metallicity environment of dwarf galaxies is characterized by higher electron temperatures and higher levels of excitation for the ISM. In theory, there may also be a more top-heavy stellar initial mass function (e.g., Bromm et al. 2002). The preponderance of massive stars profoundly affects the heating and ionization of the gas. High-mass X-ray binaries may be responsible for the ionizing photons for HeII λ4686 (Schaerer et al. 2019). If so, HeII ceases to be a useful AGN indicator in dwarf galaxies (Sartori et al. 2015, Bär et al. 2017). Massive O stars and Wolf-Rayet stars can generate sufficient extreme UV radiation to excite high-ionization lines such as [OIV] 25.89 μm (Lutz et al. 1998, Schaerer & Stasińska 1999), which renders moot any attempt to use this line to select low-mass AGNs (Georgakakis et al. 2011). [NeV] 14.32 μm, normally considered a robust AGN indicator because of its high-ionization potential of 97.12 eV (Satyapal et al. 2007, 2008, 2009; Goulding et al. 2010), is not immune either, as it can be excited by fast-shocks produced by stellar winds from massive stars and supernovae (Contini 1997, Izotov et al. 2012).

As a case in point, we draw attention to the local spheroidal NGC 185, whose nuclear optical line emission, though feeble, technically qualifies it as a Seyfert 2 galaxy (Ho et al. 1997). However, the recent detailed spatially resolved optical and X-ray analyses of this object by Vučetić et al. (2019) clearly show that the excitation of the central nebula is due to supernova remnants. NGC 185 is a fake AGN. This caveat may well impact larger samples of AGNs selected based on narrow emission lines.

Even broad emission lines are not sacrosanct. Although the presence of broad Hα lines is typically regarded as ironclad evidence of an AGN, high-velocity gas can also be of stellar origin. Wolf-Rayet galaxies, for example, often exhibit broad wings to the Hα line (Méndez & Esteban 1997), and the optical spectra of some type II supernovae bear an uncanny resemblance to Seyfert 1 nuclei (Filippenko 1989). Baldassare et al. (2016) obtained multiple-epoch observations of the type 1 sources from Reines et al. (2013) with evidence of star formation in their narrow-line spectra and discovered that in most of them the broad Hα line is transient over a baseline of several years, suggesting a supernova origin. Even when broad Hα is persistent and too strong to be explained easily by supernovae, as is the case in some blue compact dwarfs (Izotov & Thuan 2008, Izotov et al. 2010), no compelling, independent evidence for AGNs has yet surfaced. Follow-up *Chandra* observations of the metal-poor AGN candidates of Izotov & Thuan (2008) reveal that their X-ray emission is far weaker compared to their optical or mid-IR emission than expected for active galaxies (Simmonds et al. 2016). Even sensitive X-ray and radio observations do not find compelling evidence for AGNs in blue compact dwarfs (Latimer et al. 2019). There is also the converse problem, that broadened lines with ∼200–400 km s^{-1} may arise from the narrow-line region of an obscured AGN, with the width reflecting nonvirial motions associated with the AGN. In such cases, the line width may not have any relation to the black hole mass. Studies that push to ambitiously low line width may suffer this contamination (Chilingarian et al. 2018).

Several of the AGN candidates in late-type galaxies originally identified through detection of [O IV] 25.89 μm or [Ne V] 14.32 μm have since been followed up in X-rays (Gliozzi et al. 2009, Georgakakis et al. 2011, McAlpine et al. 2011, Secrest et al. 2012, Hebbar et al. 2019), and in general the X-rays are found to be weaker than expected. Diffuse, thermal emission is occasionally detected when the data are of sufficient quality. Certainly one can appeal to absorption to explain the deficit of hard X-rays, but we cannot rule out the possibility that these galaxies actually lack AGNs.

Annu. Rev. Astron. Astrophys. 2020.58:257-312. Downloaded from www.annualreviews.org
Access provided by National Astronomical Observatories, Chinese Academy of Sciences on 09/05/23. For personal use only.

4.3. Pushing Down the Luminosity Function with X-Ray or Radio Observations

Given the observation of central black holes in the Local Group with very low Eddington ratios (including Sgr A* and M31*), the minority population of highly accreting black holes identified by optical spectroscopy must be the tip of the iceberg. In addition to being faint, AGNs of low accretion rate have systematically lower ionization parameters (Ho 2009), and they may lack broad emission lines altogether (Elitzur & Ho 2009). X-ray observations provide a clean tool to overcome these problems in a wide range of circumstances. Black hole accretion invariably generates X-ray emission (Brandt & Alexander 2015), and low accretion rates have the virtue of producing proportionately even more hard X-rays (Ho 2008). The resolving power of *Chandra* and the low background of its ACIS (Advanced X-ray Astrophysics Facility CCD Imaging Spectrometer) instrument offer the ideal combination for detecting faint compact sources in nearby galaxies, even with short exposures, and the excellent astrometric accuracy of the satellite can align the optical or near-IR nucleus of the galaxy to within 1 arcsec or better. The main source of confusion comes from X-ray binaries, but the degree of contamination can be estimated once the stellar mass and star-formation rate are known (e.g., Miller et al. 2015).

A number of studies have exploited this opportunity to evaluate the incidence of AGNs in nearby late-type galaxies, succeeding in identifying X-ray nuclei in star-forming (Ghosh et al. 2008, Zhang et al. 2009, Grier et al. 2011, She et al. 2017a), dwarf irregular (Lemons et al. 2015), and local Lyman-break analog (Jiang et al. 2011) galaxies. Desroches & Ho (2009) analyzed *Chandra* images of 64 Scd-Sm spirals within 30 Mpc and discovered an X-ray core in 17 of them ($f_{\rm AGN} = 27\%$). The Sc-Sm spirals in the sample of Zhang et al. (2009) yield a consistent result ($f_{\rm AGN} = 30\%$). She et al. (2017b) extended this effort to a more comprehensive census of more than 700 galaxies within 50 Mpc; among late-type, bulgeless spirals, the detection rate of X-ray cores is $f_{\rm AGN} = 21\%$. Unlike the optically selected sources, these X-ray-selected nuclei are all highly sub-Eddington, with median $L/L_{\rm bol} \approx 10^{-4}$. Archival work searching for X-rays in ultracompact dwarfs has been far less conclusive (Pandya et al. 2016).

The above efforts, largely based on archival data, have been complemented by a series of experiments aimed at characterizing the incidence of X-ray nuclei using dedicated *Chandra* surveys of nearby, lower-mass early-type galaxies focused on the Virgo cluster (Ghosh et al. 2008, Gallo et al. 2010), on the Fornax cluster (Lee et al. 2019), and in the field (Miller et al. 2012, Gallo & Sesana 2019). Among the ∼200 early-type galaxies within 30 Mpc uniformly observed to date, Miller et al. (2015) conclude that $f_{\rm AGN} > 20\%$ in galaxies with stellar mass $M_* < 10^{10}\ M_\odot$. Their observations in this stellar-mass range are sensitive to $L/L_{\rm bol} \approx 10^{-4}$, but in more massive galaxies, the same depths probe much lower $L/L_{\rm bol}$. By assuming that the Eddington ratio distribution can be modeled as a smooth function of M_*, Miller et al. bracket the occupation fraction to fall between 30% and 100% at 1σ (see also Gallo & Sesana 2019). Work by Aird et al. (2013) supports the idea that the Eddington ratio distribution varies only very mildly as a function of stellar mass. Finally, it is very encouraging that the active fractions uncovered from X-rays in both star-forming and quiescent low-mass galaxies are comparable. These X-ray results, combined with the dynamical

ones above (Section 3), strongly suggest a high (>50%) occupation fraction in $M_* = 10^9$–10^{10} $M_\odot$ galaxies.

Recently Reines et al. (2019) used deep and high-resolution radio imaging with the Jansky Very Large Array (VLA) to follow up on 111 dwarf galaxies ($3 \times 10^7 < M_*/M_\odot < 3 \times 10^9$) with prior radio detections in FIRST data. Of these, 13 are likely to be powered by AGNs, owing to their point-like natures and luminosities relative to their star-formation rates. Only 1 of these 13 was also identified by optical spectroscopy. These data cannot be used to measure the AGN fraction in a straightforward way because of the sample selection, but they do highlight the promise of even existing radio telescopes to unveil lower-luminosity AGN populations. Intriguingly, many of the sources are found offset from their galaxy nucleus, which is perhaps consistent with predictions (Bellovary et al. 2019, Pfister et al. 2019) that in low-mass galaxies the seed black holes may never settle at galaxy centers (Section 2.1). Another possible origin for some of these sources may be fueling of wandering black holes (see also Section 5).

4.4. Going Further with the Fundamental Plane of Radio Activity

Combining radio emission with X-rays could be even more effective at probing AGNs with very low Eddington ratios. Merloni et al. (2003) and Falcke et al. (2004) found that both supermassive and stellar-mass black holes show fundamental similarities in their accretion flows in the radiatively inefficient low/hard state. Observationally, the X-ray luminosity (L_X; a product of the accretion rate and radiative efficiency) and the radio continuum luminosity (L_R; a measure of the jet power) scale with the mass of the black hole in a simple manner, such that a combination of these three quantities forms a tolerably clean two-dimensional sequence (the fundamental plane) in three-dimensional space.

A physical explanation for this fundamental plane is not necessarily straightforward, because the spectral energy distributions of accretion flows are expected to change systematically with black hole mass. There are no clear conclusions about whether most or all of the radio and X-ray emission is associated with a jet or whether the X-ray emission might instead come from a corona that is separate from the jet while still presumably being linked to the accretion flow (see, e.g., the discussion in Plotkin et al. 2012).

A major challenge in using the fundamental plane comes from the large scatter. This considerable scatter must be at least partially intrinsic, based on a number of arguments. One is that among X-ray binaries, L_R/L_X can vary by a factor of at least a few at fixed L_X (e.g., Jonker et al. 2012). Another is that even in the newest modeling of the fundamental plane—with careful restriction to objects with high-quality dynamical masses and radio and X-ray data, and consideration of the measurement uncertainties—the scatter for determining black hole masses is still large at ∼1 dex. The best-fit plane from Gültekin et al. (2019) is $\log (M/10^8\,M_\odot) = (1.09 \pm 0.10) \log (L_R/10^{38}\ \mathrm{erg\ s^{-1}}) (-0.59 \pm 0.16) \log (L_X/10^{40}\ \mathrm{erg\ s^{-1}}) + (0.55 \pm 0.22)$. We note that the use of previous fits based on careful sample selection and fitting (e.g., Plotkin et al. 2012) would give similar results within the uncertainties in most cases. Despite these uncertainties, many works have moved forward in an observational spirit to use the fundamental plane to constrain black hole masses in circumstances in which more direct measurements are prohibitively difficult or impossible.

Soon after the discovery of the fundamental plane, Maccarone (2004) pointed out that this would be a powerful tool to search for IMBHs in globular clusters (Section 5). The first high-profile use of the fundamental plane to show evidence for a modest-mass nuclear black hole was in the starburst galaxy Henize 2-10 (Reines et al. 2011). Reines et al. used the radio and X-ray data to argue for the presence of a $\log M/M_\odot = 6.3 \pm 1.1$ supermassive black hole. Follow-up very

Annu. Rev. Astron. Astrophys. 2020.58:257-312. Downloaded from www.annualreviews.org
Access provided by National Astronomical Observatories, Chinese Academy of Sciences on 09/05/23. For personal use only.

long-baseline interferometry observations constrained the radio source size to be $<3 \times 1$ pc and confirmed a nonthermal origin (Reines & Deller 2012). Higher-resolution data revealed multiple components to the central X-ray source, moving the fundamental plane mass estimate up to log $M/M_\odot \sim 7$ (Reines et al. 2016). Subsequent work showed that the X-ray spectrum of the nuclear source is more consistent with a supernova remnant than an AGN (Hebbar et al. 2019), although the possible presence of hour-scale variability would not favor this scenario (Reines et al. 2016, Hebbar et al. 2019). There is also no evidence for AGN ionization in the galaxy center (Cresci et al. 2017). In the end, given the stellar mass of 10^{10} $M_\odot$ (Nguyen et al. 2014), the detection of a black hole may be of limited relevance for IMBH studies, but it does show that use of the fundamental plane is challenging in star-forming galaxies.

Another use of the fundamental plane to find evidence for a low-mass central black hole is in the low-mass galaxy NGC 404, where the plane yielded a mass estimate of log $M/M_\odot = 6.4 \pm 1.1$ (Nyland et al. 2012). Newer observations may support an AGN interpretation of this system, although the evidence is not yet conclusive (Nyland et al. 2017). In contrast, dynamical studies of NGC 404 give a 3σ upper limit of $M_{BH} < 1.5 \times 10^5$ $M_\odot$ (Nguyen et al. 2017). These measurements are formally consistent given the large scatter in the fundamental plane but cannot be taken as a vote of confidence for the success of the fundamental plane near the IMBH regime.

Going forward, for most reasonable central black hole mass functions, volume-limited fundamental plane surveys are almost certainly needed to effectively address the question of whether IMBHs exist, due to the usual Malmquist bias that a flux-limited survey is much more likely to detect massive black holes at larger distances. If IMBHs are less common than central black holes of higher masses (see Section 9), then this bias would be exacerbated by the scatter in the fundamental plane, producing an Eddington-like bias in the IMBH candidate sample.

Consider the use of the fundamental plane to find candidate IMBHs well suited for dynamical follow-up in a nearly fixed distance sample, e.g., the *Chandra* survey of Virgo galaxies by Gallo et al. (2008). This survey found a large number of central X-ray sources with luminosities near their detection limit of $\sim 4 \times 10^{38}$ erg s^{-1}. If a subset of these sources hosted IMBHs with masses in the range of 10^4–10^5 $M_\odot$ and they obeyed the fundamental plane, the 5-GHz radio continuum flux densities would typically be only a few microjanskys. Such sensitivities are achievable with very long (10–20 h) integrations on the Jansky VLA, but the time investment for such a fishing expedition would be challenging for more than a few galaxies. However, next-generation facilities such as the Next Generation VLA (ngVLA), which has a factor of 10 higher sensitivity than the Jansky VLA, could carry out a survey of $\sim$100 galaxies with a reasonable time investment and, with a resolution of <0.1 arcsec, could pinpoint the location of any radio emission. Cross-matching with existing high-resolution HST images could weed out possible nonnuclear contaminants such as star-forming regions, supernova remnants, or background galaxies.

4.5. The Promise of Variability Selection

All AGNs vary, and this has been used as a successful selection tool (e.g., Sarajedini et al. 2006, MacLeod et al. 2011). In the near future, a number of upcoming surveys will make variability selection very powerful for IMBH searches.

Optical variability has been used to select low-mass black holes specifically (Morokuma et al. 2016), but the promise of this technique has not been fully explored yet. Heinis et al. (2016) find AGNs in galaxies with stellar masses as low as $M_* \approx 10^{9.5}$ $M_\odot$ using a variability selection. Baldassare et al. (2018, 2019) use optical variability to find AGN candidates in galaxies with M_* spanning 10^7–10^{10} $M_\odot$, a large fraction of which are not uncovered through optical emission-line selection. With upcoming surveys like LSST, this discovery space should grow.

Annu. Rev. Astron. Astrophys. 2020.58:257-312. Downloaded from www.annualreviews.org
Access provided by National Astronomical Observatories, Chinese Academy of Sciences on 09/05/23. For personal use only.

AGNs also vary at radio wavelengths, for diverse reasons both intrinsic (variations in the accretion rate, shocks in the relativistic jet) and extrinsic (scattering and/or magnification caused by interstellar plasma). Synoptic radio surveys have successfully used radio variability to select AGNs (e.g., Mooley et al. 2016). Current and future radio continuum surveys such as the VLA Sky Survey and those with the Square Kilometer Array could identify candidate IMBHs as variable radio sources associated with low-mass galaxies.

IMBHs should also leave distinct signatures in their X-ray variability signals. Specifically, because the X-ray emission region is very compact compared to more massive black holes with AGNs, the variability timescales should be short. This is clearly seen with NGC 4395 (Moran et al. 2005). Kamizasa et al. (2012) leveraged this idea to search the *XMM-Newton* archive for low-mass black hole candidates. Those they found have a median black hole mass of $\sim 10^6$ $M_\odot$ (Ho & Kim 2016), but in principle surveys like *eROSITA* may further such a search. The X-ray excess variance, while promising as a search tool, may not track black hole mass anymore below $\lesssim 10^6$ $M_\odot$, where the variance–mass relation seems to flatten (Ludlam et al. 2015, Pan et al. 2015).

4.6. Moving to Higher Redshift

In addition to pushing to deeper limits for local samples, we could gain orthogonal demographic constraints by looking at high-luminosity sources over much larger volumes; this work is in its infancy. So far, the effort to search for accreting black holes in dwarf galaxies beyond the local Universe has focused on deep X-ray observations of well-studied extragalactic fields, finding candidates from $z < 0.5$ (Schramm et al. 2013, Pardo et al. 2016, Aird et al. 2018) out to $z \approx 2.4$ (Mezcua et al. 2016, 2018a). We emphasize that these objects should be considered as candidates. In the case of the Mezcua objects in particular, many of the faint sources are proximate to more luminous objects, making the matching particularly challenging. The use of photometric redshifts with active galaxies also adds additional ambiguity. Finally, in these very high-redshift sources, the implied Eddington ratios are substantially super-Eddington. Additional follow-up is needed. As high-redshift spectroscopic samples continue to grow (e.g., Takada et al. 2014), we will continue to build reliable luminosity functions for lower-mass black holes at intermediate and high redshifts.

Studying the incidence of X-ray emission from low-mass host galaxies ($M_* = 5 \times 10^9 - 2 \times 10^{10}$ $M_\odot$) out to $z \approx 1$, Shi et al. (2008) placed a strong lower limit of 12% on the fraction of local low-mass galaxies harboring black holes. This statistical result agrees well with the surveys of nearby galaxies summarized above. In the future, along with next-generation X-ray missions, deep spectroscopic surveys with JWST and WFIRST will provide complementary samples of optically selected AGNs at moderate redshift.

5. SEARCHES FOR ACCRETING BLACK HOLES OUTSIDE OF GALAXY NUCLEI

Perhaps the most promising tool for distinguishing between seeding models comes from finding the black holes that are not in galaxy nuclei (Section 2). Thus far, dynamical searches in stellar clusters have been challenging to interpret (Section 3). However, some intriguing off-nuclear objects have surfaced because of their accretion signatures, which we review here.

5.1. Ultraluminous X-Ray Sources

ULXs provided early impetus to think about black hole formation in stellar clusters (e.g., Ebisuzaki et al. 2001), but in recent years our understanding of these objects has evolved. There are many

Annu. Rev. Astron. Astrophys. 2020.58:257-312. Downloaded from www.annualreviews.org
Access provided by National Astronomical Observatories, Chinese Academy of Sciences on 09/05/23. For personal use only.

reviews of ULXs (e.g., Kaaret et al. 2017), and we provide only a brief discussion here of the work most directly relevant to IMBHs.

Usually ULX samples are constructed from objects for which the Eddington limit is exceeded for a typical stellar-mass black hole of $\sim$10 $M_\odot$ (although the mass of the compact object may vary). ULXs were initially interpreted as strong candidates for IMBHs, largely from the simple argument that inferred isotropic luminosities $\gtrsim 10^{40}$ erg s^{-1} imply accretors above $\sim$100 $M_\odot$ (e.g., Colbert & Mushotzky 1999). By definition, ULXs are nonnuclear, to rule out quiescent or low/hard emission from central supermassive black holes.

Early surveys for ULXs were primarily statistical, because contamination from background AGNs can dominate candidate ULX samples (Zolotukhin et al. 2016). ULXs are overabundant in star-forming galaxies and indeed are primarily found near regions of recent star formation themselves (Swartz et al. 2009), which is consistent with ULXs being associated with young massive stars rather than old globular clusters or Pop III remnants. ULXs are also much more common among metal-poor stellar populations than those of solar metallicity (per unit of star formation; Prestwich et al. 2013).

X-ray spectra of ULXs show substantial variety, but overall are not congruent with the states observed for Galactic stellar-mass black holes scaled to the IMBH mass regime. Instead, some ULXs show distinct spectral states that can be physically interpreted as ultraluminous states consistent with super-Eddington accretion onto stellar-mass black holes (see discussion in Kaaret et al. 2017).

Another breakthrough in the interpretation of ULXs was the observation of X-ray pulsations in some ULXs (Bachetti et al. 2014, Fürst et al. 2016, Israel et al. 2017), proving that the accretors in these systems are neutron stars, likely with highly anisotropic accretion due to strong magnetic fields. Some ULXs mooted as IMBHs (e.g., M51 X-7; Earnshaw et al. 2016) have proved to be neutron star ULXs (Rodríguez Castillo et al. 2019).

Putting this together, there is strong evidence that most ULXs are not IMBHs. There are a few important exceptions that we discuss below.

5.2. HLX-1 and Friends

Even though most typical ULXs (with $L_X \sim 10^{39}$–10^{40} erg s^{-1}) are unlikely to be IMBHs, some rare sources have been observed with $L_X \gtrsim 10^{41}$ erg s^{-1} that cannot be easily explained even within a super-Eddington paradigm for neutron stars or stellar-mass black holes. The clearest example is HLX-1 (a so-called hyperluminous X-ray source), located in the disk galaxy ESO 243-49 ($D \sim$ 95 Mpc) at a projected distance $\sim$4 kpc from the galaxy's center (Farrell et al. 2009).

The isotropic-equivalent X-ray luminosity of HLX-1 ranges from $L_X \sim 10^{40}$–10^{42} erg s^{-1}. The association of HLX-1 with its host, and hence its extreme luminosity, have been confirmed via optical spectroscopy (Wiersema et al. 2010). Unlike typical ULXs, the source shows spectral behavior that is more similar to standard accretion disks than super-Eddington accretion, including typical high-thermal and low-hard states and state transitions (e.g., Servillat et al. 2011).

Modeling of the optical and X-ray emission through the state changes is consistent with a black hole mass of a few $\times 10^4$ $M_\odot$, with a fair degree of uncertainty (Davis et al. 2011, Godet et al. 2012, Straub et al. 2014). Radio emission associated with the state changes gives similar mass estimates, in the range of $M_{BH} \sim 10^4$–10^5 $M_\odot$ (Webb et al. 2012). The fundamental plane of X-ray/radio emission allows a mass as high as $\sim 3 \times 10^6$ $M_\odot$ (Cseh et al. 2015) and hence is of limited utility.

An intriguing puzzle in HLX-1 is the nature of the X-ray luminosity variations and state changes. Because X-ray monitoring of the source began in 2008, the state changes appeared nearly

Annu. Rev. Astron. Astrophys. 2020.58:257-312. Downloaded from www.annualreviews.org
Access provided by National Astronomical Observatories, Chinese Academy of Sciences on 09/05/23. For personal use only.

periodic at intervals of ∼1 year, leading to the idea that they were associated with the orbital period of a tidally captured companion star on an eccentric orbit (Lasota et al. 2011). Challenging this simple scenario, only a few years later the state change interval began elongating unpredictably; this was perhaps consistent with the unstable, tidally affected orbit of a compact donor such as a white dwarf (Godet et al. 2014). Other models, in which the luminosity variations do not directly reflect the orbital period of a donor star, have also been proposed (e.g., Soria et al. 2017). Future state changes, or a lack thereof, can provide additional constraints on these models.

Observations of the surrounding stellar population give additional insight into HLX-1. Although the modeling of the data is not conclusive owing to optical emission associated with HLX-1 itself, the photometry is most consistent with a relatively massive (about a few $\times 10^6$ $M_\odot$) star cluster dominated by an intermediate to old stellar population (Soria et al. 2017). No compelling evidence for a recent major merger has been observed around the galaxy (Webb et al. 2017), but nevertheless a self-consistent scenario is that HLX-1 represents a central massive black hole on the low-mass end of the mass distribution of nucleated $\sim 10^9$–$10^{10} M_*$ galaxies whose parent galaxy was accreted and tidally stripped, leaving only the bare nuclear star cluster (e.g., Mapelli et al. 2013). Star formation, perhaps due to the merger, could have increased the capture rate for a central black hole to acquire a companion star on which it is currently feeding. In this scenario, HLX-1 does not represent a unique formation channel for IMBHs, but it is one of the best candidates we have for a (previously central) $\sim 10^4$-$M_\odot$ black hole. HLX-1 and similar systems could help inform our understanding of low-mass central black holes in galaxies.

Besides HLX-1, no other very luminous ULXs are as convincing as IMBH candidates. Pasham et al. (2014) argue that M82 X-1 (which can reach $L_X \sim 10^{41}$ erg s^{-1}) contains an $\sim 430 \pm 100$-$M_\odot$ IMBH via an extrapolation of a stellar-mass black hole scaling relation for X-ray quasi-periodic oscillations. Brightman et al. (2016) model X-ray data of the source over a wide range of energies and prefer a model of super-Eddington accretion onto a stellar-mass black hole, although depending on the spin, the black hole mass might be as high as $\sim 100\, M_\odot$. The interpretation of these data is not settled, and may require future X-ray missions; confusion with the bright ULX pulsar M82 X-2 is a challenge for low-resolution observations. M82 is a starburst dwarf only ∼3.5 Mpc distant, and a confirmation of a luminous IMBH at such a distance would suggest a high space density of IMBHs.

Another source of recent interest is an off-nuclear ULX in the Seyfert galaxy NGC 5252 at ∼100 Mpc (Kim et al. 2015). This ULX has an associated optical and radio source that has been studied at high resolution with the HST and very long baseline interferometry. Overall, these data are consistent with a massive black hole in the $\sim 10^5$–10^6-$M_\odot$ regime whose stars have been stripped, though a somewhat lower mass in the IMBH range cannot be excluded (Mezcua et al. 2018b).

An even less settled case is that of NGC 2276-3c, an $L_X = 2 \times 10^{40}$ erg s^{-1} ULX in a face-on starburst spiral at ∼33 Mpc. The source was associated with a large (hundreds of parsecs) radio nebula in VLA radio imaging (Mezcua et al. 2013). Follow-up quasi-simultaneous X-ray and very long baseline radio data were used to find unresolved hard X-ray emission and detect a compact parsec-scale radio jet at modest significance (Mezcua et al. 2015). A compact, steady jet is consistent with an AGN in the low/hard state, and the fundamental plane was then used to estimate a mass of $\sim 5 \times 10^4$ $M_\odot$ (all such mass estimates have uncertainties of at least 1 dex). However, Yang et al. (2017) independently reduced the radio data and did not confirm the high-resolution radio detection. Furthermore, there is no claimed optical counterpart to the ULX, which might be expected in a scenario in which the IMBH is associated with a star cluster or stripped nucleus. The large number of ULXs found in NGC 2276 (Wolter et al. 2015) suggests that NGC 2276-3c is truly associated with the galaxy. Nonetheless, given the galaxy's high star-formation rate, the

Annu. Rev. Astron. Astrophys. 2020.58:257-312. Downloaded from www.annualreviews.org
Access provided by National Astronomical Observatories, Chinese Academy of Sciences on 09/05/23. For personal use only.

lack of an optical counterpart, and uncertain compact jet detection, it seems more likely that NGC 2276-3c is a super-Eddington stellar-mass black hole or a neutron star ULX rather than an IMBH. In this scenario, the extended radio emission might well be associated with NGC 2276-3c, as radio nebulae due to ULXs are not uncommon (see the discussion in Urquhart et al. 2018).

5.3. Fundamental Plane Searches in Globular Clusters

Accretion constraints on the presence of IMBHs in globular clusters rest on the assumption that, in a manner analogous to that of low-luminosity AGNs, such IMBHs will accrete a fraction of the gas within their sphere of influence, resulting in detectable radio or X-ray emission from the accretion flow or jet (Maccarone 2004). To convert a measurement or upper limit in radio or X-ray luminosity to a corresponding IMBH mass or limit requires assumptions about the accretion rate and radiative efficiency of the accretion process.

In a globular cluster, the winds of evolved stars represent a source of low-velocity gas that is continually replenished: No long-term accumulation of gas is needed to produce an observable level of accretion. Assuming that the gas is ionized, the expected electron density is $n_e \sim 0.05$–0.5 cm^{-3}(Pfahl & Rappaport 2001). The predicted level of ionized gas was first observed in the core of the globular cluster 47 Tuc by Freire et al. (2001), using the radial distribution of the dispersion measure of millisecond pulsars. This single observation has had little follow-up in subsequent years, because the method requires (*a*) a large population of millisecond pulsars and (*b*) a low foreground of ionized material. This combination is, at present, still only satisfied for 47 Tuc. Nonetheless, Abbate et al. (2018) revisit the measurement for this well-studied cluster with updated pulsar parameters, finding an even larger gas density than that in the original paper ($n_e = 0.23 \pm 0.05$ cm^{-3}, compared to $\sim$0.07 cm^{-3}). This measurement is consistent with theory and supports the basic underpinning of the accretion-based mass constraints: Globular clusters should have some amount of gas that is available to be accreted by an IMBH. Other routes to fueling at higher rates are also available, such as winds or tidally stripped material from binary companion stars acquired dynamically (MacLeod et al. 2016b).

Because the X-ray luminosity (L_X) is observed to be a nonnegligible fraction of the bolometric luminosity for known low-luminosity AGNs, it is the most directly accessible tracer of the accretion rate. Given the expected gas density, IMBHs with 10^3–10^4 $M_\odot$ accreting at the Bondi rate with high ($\epsilon \sim 0.05$–0.1) radiative efficiency would be X-ray sources with $L_X \sim 10^{34}$–10^{36} erg s^{-1} at the centers of globular clusters. X-ray sources are observed at this L_X but are identified as individual X-ray binaries rather than IMBHs. Hence, it is clear that if IMBHs are present in Galactic globular clusters, they accrete at levels below that of the Bondi rate or with lower radiative efficiency.

Maccarone (2004) first pointed out that, based on the fundamental plane, radio continuum observations put the most stringent accretion constraints on IMBHs accreting at low radiative efficiency, at least for typical observational sensitivities of radio and X-ray data. Assuming radiatively inefficient accretion and the sub-Bondi accretion rates observed for nearby low-luminosity AGNs (e.g., Pellegrini 2005), many papers have used the fundamental plane and radio upper limits to set stringent constraints on the presence of accreting IMBHs in globular clusters (Maccarone et al. 2005, Maccarone & Servillat 2008, Cseh et al. 2010, Lu & Kong 2011, Strader et al. 2012).

These observational efforts culminated in a study by Tremou et al. (2018), which uses a similar formalism but a much larger sample of deep radio continuum imaging of 50 Galactic globular clusters from the Jansky VLA and the Australia Telescope Compact Array. No emission consistent with an IMBH was observed for any cluster or for a cluster stack, including clusters with dynamical IMBH claims, such as ω Cen, M54, and NGC 6388 (see above). For the clusters with more sensitive VLA data, using the assumed formalism, the median 3σ upper limit to an IMBH

Annu. Rev. Astron. Astrophys. 2020.58:257-312. Downloaded from www.annualreviews.org
Access provided by National Astronomical Observatories, Chinese Academy of Sciences on 09/05/23. For personal use only.

is $\lesssim$1,100 $M_\odot$, which corresponds to very low accretion rate upper limits of less than about a few $\times 10^{-11}$ $M_\odot$ year^{-1}.

There are plausible mechanisms that could temporarily remove all gas from the immediate vicinity of the IMBH, rendering it invisible in radio continuum emission. Hence, the lack of radio emission alone does not definitively prove the absence of an IMBH in a particular cluster. However, scatter in the accretion rate and efficiency is expected in both directions, so if IMBHs were common, at least some obvious sources would be observed. They are not.

It is reasonable to use the full sample of objects with radio constraints to set limits on the occupation fraction. The Tremou et al. (2018) work is sensitive to $\gtrsim$1,000-$M_\odot$ IMBHs and searches $\gtrsim 10^5$-$M_\odot$ globular clusters. Assuming the conservative accretion luminosities outlined by Tremou et al. (2018), their nondetections set a 3σ upper limit of 10–15% on the fraction of such massive globular clusters that could host $\sim$1,000-$M_\odot$ black holes just based on Poisson statistics. The modest size of the Galactic globular cluster system overall makes it challenging to substantially improve this limit on the occupation fraction with future data, except to push to fainter emission levels and hence lower (or more conservative) mass limits. Deep X-ray observations can also provide complementary constraints if the observing times are sufficiently long (Grindlay et al. 2001, Haggard et al. 2013).

Perhaps the best way to improve the limit, especially if IMBHs closer to 10^4 $M_\odot$ are being considered, is with observations of extragalactic globular clusters in nearby galaxies with next-generation radio continuum telescopes: The large number of clusters (hundreds to thousands per galaxy) should allow the detection of the high accretion tail of the distribution even if the occupation fraction is modest (Wrobel et al. 2016, 2019).

6. IMBH SEARCHES WITH TRANSIENT PHENOMENA

Thus far, we have focused on search techniques specialized for either galaxy nuclei that can extend downward to the upper end of the IMBH regime or stellar-cluster-focused work aiming to identify sources in the 10^3-$M_\odot$ realm. However, tidal disruptions and gravitational waves have the potential to work across these boundaries and potentially find wandering black holes in lower-mass stellar systems, should they exist.

6.1. Tidal Disruption Events

TDEs are the electromagnetic signature that may result if a star passes within its tidal radius of a black hole (e.g., Rees 1988). TDEs are powered by accretion onto massive black holes, but their rates and environments provide an independent probe of the space density of IMBHs, because the rates depend on stellar (rather than gas) dynamics. In principle it is possible to derive $M_{\rm BH}$ from modeling of the TDE light curve itself (Lodato et al. 2009, Guillochon & Ramirez-Ruiz 2013, Mockler et al. 2019), as the emission from these events depends on both the mass and radius of the star and the mass of the black hole (e.g., Law-Smith et al. 2017). The TDE literature merits its own review; we focus here only on aspects that may bear directly on IMBH demographics.

6.1.1. Nuclear events. Wevers et al. (2017) present black hole masses for a sample of optically selected TDEs using stellar velocity dispersion measurements. Wevers et al. (2019) play a similar game for X-ray-selected samples, but in those cases identifying a reliable optical counterpart is more complicated, so we focus on the optical samples here. We also note an X-ray-detected transient that is a likely TDE with an $M_{\rm BH}$–σ_*-based mass estimate of 1.3–6.3 $\times$ 10^5 $M_\odot$ (Maksym et al. 2013). If the $M_{\rm BH}$–σ_* relation can be extrapolated below $\sigma_*\sim$100 km s^{-1} (we provide direct

Annu. Rev. Astron. Astrophys. 2020.58:257-312. Downloaded from www.annualreviews.org
Access provided by National Astronomical Observatories, Chinese Academy of Sciences on 09/05/23. For personal use only.

support for this in Section 8), then it is very likely some $<10^6$-$M_\odot$ black holes have already produced detectable TDEs.

Van Velzen (2018) goes a step further and claims that a constant black hole occupation fraction from stellar masses $M_* \approx 5 \times 10^9$ $M_\odot$ to 3×10^{10} $M_\odot$ is required to reproduce the observed TDE rate as a function of mass. This result highlights the promise of TDE observations to independently constrain the occupation fraction and is consistent with our inferences from dynamics (Section 3) and X-ray observations of local galaxies (Section 4) above. That said, to fully utilize the promise of TDEs, some key assumptions need to be explicitly checked. We do not know how TDE rates in low-mass galaxies may depend on star-formation rate or galaxy structure, although we know that TDE rates in more massive galaxies are a function of galaxy properties (e.g., Arcavi et al. 2014). Another open question is whether the TDE emission properties depend systematically on $M_{\rm BH}$ in a way that biases the mass distributions of samples as a function of their selection (e.g., Strubbe & Quataert 2009). Finally, for white dwarf disruptions, there is interesting literature comparing the emission signatures to those of type Ia supernovae (Rosswog et al. 2009, MacLeod et al. 2016a, Anninos et al. 2018). These events are particularly exciting because they could be accompanied by the gravitational wave signature of an extreme-mass-ratio inspiral (Section 6.2).

TDE rates are so uncertain that in theory, all AGN activity in low-mass galaxies may be powered by TDEs, and most black hole mass density at low mass may be built up through tidal capture and TDEs (Milosavljević et al. 2006, MacLeod et al. 2016a, Stone et al. 2017, Zubovas 2019). Zubovas in particular claims that the AGN fraction matches TDE expectations at low mass by assuming (*a*) rates from Stone & Metzger (2016) and (*b*) unity occupation fraction. It should be possible to use multiepoch observations of active nuclei in low-mass galaxies to test whether they fade, as would be expected for TDEs, but at present our time baselines of ∼10 years are too short to be discriminating (e.g., Baldassare et al. 2016, 2018). On the positive side, Jonker et al. (2019) present some hopeful evidence for persistent (5–10 years) X-ray emission from optically identified TDEs, suggesting that *eROSITA* may find as many as thousands of TDEs powered by low-mass black holes.

6.1.2. Peculiar explosions and possible off-nuclear tidal disruption events. In theory there may be numerous off-nuclear IMBHs living in globular clusters or wandering with only a small number of tightly bound stars (O'Leary & Loeb 2012, Fragione et al. 2018), which may give rise to off-nuclear TDEs observed as peculiar transients. For instance, there is a class of rapid blue transients (e.g., Drout et al. 2014, Vinkó et al. 2015, Tanaka et al. 2016, Pursiainen et al. 2018, Perley et al. 2019) that are not easily explained as standard classes of supernovae. These do not occur in galaxy centers nor do they quite look like TDEs. Various groups have suggested that the object presented by Vinkó et al. (2015) may be powered by the tidal disruption of a white dwarf (e.g., Law-Smith et al. 2017). By contrast, Margutti et al. (2019) argue that AT2018cow (Perley et al. 2019) has too much circumstellar material to be explained by an IMBH TDE (although see also Kuin et al. 2019).

Another class of TDE candidate is associated with off-nuclear sources that show transient X-ray emission, often ascribed to a large temporary increase in the accretion rate of the putative IMBH associated with a TDE. Perhaps the most compelling of these is 3XMM J215022.4–055108, which is an X-ray source associated with a $z \sim 0.06$ lenticular galaxy (Lin et al. 2018). This source shows a TDE-like X-ray light curve measured over 10 years, with a luminosity of at least 10^{43} erg s^{-1}. The X-ray source matches the position of a compact star cluster (possibly a stripped nucleus) with an old stellar population and a mass of $\sim 10^7$ $M_\odot$. Fitting the X-ray spectra suggests a black hole mass of 5×10^4–10^5 $M_\odot$, depending on the unknown spin of the black hole. The position of the source

Annu. Rev. Astron. Astrophys. 2020.58:257-312. Downloaded from www.annualreviews.org
Access provided by National Astronomical Observatories, Chinese Academy of Sciences on 09/05/23. For personal use only.

on a diagram of luminosity and temperature for a standard thin accretion disk is very similar to that of HLX-1, suggesting a similar mass.

Other similar sources have been discovered (e.g., Lin et al. 2016, 2017), although the evidence for a TDE-like decay (rather than typical AGN activity) is less compelling owing to a smaller number of deep observations over time, and generally the masses of the associated black holes are more in the regime of normal low-mass central black holes (masses 10^5–10^6 $M_\odot$) rather than in the IMBH regime. If TDEs associated with low-mass central black holes in stripped nuclei are as common as suggested by these recent works, then future sensitive X-ray missions such as the *Athena X-Ray Observatory* should confirm such sources in substantial quantities, with possible rates of up to ∼100 $year^{-1}$ (Cassano et al. 2018, Lin et al. 2018).

Although these TDE-like sources decay over timescales of years, another type of source is worth a quick mention: Irwin et al. (2016) found extremely brief (hundreds of seconds), luminous ($L_X \sim 10^{40}$–10^{41} erg s^{-1}) X-ray flares from star clusters associated with two nearby early-type galaxies. One of the clusters appears to be a typical massive globular cluster, whereas the other has properties consistent with being a stripped nucleus. These X-ray sources show properties most similar to flares from young pulsars with strong magnetic fields—sources not expected to exist in old stellar populations. If the flares are Eddington-limited, then they could represent accretion onto IMBHs with masses of ∼100–1,000 $M_\odot$. So far, these results are only suggestive, and other evidence (such as radio emission from the sources in their lower state) would be necessary to provide stronger evidence for an IMBH classification.

Very likely, these peculiar objects have diverse origins, and only with next-generation observations, along with detailed modeling, will we be in a position to find the most likely TDE candidates among all the rich stellar death phenomenology.

6.2. Gravitational Waves

Given the range of mass and mass ratio that we can hope to detect with gravitational waves in the upcoming decades, we summarize some of the expected discoveries related to IMBHs from LIGO and LISA.

6.2.1. IMBH–IMBH mergers at high redshift. LISA will be sensitive to black hole mergers with mass ratios $q \sim 0.1$–1 for $M_{BH} \sim 10^4$–10^5 $M_\odot$ out to very high redshift ($z \approx 20$). The black hole masses and redshifts can be measured from high S/N gravitational waveforms (Amaro-Seoane et al. 2017). These measurements will provide insight into the seeding mechanisms and fueling rates (e.g., Sesana et al. 2011). However, in detail the rates will depend not only on the seeding mechanism(s) at play but also on the accretion history and the dynamics driving the mergers of the black holes (e.g., Sesana et al. 2007, Klein et al. 2016). In practice it will not be trivial to disentangle these effects. Observations in the X-ray and optical/IR with missions like JWST and the *Lynx X-ray Observatory* that should detect the actively accreting 10^5–10^6 $M_\odot$ black holes at similar epochs would be very complementary (e.g., Haiman et al. 2019; see Section 10).

6.2.2. Low-redshift constraints from intermediate- and extreme-mass-ratio inspirals. If there are IMBHs floating around in more massive halos, then occasionally they should merge with the primary supermassive black hole in an intermediate-mass-ratio inspiral event (e.g., Holley-Bockelmann et al. 2010). In addition, an IMBH embedded in a star cluster (nuclear or otherwise) could merge with a stellar-mass black hole in an extreme-mass-ratio inspiral with even lower-mass ratios (e.g., Gair et al. 2010). Again, the rates of both events are heavily dependent on a number of unknown factors, including the spin of the black hole, the dynamics of the surrounding

Annu. Rev. Astron. Astrophys. 2020.58:257-312. Downloaded from www.annualreviews.org
Access provided by National Astronomical Observatories, Chinese Academy of Sciences on 09/05/23. For personal use only.

Table 2 Detections in nuclei

Object	Distance (Mpc)	Determination method	M_{BH} ($M_\odot$)	$M_{cluster}$ ($M_\odot$)	M_*[a] ($M_\odot$)	σ_*[b] (km s^{-1})	Reference
NGC 205	0.82	Dynamics	$(6.8^{+32}_{-2.2}) \times 10^3$	1.8×10^6	9.7×10^8	40.0	Nguyen et al. 2019b
NGC 5102	3.2	Dynamics	$(9.1^{+0.61}_{-0.51}) \times 10^5$	7×10^6	5.9×10^9	42.3	Nguyen et al. 2019b
NGC 5206	3.5	Dynamics	$(6.3^{+0.69}_{-0.61}) \times 10^5$	1.7×10^6	2.4×10^9	35.4	Nguyen et al. 2019b
NGC 4395	4.4	Dynamics	$(4.0^{+8}_{-3}) \times 10^5$	2×10^6	2×10^9	<30	den Brok et al. 2015
NGC 4395	4.4	RM	$(3.6 \pm 1.1) \times 10^5$	2×10^6	2×10^9	<30	Peterson et al. 2005
NGC 4395	4.4	RM	$(9.1^{+1.5}_{-1.6}) \times 10^3$	2×10^6	2×10^9	<30	Woo et al. 2019
UGC 6728	27	RM	$(5.2 \pm 2.9) \times 10^5$	ND	7.5×10^9	52	Bentz et al. 2016
iPTF16fnl	67	M_{BH}–σ^*	3.2×10^5	ND	9.7×10^9	55	Wevers et al. 2017, Blagorodnova et al. 2017
ASASSN-14ae	200	M_{BH}–σ^*	2.6×10^5	ND	6.3×10^9	53	Wevers et al. 2017, Holoien et al. 2014
PTF-09axc	536	M_{BH}–σ^*	4.8×10^5	ND	1.2×10^{10}	60	Wevers et al. 2017, Arcavi et al. 2014
PS1-10jh	822	M_{BH}–σ^*	7.1×10^5	ND	3.6×10^9	65	Wevers et al. 2017, Gezari et al. 2012
PTF-09djl	900	M_{BH}–σ^*	6.6×10^5	ND	1.9×10^{10}	64	Wevers et al. 2017, Arcavi et al. 2014
WINGS J1348	265	M_{BH}–σ^*	$5.1–5.6 \times 10^5$	ND	2.5×10^8	<50	Maksym et al. 2013, 2014

Abbreviations: ND, no data; RM, reverberation mapping.
[a]Stellar mass when galaxy host.
[b]Stellar velocity dispersion, cluster or galaxy.

stellar cluster, and the number density of IMBHs (e.g., Amaro-Seoane et al. 2015, Fragione et al. 2018, Berry et al. 2019), which hopefully can be partially determined through complementary electromagnetic observations.

6.2.3. Gravitational runaway constraints at low redshift. As alluded to in Section 2 above, if the gravitational runaway channel operates to make seeds, then it should be operating at present in young and forming star clusters. It should be possible to catch the early stages of this process with LIGO detections (Kovetz et al. 2018, Antonini et al. 2019). Current limits on the merger of ~100-$M_\odot$ black holes are not yet constraining (Abbate et al. 2018) but should become so as LIGO progresses. The one caveat relates to the possible subset of runaway processes involving stars (as opposed to black holes) that may require low metallicity. If so, this channel also may operate only at high redshift. We have argued, based on the similarity of observed properties of globular clusters as a function of metallicity, that metallicity dependence is in some tension with observations.

7. IMBH CANDIDATE TABLES

We summarize the prior three sections in three tables containing all of the credible IMBH candidates in the literature to date. For clarity, we separate measurements in nuclei (**Table 2**) from off-nuclear candidates (**Table 3**) and constraining limits (**Table 4**). To be included in the table, an object must have a published black hole mass or limit that falls below 10^6 $M_\odot$. Furthermore, the mass must be based on a primary or secondary black hole mass determination method. We include M_{BH} estimates based on stellar and gas dynamics, reverberation mapping, and scaling from

Annu. Rev. Astron. Astrophys. 2020.58:257-312. Downloaded from www.annualreviews.org
Access provided by National Astronomical Observatories, Chinese Academy of Sciences on 09/05/23. For personal use only.

Table 3 IMBH candidates outside nuclei

Object	Distance (Mpc)	Determination method	M_{BH}[a] ($M_\odot$)	$M_{cluster}$ ($M_\odot$)	σ_*[b] (km s^{-1})	Reference
47 Tuc	0.005	Dynamics	2,300	7.8×10^5	12.2	Kızıltan et al. 2017
47 Tuc	0.005	Dynamics	<1,650	7.8×10^5	12.2	Mann et al. 2019
47 Tuc	0.005	FP	<1,040	7.8×10^5	12.2	Tremou et al. 2018
ω Cen	0.005	Dynamics	$(4.7 \pm 1.0) \times 10^4$	3.6×10^6	17.6	Noyola et al. 2010
ω Cen	0.005	Dynamics	$<1.8 \times 10^4$	3.6×10^6	17.6	van der Marel & Anderson 2010
ω Cen	0.005	FP	<1,000	3.6×10^6	17.6	Tremou et al. 2018
M62	0.007	Dynamics	(2,000 ± 1,000)	7.1×10^5	15.2	Lützgendorf et al. 2013
M62	0.007	FP	<1,130	7.1×10^5	15.2	Tremou et al. 2018
NGC 6624	0.008	Dynamics	>7,500	7.3×10^4	6.1	Perera et al. 2017
NGC 6624	0.008	Dynamics	<650	7.3×10^4	6.1	Gieles et al. 2018a
NGC 6624	0.008	Dynamics	<1,000	7.3×10^4	6.1	Baumgardt et al. 2019
NGC 6624	0.008	FP	<1,550	7.3×10^4	6.1	Tremou et al. 2018
M15	0.010	Dynamics	1,700–3,200	4.5×10^5	12.9	Gerssen et al. 2002
M15	0.010	Dynamics	<2,000	4.5×10^5	12.9	Baumgardt et al. 2003
M15	0.010	FP	<1,530	4.5×10^5	12.9	Tremou et al. 2018
NGC 6388	0.011	Dynamics	$(2.8 \pm 0.4) \times 10^4$	1.1×10^6	13.1	Lützgendorf et al. 2015
NGC 6388	0.011	Dynamics	<2,000	1.1×10^6	13.1	Lanzoni et al. 2013
NGC 6388	0.011	FP	<1,770	1.1×10^6	13.1	Tremou et al. 2018
NGC 1904	0.013	Dynamics	(3,000 ± 1,000)	1.7×10^5	8.7	Lützgendorf et al. 2013
M54	0.024	Dynamics	9,400	1.4×10^6	20.2	Ibata et al. 2009
M54	0.024	Dynamics	1.1×10^4	1.4×10^6	20.2	Baumgardt 2017
M54	0.024	FP	<3,000	1.4×10^6	20.2	Tremou et al. 2018
M31/G1	0.780	Dynamics	$(1.8 \pm 0.5) \times 10^4$	3.1×10^6	25.8	Gebhardt et al. 2005
M31/G1	0.780	Dynamics	~0	3.1×10^6	25.8	Baumgardt et al. 2003
M31/G1	0.780	FP	<9,700	3.1×10^6	25.8	Miller-Jones et al. 2012
HLX-1	95	X-ray spectra	$\sim 10^4$–2×10^5	2×10^5–3×10^6	ND	Straub et al. 2014
HLX-1	95	State changes	$\sim 10^4$–10^5	2×10^5–3×10^6	ND	Webb et al. 2012
HLX-1	95	FP	$<3 \times 10^6$	2×10^5–3×10^6	ND	Cseh et al. 2015
M82 X-1	3.5	X-ray QPOs	430 ± 100	ND	ND	Pasham et al. 2014
M82 X-1	3.5	X-ray spectra	<100	ND	ND	Brightman et al. 2016
NGC 5252-ULX1	100	FP	3,000–2×10^6	ND	ND	Mezcua et al. 2018b

Abbreviations: FP, fundamental plane; ND, no data; QPO, quasi-periodic oscillation.
[a]When limits are listed, an effort has been made to quote a 3σ limit.
[b]Stellar velocity dispersion, cluster or galaxy.

the M_{BH}–σ_* relation in the specific case of TDE events that seem to have reliable determinations of the host galaxies. We also include a small number of measurements based on modeling of the X-ray emission or on the radio/X-ray fundamental plane. We do not include single-epoch virial black hole mass estimates for AGNs (but see references in Section 4). For the credible candidates, we also include other representative published measurements or limits, which in many cases are contradictory. However, we do not include off-nuclear sources that have only limits with no claimed detections.

Annu. Rev. Astron. Astrophys. 2020.58:257-312. Downloaded from www.annualreviews.org
Access provided by National Astronomical Observatories, Chinese Academy of Sciences on 09/05/23. For personal use only.

Table 4 Constraining upper limits determined via stellar dynamics

Object	Distance (Mpc)	M_{BH}[a] ($M_\odot$)	$M_{cluster}$[b] ($M_\odot$)	M_*[c] ($M_\odot$)	σ_*[d] (km s^{-1})	Reference
Fornax	0.135	$<1 \times 10^5$	ND	4×10^7	10	Jardel & Gebhardt 2012
UMi	0.076	$<3 \times 10^4$	ND	4.5×10^5	ND	Lora et al. 2009
IC 342	1.9	$<3.3 \times 10^5$	6×10^6	ND	33	Böker et al. 1999
NGC 300	2.2	$<1 \times 10^5$	1×10^6	2.0×10^9	13	Neumayer & Walcher 2012
NGC 404	3.1	$<1.5 \times 10^5$	1×10^7	8.5×10^8	40	Nguyen et al. 2017
NGC 428	16.1	$<7 \times 10^4$	3×10^6	6.3×10^9	24	Neumayer & Walcher 2012
NGC 1042	18.2	$<3.0 \times 10^6$	3×10^6	1.0×10^{10}	32	Neumayer & Walcher 2012
NGC 1493	11.4	$<8.0 \times 10^5$	2×10^6	4.0×10^9	25	Neumayer & Walcher 2012
NGC 2139	23.6	$<4.0 \times 10^5$	8×10^5	1.3×10^{10}	17	Neumayer & Walcher 2012
NGC 3423	14.6	$<7.0 \times 10^5$	3×10^6	7.9×10^9	30	Neumayer & Walcher 2012
NGC 3621	6.6	$<3.0 \times 10^6$	1×10^7	1.6×10^{10}	43	Barth et al. 2009
NGC 4244	4.4	$<5.0 \times 10^5$	1.6×10^7	2.0×10^9	28	De Lorenzi et al. 2013
NGC 7418	18.4	$<9.0 \times 10^6$	6×10^7	1.6×10^{10}	34	Neumayer & Walcher 2012
NGC 7424	10.9	$<4.0 \times 10^5$	1×10^6	4.0×10^9	16	Neumayer & Walcher 2012
NGC 7793	3.3	$<8.0 \times 10^5$	8×10^6	4.0×10^9	25	Neumayer & Walcher 2012

Abbreviation: ND, no data.

[a]Black hole mass limit, 3σ when possible. For the Neumayer & Walcher (2012) sample, we use their maximum black hole masses.

[b]Star cluster mass, when relevant.

[c]Stellar mass when galaxy host.

[d]Stellar velocity dispersion, cluster or galaxy.

The tables neatly summarize the state of the field. We have high confidence that nuclear black holes extend downward to $\sim 10^5$ $M_\odot$. There is tantalizing evidence for objects below this limit in galaxy nuclei (NGC 205 and upper limits) but not definitive evidence to date. HLX-1 and objects like it provide additional circumstantial evidence for black holes with masses in the 10^4–10^5 $M_\odot$ range. There is no compelling evidence yet for any object with $M_{BH} \sim 10^3$ $M_\odot$, and it is likely that many of the candidates listed in the table will not be confirmed as IMBHs.

Although all the search techniques described above have their own challenges, there are a few themes worth drawing out that are special roadblocks when searching for IMBHs. Angular resolution is currently the limiting factor for dynamical methods, and higher resolution likewise enhances accretion searches by eliminating contamination from stellar sources and enabling one to better tease out the signal from low-level accretion (e.g., Dickey et al. 2019).

However, even the order-of-magnitude improvements in angular resolution coming soon will not completely eliminate this confusion. Indeed, nearly all techniques suffer contamination from stars. Even at high Eddington ratio, IMBHs cannot be uniquely distinguished on the basis of their luminosity, and for a short period of time luminous supernovae can masquerade as accreting black holes (Filippenko 1989, Baldassare et al. 2015). We have already hit a confusion floor with X-ray observations because going deeper than $\sim 10^{38}$ erg s^{-1} simply yields large samples of low-mass X-ray binaries. In principle, incorporating radio observations could help. However, in nearly all accreting objects the X-ray and radio emission are linked in some manner, leading the fundamental plane to return a seemingly reasonable mass even in cases in which its use turns out later to have been not justified. For example, early discussions of ULXs argued that the fundamental plane might support their identification as IMBHs (e.g., Miller 2005, Kaaret et al. 2009), though at least some of these sources turned out to be pulsars. Even dynamical masses in nuclei for sources with

Annu. Rev. Astron. Astrophys. 2020.58:257-312. Downloaded from www.annualreviews.org
Access provided by National Astronomical Observatories, Chinese Academy of Sciences on 09/05/23. For personal use only.

$M_{BH} < 10^4\ M_\odot$ will suffer from confusion with clusters of compact objects, and measurements in globular clusters are very challenging owing to this confusion.

8. SCALING RELATIONS

Scaling relations between M_{BH} and macroscopic galaxy properties are useful as a tool to estimate M_{BH} for exciting objects (e.g., Wevers et al. 2017) or to calculate the black hole mass density in the Universe (e.g., Marconi et al. 2004). These relations may also encode the evolutionary history of black holes. In the case of IMBHs, scaling relations at low mass might differ based on seeding mechanisms (e.g., Volonteri et al. 2008, van Wassenhove et al. 2010), although accretion processes at early times may also wash out these signatures (e.g., Volonteri & Gnedin 2009).

8.1. M_{BH}–σ_*

We consider the low-mass end of the M_{BH}–σ_* relation, based on dynamical masses from Kormendy & Ho (2013), supplemented with more recent work (Greene et al. 2016, Saglia et al. 2016, Krajnović et al. 2018, Thater et al. 2019), particularly at low masses (den Brok et al. 2015; Nguyen et al. 2018, 2019b), although our results do not change if we focus exclusively on Kormendy & Ho's data augmented by low-mass objects. Crucially, we explore the importance of including upper limits (Böker et al. 1999, Barth et al. 2009, Neumayer & Walcher 2012, Nguyen et al. 2017). There has been considerable literature on the scatter in scaling relations as a function of galaxy properties (Hopkins et al. 2007, Kormendy & Ho 2013, Saglia et al. 2016). We do not attempt to address these issues, because the measurement uncertainties are still very large in the low-mass systems that concern us here. Finally, because we need it for our black hole mass function determinations below, we also split the sample into early- (elliptical and S0) and late-type (spiral) galaxies, using the Hubble types from Saglia et al. (2016) where available and the individual papers for all other galaxies (**Supplemental Tables 2–4**).

Supplemental Material >

As we show, including the constraining upper limits on low-mass galaxies (Barth et al. 2009, Neumayer & Walcher 2012, De Lorenzi et al. 2013) makes a real difference in the fitted slopes of the relations. We note that Neumayer & Walcher (2012) provide both a best and maximum allowed black hole mass, using the best and minimum M/L from population synthesis models. We use their maximum value as the upper limits in the fits.

Assuming that $\log(M_{BH}/M_\odot) = \alpha + \beta \log(\sigma^*/160\,\mathrm{km\,s^{-1}}) + \epsilon$, where ϵ is the intrinsic scatter, we present our fits in **Supplemental Table 5** and **Figure 3**. Our results are broadly consistent with prior work. However, we explore some additional issues due to the inclusion of low-mass M_{BH} measurements and limits. First of all, when only detections are included in the fitting, the slope we fit to the late-type galaxies alone is very shallow, likely due to the bias in M_{BH} measurements toward the most massive black holes at a given galaxy property (see also Batcheldor 2010, Pacucci et al. 2018). Similar flattening or breaks have been reported based on AGN-based M_{BH} values (e.g., Greene & Ho 2006, Martín-Navarro & Mezcua 2018), perhaps suffering from a similar bias. When limits are included, the fit to late- and early-type galaxies becomes much more similar. In either case, the limits mitigate the bias seen in the detections, and we see no evidence for a change in M_{BH}–σ_* relations at low σ_* (as also concluded by Barth et al. 2005, Neumayer & Walcher 2012).

Early work raised the exciting prospect that the shape and scatter in the M_{BH}–σ_* relation for low M_{BH} objects might depend on the seeding mechanism (Volonteri et al. 2008, Volonteri & Natarajan 2009). Certainly, if all seeds were made at or above $10^5\ M_\odot$, then the scaling relations would flatten at low mass. As of now, we do not see evidence for flattening at $10^5\ M_\odot$, but NGC 205 and the published upper limits argue for a broad distribution of M_{BH} at the low-mass

Annu. Rev. Astron. Astrophys. 2020.58:257-312. Downloaded from www.annualreviews.org
Access provided by National Astronomical Observatories, Chinese Academy of Sciences on 09/05/23. For personal use only.

Annu. Rev. Astron. Astrophys. 2020.58:257-312. Downloaded from www.annualreviews.org
Access provided by National Astronomical Observatories, Chinese Academy of Sciences on 09/05/23. For personal use only.

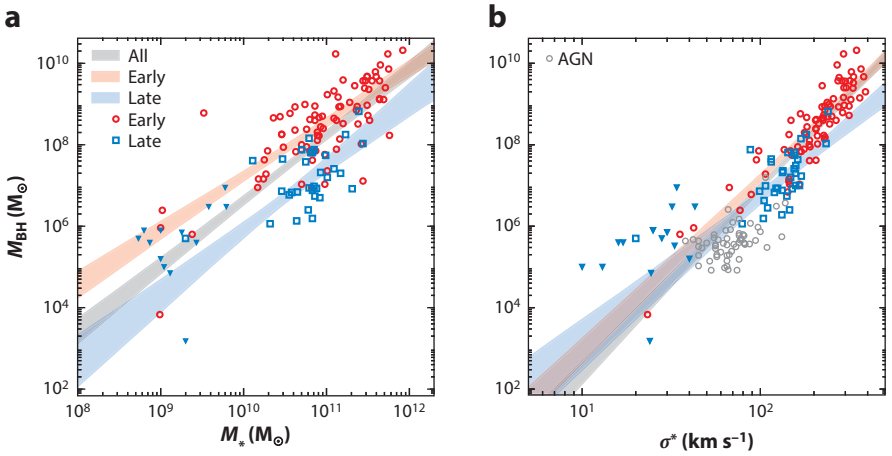


Figure 3

(*a*) The relationship between M_{BH} and M_* for dynamical early-type galaxies (*red open circles*) and late-type galaxies (*blue open squares*), and dynamical upper limits (*blue triangles*). We show fits to the early- and late-type galaxies (*red* and *blue shaded regions*) and the full sample (*gray*). The late-type galaxy fits have comparable slopes but lower normalization in comparison with the early-type galaxy fits. We also see hints for increased scatter at low mass, in part perhaps due to nonunity occupation fraction at low mass. (*b*) Same as panel *a*, but for M_{BH} versus σ_*. Here, we include the sample of AGNs from Xiao et al. (2011; *gray open circles*). By construction through f_{vir}, the AGN points are consistent with the late-type galaxies. Abbreviation: AGN, active galactic nucleus.

end, particularly given the additional evidence for a high occupation fraction in this stellar-mass range. Nominally, the observed M_{BH}–σ_* relation disfavors heavy seed models that make exclusively $M_{BH} \gtrsim 10^5$ $M_\odot$.

8.2. M_{BH}–M_*

Unfortunately, σ_* functions are not measured for low-mass galaxies, and bulge fractions are no longer meaningful in these galaxies either (e.g., MacArthur et al. 2003), although see Schutte et al. (2019). For these reasons, we revisit the correlation between M_{BH} and M_* from dynamical studies including black holes with $M_{BH} < 10^6$ $M_\odot$. We then use this relation to estimate the black hole mass function in that same mass range.

Recently, Reines & Volonteri (2015) presented a fit to the M_{BH}–M_* relation using the dynamical sample by Kormendy & Ho (2013). We add additional galaxies that have been published since then as above (Greene et al. 2016, Saglia et al. 2016, Krajnović et al. 2018, Thater et al. 2019), including low-mass black holes (den Brok et al. 2015; Nguyen et al. 2018, 2019b).

As for Kormendy & Ho (2013), we measure *K*-band magnitudes and *B*–*V* colors for the new galaxies. We use this single color and the fitting functions from Bell et al. (2003) to calculate M_* for all samples, so that all M_* estimates share a common initial mass function and stellar population assumptions. The one exception is the low-mass galaxies ($M_* < 10^{10}$ $M_\odot$), where we use the stellar masses from the dynamical papers. Nguyen et al. (2019b) gives a more detailed comparison of different color–M/L relations. All black hole mass measurements and stellar masses used in this fit are tabulated in **Supplemental Tables 2–4**.

Supplemental Material >

In **Figure 3** (see also **Supplemental Table 5**), we present the updated M_{BH}–M_* scaling relation. One thing that is immediately apparent is that, when plotted against M_*, the dearth of

FEEDBACK

One plausible explanation of black hole–galaxy scaling relations more generally is that there is a feedback loop between black hole growth and star formation, such that black holes are able to remove or heat gas in galaxies when they reach a critical mass relative to the galaxy potential (e.g., Silk & Rees 1998). For low-mass galaxies in particular, AGN feedback has largely been ignored. However, recent theoretical interest and observational evidence have brought the possibility of AGN feedback in dwarf galaxies to the fore.

Silk (2017) argues on theoretical grounds that AGN feedback in low-mass galaxies may be important to solve small-scale challenges for ΛCDM (see also Dashyan et al. 2018). Penny et al. (2018) present evidence for AGN activity in 10% of LMC-mass quenched galaxies. They interpret misaligned kinematics as signs of AGN-driven feedback. Manzano-King et al. (2019) also present some evidence that AGN outflows in dwarfs may be suppressing star formation. Dickey et al. (2019) examine 20 of the rare $M_* \approx 10^9$-$M_\odot$ galaxies that are both isolated and non-star-forming and find evidence for AGN activity in 16 of them (see also Bradford et al. 2018). Dickey et al. conclude that AGN activity can self-quench even relatively isolated low-mass galaxies that otherwise are blue (Geha et al. 2012). Nyland et al. (2017) also identify possible evidence for feedback in the jet in NGC 404. In short, there is now intriguing evidence that even dwarf galaxies with low-mass black holes may suffer the impacts of AGN feedback. We do not yet know whether these episodes are crucial in setting scaling relations in this regime.

Annu. Rev. Astron. Astrophys. 2020.58:257-312. Downloaded from www.annualreviews.org
Access provided by National Astronomical Observatories, Chinese Academy of Sciences on 09/05/23. For personal use only.

dynamical black hole mass measurements for $M_* < 3 \times 10^{10}$ $M_\odot$ is striking. A high priority for understanding black hole demographics at low M_* is studying the supermassive black hole demographics in Milky Way–mass galaxies (Krajnović et al. 2018, Nguyen et al. 2019a).

Focusing on the IMBH regime, again we find that without upper limits, the fit to late-type galaxies returns a very shallow relation, because the measured $M_{\rm BH}$ values are biased high. When we include the limits, however, the slope of the relation becomes consistent between the red and blue populations. By contrast, the overall normalization for the late-type galaxies is considerably lower than that for the early-type galaxies (in agreement with Greene et al. 2010, 2016; Reines & Volonteri 2015; Läsker et al. 2016). This difference has been interpreted to mean that black hole mass does not correlate with disk mass (e.g., Kormendy & Richstone 1995), although the different trends have also been used to constrain the relationship between star formation and black hole growth (Caplar et al. 2015). We note that our fit to the full sample including limits has a lower normalization and slightly steeper slope than the Reines & Volonteri fit, whereas it is very similar to that presented recently by Gallo & Sesana (2019). We do not discuss the physical origins of the scaling relations, but see the sidebar titled Feedback.

8.3. Using Active Galactic Nuclei to Probe Scaling Relations

We overplot the sample of low-mass AGNs from Xiao et al. (2011) in the $M_{\rm BH}$–σ_* plane (**Figure 3**; excluding those with uncertain broad lines). We adjust the single-epoch virial masses to an $f_{\rm vir}$ calibrated with late-type galaxies, as advocated by Ho & Kim (2014). By construction, the AGNs align with the late-type galaxy fit. We again see no evidence in the AGN sample for any flattening or offset at low mass, given the caveat that we do not know the absolute black hole masses of these objects. Given the large uncertainty in the single-epoch masses, we cannot make any additional statements about scatter from this sample.

More generally, we would urge extreme caution in using AGN signatures to infer scaling relations, particularly in this low-mass regime. Even the nearby AGN NGC 4395 ($D \approx 4$ Mpc) has published reverberation-mapping masses that differ by more than an order of magnitude

(Peterson et al. 2005, Edri et al. 2012, Woo et al. 2019). We do not yet know how to fully interpret reverberation-based masses. One problem is the f_{vir} uncertainty. Beyond that, in the case of NGC 4395, the disagreement in black hole mass is mostly attributable to different line widths between the UV resonance line CIV and the optical recombination line Hα. Much more work is needed to effectively harness reverberation mapping for AGNs with low-mass black holes.

8.4. Scaling with Nuclear Star Clusters

In addition to scaling relations between galaxy properties and black hole mass, we consider possible scaling relations between the central black hole and the surrounding nuclear star cluster. We observe a high incidence of black holes in nuclear star clusters. As we argue below (Section 9), a fraction >50% of 10^9–10^{10}-$M_\odot$ galaxies harbor black holes, and nearly all such galaxies harbor nuclear star clusters. Nuclear star clusters do not seem to replace black holes as the central compact object (Ferrarese et al. 2006). Rather the two appear to coexist often at low galaxy mass (Seth et al. 2008). In contrast, most higher-mass galaxies contain supermassive black holes (Gültekin et al. 2011) but show a very low incidence of nuclear star clusters (e.g., Graham & Spitler 2009). Likely the growing black hole contributes to the demise of the nuclear star cluster (Antonini et al. 2019).

It is not obvious what (if any) causal relationship exists between black holes and nuclear star clusters. We have already discussed the possibility that black holes form via gravitational runaway processes in stellar clusters (Section 2) and the dearth of concrete observational evidence to date for black holes with $M_{BH} > 1{,}000\ M_\odot$ in globular clusters (Tremou et al. 2018, Section 5). Nuclear star clusters are different from globular clusters in four key ways: They have higher stellar densities (and thus higher interaction rates), they have longer relaxation times, they have deeper potential wells (and hence higher escape velocities), and they have well-documented multiage populations (e.g., Kacharov et al. 2018). Although some theoretical work postulated a higher likelihood of gravitational runaway in clusters with the highest σ_* (Miller & Davies 2012), more recent work suggests that massive black holes likely can only form via rapid processes in nuclear star clusters (Breen & Heggie 2013, Stone et al. 2017).

Instead, the high coincidence of black holes and nuclear star clusters may suggest that globular clusters with IMBHs are more successful at surviving and migrating to a galaxy center, where through continued gas accretion they can become a nuclear star cluster. Or, the black hole may form early via other means (Section 2) and then grow along with the present-day nuclear star cluster.

Going beyond occupation fractions, the mass fraction of the cluster bound up in the black hole may constrain models. We extend the work by Seth et al. (2008), Zasov & Cherepashchuk (2013), Georgiev et al. (2016), and Nguyen et al. (2018) based on the increased number of dynamical black hole masses available now in the literature (**Figure 4** and **Supplemental Table 6**). Our full sample includes upper limits on M_{BH} in globular clusters from Tremou et al. (2018), ultracompact dwarfs with dynamical black hole mass measurements or upper limits (Seth et al. 2014; Ahn et al. 2017, 2018; Afanasiev et al. 2018), and dynamical black holes in low-mass galaxies (Section 3), drawing nuclear star cluster masses from those papers. For the black hole masses and limits of Krajnović et al. (2018) and Pechetti et al. (2017), we calculate the nuclear star cluster masses using color and luminosity information from Côté et al. (2006) and the relations of Bell et al. (2003). Finally, we include NGC 1023 and NGC 3384, two early-type galaxies that Lauer et al. (2005) identify as containing stellar nuclei, with the caveat that in some cases it can be challenging to determine whether these point sources are stellar or nonthermal in nature (e.g., Ravindranath et al. 2001).

Supplemental Material >

Roughly ~0.1% mass fractions are predicted from gravitational runaway scenarios (Section 2). The observed mass fractions in nuclear star clusters far exceed these limits. We see from **Figure 4**

Annu. Rev. Astron. Astrophys. 2020.58:257-312. Downloaded from www.annualreviews.org
Access provided by National Astronomical Observatories, Chinese Academy of Sciences on 09/05/23. For personal use only.

Annu. Rev. Astron. Astrophys. 2020.58:257-312. Downloaded from www.annualreviews.org
Access provided by National Astronomical Observatories, Chinese Academy of Sciences on 09/05/23. For personal use only.

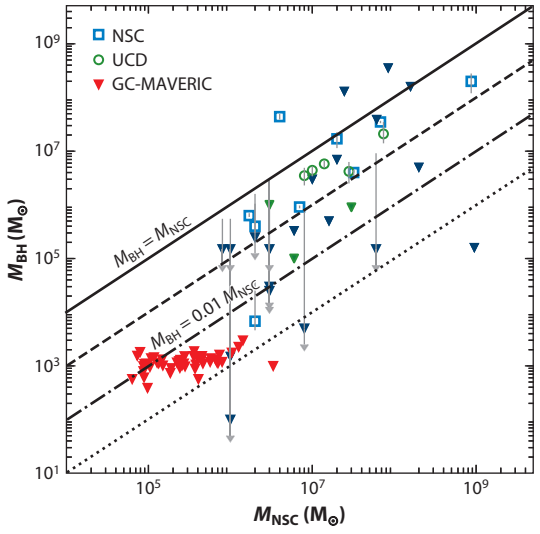


Figure 4

The ratio of black hole to cluster mass, with limits shown as gray arrows. We include limits on black hole masses in GCs from Tremou et al. (2018; *red triangles*) and dynamical black hole mass measurements with known NSCs from the literature (*blue squares*; building on Seth et al. 2008, Nguyen et al. 2018). The upper-most extent of the arrows for the Neumayer & Walcher (2012) measurements represents their maximum allowed black hole mass, whereas the gray circles are their best measurement. We further include UCDs with $M_{\rm BH}$ masses or upper limits (*green circles*). Whenever available from the literature, we plot the inner component of the UCD, not the entire galaxy mass. The median ratio of $M_{\rm BH}$ to NSC mass for objects with black holes detected is ∼25%, but with a factor of two scatter. The GCs are consistent with a 0.1% mass fraction for a small fraction of the Milky Way GC system. Abbreviations: GC, globular cluster; NSC, nuclear star cluster; UCD, ultracompact dwarf.

that in most cases $M_{\rm BH}$ comprises a much higher fraction of the nuclear star cluster mass: The median value of $M_{\rm BH}/M_{\rm NSC}$ for the objects with black hole detections is ∼0.3, with more than a factor of two scatter. There is even more scatter when the limits are considered. This scatter likely reflects both a lack of black holes in some clusters and intrinsic scatter in the growth histories of both constituents. Interestingly, the largest outliers with low ratios of black hole–to–nuclear star cluster mass are found in the low-mass and late-type spiral galaxies.

Given the wide range of $M_{\rm BH}/M_{\rm NSC}$ that we observe, it seems possible that stochastic late-time fueling and/or merging plays a substantial role in the growth of each component (e.g., Naiman et al. 2015). Ultracompact dwarfs provide an interesting testing ground for how much black hole growth occurs via later-time accretion versus initial formation. Because ultracompact dwarfs were stripped, likely quite early in some cases (Pfeffer et al. 2014), we would expect less late-time growth, leaving their $M_{\rm BH}/M_{\rm NSC}$ ratios closer to their value at formation, whereas there may be more scatter in the population due to different stripping times. So far, the ultracompact dwarfs do not obviously segregate in this plane, but the constraint will be more interesting as their number with $M_{\rm BH}$ constraints continues to grow.

9. DEMOGRAPHICS

9.1. Existing Limits on the Occupation Fraction

After Gebhardt et al. (2001) published an upper limit of <1,500 $M_\odot$ on any putative black hole in the nuclear star cluster in M33, the community assumed that massive black holes were rare in

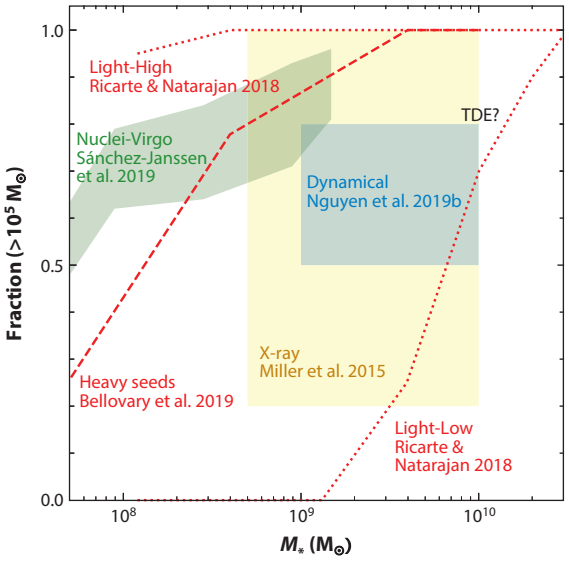


Figure 5

Multiple constraints are converging toward a relatively high value of occupation fraction (>50%) of black holes with $M_{\rm BH} \gtrsim 10^5$ $M_\odot$ in galaxies with stellar masses in the range of $10^9 < M_*/M_\odot < 10^{10}$. Observational constraints from Miller et al. (2015; *yellow box*) are from X-ray observations of low-mass red galaxies. Dynamical constraints are summarized by Nguyen et al. (2019b; *blue box*) and suggest occupation fractions >50%. Likewise, the TDE mass function suggests a high occupation fraction (van Velzen 2018) even below 10^{10} $M_\odot$. Intriguingly, the nuclear star cluster occupation fraction is consistent with existing black hole limits as well, as exemplified by the green region derived from Virgo by Sánchez-Janssen et al. (2019). For reference, we include predictions from three models (*red*). We include Ricarte & Natarajan (2018; *dotted*) predictions for black holes more massive than 3×10^5 $M_\odot$. Their Population III models span the full range shown here, with the light-low case corresponding to their power-law accretion mode while the light-high case is their main-sequence accretion mode. Their direct-collapse seeds fall in between these two limiting cases. We also show the limits on occupation fraction from Bellovary et al. (2019; *dashed*), which is effectively a heavy seeding model. Abbreviation: TDE, tidal disruption event.

low-mass, late-type galaxies with little or no bulge component. In fact, black holes do not appear to be rare, at least in galaxies with $10^9 < M_*/M_\odot < 10^{10}$.

Recall that there are 10 galaxies within 4 Mpc and $10^9 < M_*/M_\odot < 10^{10}$ $M_\odot$ with published dynamical masses or limits (Section 3). Of these, 5 are detections. From the dynamical measurements, we infer an occupation fraction >50% (**Figure 5**). If the upper limit in M33 of $M_{\rm BH} <$ 1,500 $M_\odot$ is taken at face value, it would suggest that the occupation fraction is not unity for $M_{\rm BH} = 10^3$–10^6-$M_\odot$ black holes in galaxies with $M_* \approx 10^9$ $M_\odot$. However, better statistics and more limits are needed.

In addition to dynamical constraints, X-ray surveys of local galaxies also allow us to make a concrete measurement of the occupation fraction. Just based on the number of detected X-ray sources in galaxies with $M_* = 10^9$–10^{10} $M_\odot$, Miller et al. (2015) and She et al. (2017b) both find a lower limit of 20% on the occupation fraction. Miller et al. argue for a likely occupation fraction of ∼70% based on jointly modeling the $L_{\rm X}/M_*$ relation and the occupation fraction. Taking ∼20% as the lower limit, we find that sensitive X-ray surveys of local galaxies already point toward relatively high occupation fractions, which is in agreement with the dynamics (**Figure 5**).

Our fits in Section 8 suggest that blue galaxies might harbor black holes with masses lower than red galaxies at fixed mass. As yet, we see no concrete evidence for differences in mass distribution

Annu. Rev. Astron. Astrophys. 2020.58:257-312. Downloaded from www.annualreviews.org
Access provided by National Astronomical Observatories, Chinese Academy of Sciences on 09/05/23. For personal use only.

between red and blue low-mass galaxies in this stellar-mass regime, which also appears to hold for the X-ray detection fractions described above Section 4. Given the small numbers involved, we cannot test for a difference yet. Because blue galaxies are far more common than red galaxies at these masses, any difference could have significant ramifications for the black hole mass density.

The growing field of tidal disruptions will soon start to put competitive constraints on the occupation fraction if we can understand the rates (Section 6). Van Velzen (2018) makes a first attempt. He finds that the observed luminosity function of TDEs can only be explained if the occupation fraction is basically flat from LMC- to Milky Way–mass galaxies. Although this result is hard to turn into an exact occupation fraction, it certainly argues that a high fraction of galaxies in this mass range host an IMBH.

As a point of comparison, we also plot the fraction of Virgo galaxies with $M_* < 10^9$ $M_\odot$ containing nuclear star clusters (Sánchez-Janssen et al. 2019). It is interesting to see that if most nuclear star clusters host a central black hole, then the black hole occupation fraction would be within the limits derived by other methods (see also Seth et al. 2008, Foord et al. 2017). Below, when we calculate limits on the black hole mass function, we use the measured nuclear star cluster fraction as one estimate of the black hole occupation fraction for illustrative purposes. We also show predictions from recent models for the occupation fraction (**Figure 5**). The Ricarte & Natarajan (2018) models with Pop III seeds span nearly all possible occupation fractions, depending on their fueling model (**Figure 5**), whereas the direct-collapse models lie in between, consistent with (Bellovary et al. 2019). In summary, at least $\gtrsim$50% of galaxies with $M_* \approx 10^9$–10^{10} $M_\odot$ host a massive black hole with $M_{\rm BH} \sim 10^4$–10^6 $M_\odot$.

9.2. Inferred Black Hole Mass Functions at Low Mass

Predictions for the rates of events like tidal disruptions (e.g., Stone & Metzger 2016) or extreme-mass-ratio inspirals (e.g., Gair et al. 2010) depend on the black hole mass function in the IMBH mass range. However, there are few observational constraints on the $M_{\rm BH}$ mass function below $\sim 10^6$ $M_\odot$ (e.g., Marconi et al. 2004, Greene & Ho 2007c). We now have the ingredients needed to calculate a range of possible black hole mass functions down to $\sim 10^4$ $M_\odot$, albeit with significant uncertainty.

Using the $M_{\rm BH}$–M_* relation derived in Section 8 above, we convert the observed galaxy mass function into a black hole mass function (e.g., Marconi et al. 2004). The mass function of Wright et al. (2017) extends to $M_* \approx 10^6$ $M_\odot$ and thus allows us to explore the ramifications of a nonzero occupation fraction to very low stellar mass. The galaxy stellar mass is converted into black hole mass density using the $M_{\rm BH}$–M_* relation that we fitted in Section 8, including intrinsic scatter. We consider the red and blue galaxies separately, because they have different scaling zero points (see also Shankar et al. 2016), and for this we take guidance from the red- and blue-galaxy luminosity functions presented by Blanton & Moustakas (2009). We thus input a galaxy mass function that is dominated by blue galaxies below, and red galaxies above, $M_* = 10^{10}$ $M_\odot$.

Below $M_* \approx 10^{10}$ $M_\odot$, the occupation fraction may deviate from unity. We adopt two different forms for the occupation fraction, both of which are consistent with the current data and models (**Figure 6**). As a pessimistic case, we assume that the occupation fraction drops linearly from unity at 10^{10} to 0 at 3×10^7 $M_\odot$. As an optimistic limit, we take the fraction of galaxies with nuclear star clusters and assume that every nuclear star cluster harbors a massive black hole (derived in Virgo by Sánchez-Janssen et al. 2019). In the default mass function, there are only nuclear black holes and a single power-law relation between stellar and black hole masses. The resulting range of possible mass functions are shown in **Figure 6** (**Supplemental Table 7**). There is a range of possible

Supplemental Material >

Annu. Rev. Astron. Astrophys. 2020.58:257-312. Downloaded from www.annualreviews.org
Access provided by National Astronomical Observatories, Chinese Academy of Sciences on 09/05/23. For personal use only.

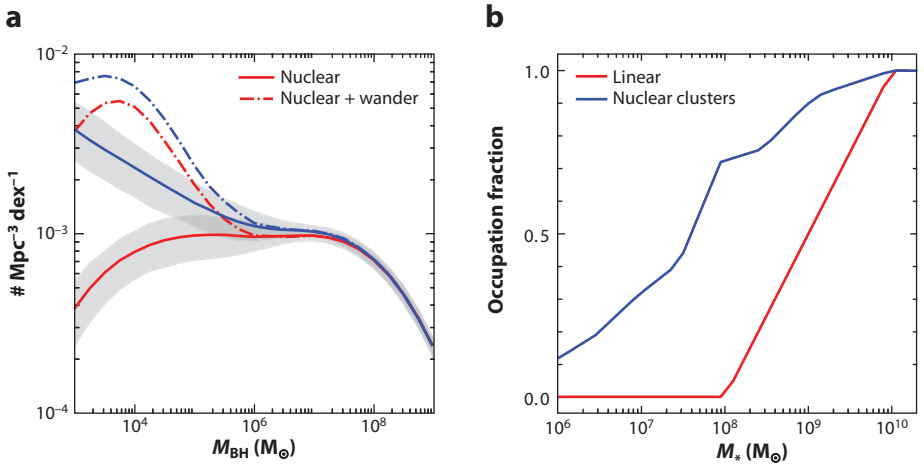


Figure 6

(*a*) Inferred black hole mass function based on the GAMA stellar-mass function (Wright et al. 2017) and the M_{BH}–M_* relation from Section 8. We show two occupation fractions as illustrated in panel *b*, with the optimistic "nuclear cluster" model (*blue*) that assumes every nuclear star cluster houses an intermediate-mass black hole, and the nucleation fraction from Sánchez-Janssen et al. (2019), whereas the more pessimistic line (*red*) is meant to be consistent with existing observations. In the solid lines, we show the black hole mass density from nuclear sources alone, assuming power-law relations between M_{BH} and M_* that differ for red and blue galaxies. We additionally add to the default model a wandering black hole component with a number density tied to ultracompact dwarfs (*dash-dot*).

M_{BH} densities for $M_{BH} < 10^6\ M_\odot$. We note again that we have assumed comparable occupation fractions for red and blue galaxies, which is a systematic uncertainty that must be tested.

We also explore what a contribution from wandering black holes might look like (Section 2). These black holes may reveal themselves in our own Galaxy through dynamical signatures, and they may be the sites of extreme-mass-ratio inspirals or white dwarf TDEs as well. We tie the number of wandering black holes to the number of ultracompact dwarfs, as described in Section 2.1. In short, we take the number of ultracompact dwarfs as a proxy for the number of disrupted satellites and then assume a 10–50% occupation fraction for them. We are not adopting a cosmologically motivated mass spectrum of satellites, nor do we have an empirical way to assign black hole masses to this population. The ultracompact dwarfs with known black holes orbit more massive hosts and likely had more massive progenitors than those we consider here (Seth et al. 2014, Voggel et al. 2019). Thus, we simply take a typical black hole mass of $3 \times 10^3\ M_\odot$, chosen to fall below current detection limits, and a log-normal width of 0.5 dex. These are arbitrary, but they at least qualitatively demonstrate how much higher the black hole mass density might be for relatively conservative estimates on wandering populations.

There are a number of systematic uncertainties here, including the shape of the M_{BH}–M_* relation and all the challenges inherent in calculating stellar masses (Conroy 2013). Gallo & Sesana (2019) nicely demonstrate the systematic effect of different scaling relation fits (see also Shankar et al. 2016). Furthermore, we do not know the functional form of the occupation fraction with stellar mass. Because the stellar-mass function rises steeply, even a small occupation fraction in low-mass galaxies dramatically changes the black hole mass density at low mass. Nevertheless, the mass functions we present here may be used to bracket the expected event rates of TDEs and extreme-mass-ratio inspirals.

Annu. Rev. Astron. Astrophys. 2020.58:257-312. Downloaded from www.annualreviews.org
Access provided by National Astronomical Observatories, Chinese Academy of Sciences on 09/05/23. For personal use only.

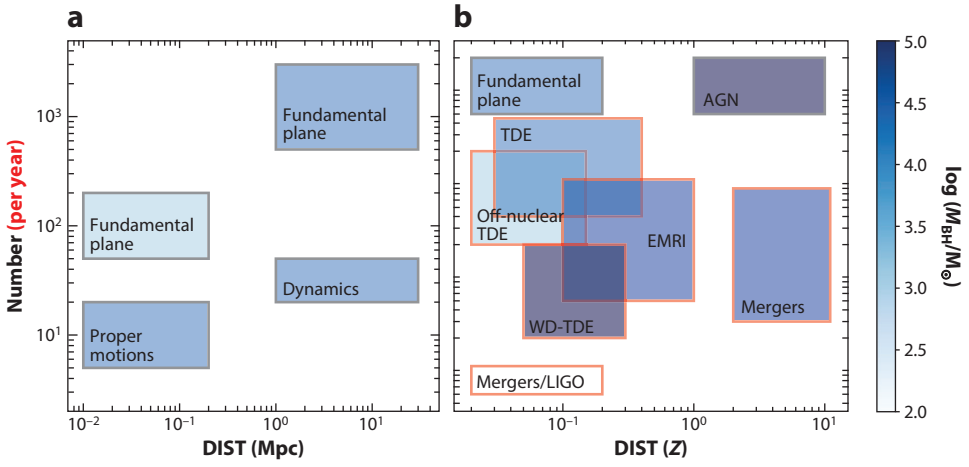


Figure 7

(*a*) Volume and number of targets to be reached by next-generation facilities. The color bar reflects the black hole mass range (from 100–10^5 $M_\odot$, with darker color for more massive black holes). (*b*) Same as panel *a*, but for more distant black holes. The red outline signals that we tabulate a rate per year rather than a number. Abbreviations: AGN, active galactic nucleus; EMRI, extreme-mass-ratio inspiral; TDE, tidal disruption event; WD, white dwarf.

10. THE FUTURE

In the coming two decades, we hope to break into the elusive ∼100–10^4 $M_\odot$ regime with robust dynamical constraints from stars, gas, and gravitational wave detections. We provide a short synopsis of the most promising ongoing and upcoming experiments, along with the distance distributions and available number of objects that they can each explore (**Figure 7**). We provide a full explanation for the numbers used in the figure in the **Supplemental Materials**.

Supplemental Material >

If we are to take full advantage of these next-generation opportunities, we must begin to lay the groundwork now to be maximally ready to exploit upcoming surveys. We present here a list of our high-priority items.

Next-generation extremely large telescopes and the Atacama Large Millimeter Array (ALMA) at full capacity will have stunning spatial resolution, but we will only be able to find putative $<10^5$-$M_\odot$ black holes in $<10^9$-$M_\odot$ galaxies if we know where to look. We must use all the tools at our disposal, from astrometry with *Gaia* to gas kinematics, to determine centers for Local Group dwarfs (van der Marel & Kallivayalil 2014). Moving out to larger radii, a complete sample of nuclear star clusters within 5 Mpc would be immensely useful in planning for next-generation dynamical searches. Likewise a survey of the molecular gas content of $<10^9$-$M_\odot$ galaxies in the south to identify good ALMA targets is needed. Finally, it is a high priority to start mining *Gaia* for potential wandering black hole candidates.

We have assumed throughout that red and blue low-mass galaxies have similar black hole occupation fractions, which is consistent with the current X-ray and dynamical results. Even a larger sample of constraining limits for more nuclear star clusters (Neumayer & Walcher 2012), particularly including all the available red galaxies within 10 Mpc, could potentially shed light on this important issue before many more detections are in reach. Because red and blue galaxies have very different number densities at low mass, it is important to know if there are differences in their occupation fractions.

Annu. Rev. Astron. Astrophys. 2020.58:257-312. Downloaded from www.annualreviews.org
Access provided by National Astronomical Observatories, Chinese Academy of Sciences on 09/05/23. For personal use only.

We will continue to rely on accretion signatures, even as dynamical capabilities grow. We urgently need theoretical predictions for the spectral energy distributions and presence or absence of broad lines in 10^3–10^5-$M_\odot$ black holes (e.g., Cann et al. 2019) to search effectively for them with upcoming sensitive instruments like JWST and/or *Lynx*. Standard AGN search techniques have identified targets with inferred masses pushing toward 10^4 $M_\odot$ (e.g., Baldassare et al. 2015), but we may be unable to identify the majority of sources at this black hole mass because their accretion signatures do not match our expectations (Cann et al. 2019). This question is important not only for selection reasons but also because the ionizing spectrum of low-mass black holes is needed to think about the impact of IMBHs on reionization (e.g., Madau & Haardt 2015).

There are indications that the spectral energy distributions of accreting black holes may be changing in interesting ways as we push to low mass. Most concretely, AGNs with inferred low black hole mass and high Eddington ratio show a very pronounced soft X-ray excess, which may even be the tail of emission from the accretion disk itself (e.g., Done et al. 2012, Jin et al. 2012, Yuan et al. 2014), as would be expected in the low-mass regime. Such objects are also highly variable (Kamizasa et al. 2012). Along with this, the ratio of optical–to–X-ray emission also shows interesting behavior among the low-mass black holes (e.g., Dong et al. 2012a, Plotkin et al. 2016), but these changes may be tied more closely to the high Eddington ratios rather than low masses of this sample. On the flip side, Ludwig et al. (2012) did not find the ratio of HeII/Hβ to depend on black hole mass, as one would expect if the big blue bump moves to higher temperature at lower masses.

At the low accretion rate end, there is a need for theoretical guidance in terms of the expected radio and X-ray emission. We would like to see calculations like those of Ressler et al. (2019), which are built for the Galactic Center, applied to the globular cluster context to directly predict accretion rates based on the angular momentum of the stellar winds.

11. SUMMARY

By reviewing the observational literature, we draw the following conclusions about IMBH populations:

- There are clear and compelling cases for black holes in the mass range of 10^5–10^6 $M_\odot$ in the nuclei of low-mass galaxies. Moving downward into the true IMBH regime, there are tantalizing hints from NGC 205 and some constraining limits for lower-mass black holes, whereas HLX-1 and a handful of similar objects provide additional circumstantial evidence that black holes of $\sim 10^4$ $M_\odot$ exist. There is not even circumstantial evidence yet for 10^3-$M_\odot$ black holes.
- Excepting HLX-1, most ULXs are not powered by IMBHs.
- Among $M_* > 10^5$-$M_\odot$ globular clusters in the Milky Way, observations limit the occupation fraction of $\sim 10^3$-$M_\odot$ black holes to 10–15%. In contrast, both dynamical measurements and X-ray observations in 10^9–10^{10}-$M_\odot$ galaxies argue for >50% occupation fractions of black holes in these galaxies.
- The most promising avenues to find $\sim$100–10^3-$M_\odot$ black holes are either to identify stellar binaries, which are expected to be common, or to detect them in gravitational radiation. Ground-based gravitational wave limits on the low end of this mass regime are continuing to improve.
- We do not see evidence for a change in the $M_{\rm BH}$–σ_* relation for $\sigma_* < 100$ km s^{-1}. However, the existing limits suggest there is a broad range of black hole masses in these galaxies just below our detection limit, particularly because observations suggest that a large fraction of these galaxies do host black holes with $M_{\rm BH} \gtrsim 10^4$ $M_\odot$.

Annu. Rev. Astron. Astrophys. 2020.58:257-312. Downloaded from www.annualreviews.org
Access provided by National Astronomical Observatories, Chinese Academy of Sciences on 09/05/23. For personal use only.

- Folding together the empirically allowed range of occupation fractions with the observed correlation between stellar mass and black hole mass, we are able to bracket the allowed range of black hole number density down to $\sim 10^4$ $M_\odot$. More dynamical observations of black holes in $<10^{10}$-$M_\odot$ galaxies, which will be facilitated by ALMA at full capacity along with extremely large telescopes in the coming decade, are needed to determine the scaling relations and occupation fractions for both red and blue galaxies.

By putting together theoretical predictions of occupation fractions with galaxy luminosity functions, we evaluate the current constraints on seeding mechanisms:

- Early seeding mechanisms—direct-collapse-type models or Pop III stars—will be hard to distinguish using local observations alone, because varied accretion histories can wash out the early differences in these models. However, luminosity functions and gravitational wave observations at high redshift could help.
- Theoretical predictions are quite divided on whether direct-collapse scenarios can produce sufficient black holes. If direct-collapse models do operate, the typical formation mass must be $<10^5$ $M_\odot$.
- From both theoretical and observational perspectives, gravitational runaway is unlikely to take off in typical globular clusters, but the most massive star clusters may still host such events.

We highlight a few concrete conclusions related to next-generation measurements here:

- Due to mass segregation, the total number of stars within the sphere of influence of an $\sim$1,000-$M_\odot$ black hole may be insufficient to place stringent dynamical constraints on objects in this mass range even with extremely large telescopes, whereas $\sim$3,000-$M_\odot$ black holes should be measurable.
- To unlock the potential of the fundamental plane for understanding black hole demographics, next-generation radio telescopes will be crucial to detect low-mass, low-accretion-rate black holes in dwarf galaxies.
- The growing number of ultracompact dwarfs with black holes may help illuminate the relative importance of birth and accretion for black holes in nuclear clusters, because their accretion histories were likely truncated by falling into a bigger halo.
- Nuclear TDEs are on the cusp of providing important clues to black hole demographics, but we must understand the rates as a function of galactic environment.
- It should be possible to identify (or rule out) wandering black holes in our Galaxy by searching for compact and low-mass star clusters with *Gaia*. Complementary off-nuclear TDEs offer a promising avenue for getting large-scale statistics of such objects, again provided we can understand the rates and emission mechanisms.

We are very excited about prospects for finding true IMBHs in the coming decades with the promise of improved sensitivity and frequency range for gravitational wave detection; the leap in angular resolution and sensitivity afforded by next-generation optical, radio, and X-ray telescopes; and the expanding reach of time-domain surveys.

DISCLOSURE STATEMENT

The authors are not aware of any affiliations, memberships, funding, or financial holdings that might be perceived as affecting the objectivity of this review.

Annu. Rev. Astron. Astrophys. 2020.58:257-312. Downloaded from www.annualreviews.org
Access provided by National Astronomical Observatories, Chinese Academy of Sciences on 09/05/23. For personal use only.

ACKNOWLEDGMENTS

We thank Gillian Bellovary, Ruben Sanchez-Janssen, and Angelo Ricarte for sharing their data. We thank Ruancun Li for performing bespoke 2MASS fitting and providing luminosities and colors for more than 40 galaxies. We are grateful to Suvi Gezari, Zoltan Haiman, Morgan MacLeod, Nadine Neumayer, Anil Seth, Sjoert van Velzen, Marta Volonteri, and Joan Wrobel for useful discussions. L.C.H. is supported by the National Science Foundation of China (11721303 and 11991052) and the National Key R&D Program of China (2016YFA0400702). J.S. acknowledges support from the Packard Foundation and from National Science Foundation grant AST-1514763. J.E.G. acknowledges support from National Science Foundation grants AST-1713828 and AST-1815417.

LITERATURE CITED

Abadi MG, Navarro JF, Steinmetz M. 2009. *Ap. J. Lett.* 691:L63–66
Abbate F, Possenti A, Ridolfi A, et al. 2018. *MNRAS* 481:627–38
Afanasiev AV, Chilingarian IV, Mieske S, et al. 2018. *MNRAS* 477:4856–65
Ahn CP, Seth AC, Cappellari M, et al. 2018. *Ap. J.* 858:102
Ahn CP, Seth AC, den Brok M, et al. 2017. *Ap. J.* 839:72
Ai YL, Yuan W, Zhou HY, Wang TG, Zhang SH. 2011. *Ap. J.* 727:31
Aird J, Coil AL, Georgakakis A. 2018. *MNRAS* 474:1225–49
Aird J, Coil AL, Moustakas J, et al. 2013. *Ap. J.* 775:41
Alexander T, Bar-Or B. 2017. *Nat. Astron.* 1:0147
Alexander T, Natarajan P. 2014. *Science* 345:1330–33
Ali-Haïmoud Y, Kovetz ED, Kamionkowski M. 2017. *Phys. Rev. D* 96:123523
Alvarez MA, Wise JH, Abel T. 2009. *Ap. J. Lett.* 701:L133–37
Amaro-Seoane P, Audley H, Babak S, et al. 2017. arXiv:1702.00786
Amaro-Seoane P, Gair JR, Pound A, Hughes SA, Sopuerta CF. 2015. *J. Phys. Conf. Ser.* 610:012002
Anninos P, Fragile PC, Olivier SS, et al. 2018. *Ap. J.* 865:3
Antonini F, Gieles M, Gualandris A. 2019. *MNRAS* 486:5008–21
Antonini F, Rasio FA. 2016. *Ap. J.* 831:187
Arcavi I, Gal-Yam A, Sullivan M, et al. 2014. *Ap. J.* 793:38
Bachetti M, Harrison FA, Walton DJ, et al. 2014. *Nature* 514:202–4
Bahcall JN, Ostriker JP. 1975. *Nature* 256:23–24
Baldassare VF, Geha M, Greene J. 2018. *Ap. J.* 868:152
Baldassare VF, Geha M, Greene J. 2019. *Ap. J.* Submitted. arXiv:1910.06342
Baldassare VF, Reines AE, Gallo E, et al. 2016. *Ap. J.* 829:57
Baldassare VF, Reines AE, Gallo E, Greene JE. 2015. *Ap. J. Lett.* 809:L14
Baldassare VF, Reines AE, Gallo E, Greene JE. 2017. *Ap. J.* 850:196
Baldwin JA, Phillips MM, Terlevich R. 1981. *Publ. Astron. Soc. Pac.* 93:5–19
Bañados E, Venemans BP, Mazzucchelli C, et al. 2018. *Nature* 553:473–76
Bär RE, Weigel AK, Sartori LF, et al. 2017. *MNRAS* 466:2879–87
Barrows RS, Mezcua M, Comerford JM. 2019. *Ap. J.* 882:181
Barth AJ, Greene JE, Ho LC. 2005. *Ap. J. Lett.* 809:L151–54
Barth AJ, Greene JE, Ho LC. 2008. *Astron. J.* 136:1179–200
Barth AJ, Ho LC, Rutledge RE, Sargent WLW. 2004. *Ap. J.* 607:90–102
Barth AJ, Strigari LE, Bentz MC, Greene JE, Ho LC. 2009. *Ap. J.* 690:1031–44
Batcheldor D. 2010. *Ap. J. Lett.* 809:L108–11
Baumgardt H. 2017. *MNRAS* 464:2174–202
Baumgardt H, Gualandris A, Portegies Zwart S. 2006. *MNRAS* 372:174–82
Baumgardt H, He C, Sweet SM, et al. 2019. *MNRAS* 488:5340–51
Baumgardt H, Makino J, Hut P, McMillan S, Portegies Zwart S. 2003. *Ap. J. Lett.* 809:L25–28

Annu. Rev. Astron. Astrophys. 2020.58:257-312. Downloaded from www.annualreviews.org
Access provided by National Astronomical Observatories, Chinese Academy of Sciences on 09/05/23. For personal use only.

Annu. Rev. Astron. Astrophys. 2020.58:257-312. Downloaded from www.annualreviews.org
Access provided by National Astronomical Observatories, Chinese Academy of Sciences on 09/05/23. For personal use only.

Begelman MC. 2010. *MNRAS* 402:673–81
Begelman MC, Rees MJ. 1978. *MNRAS* 185:847–60
Begelman MC, Volonteri M, Rees MJ. 2006. *MNRAS* 370:289–98
Bell EF, McIntosh DH, Katz N, Weinberg MD. 2003. *Ap. J. Suppl.* 149:289–312
Bellovary JM, Cleary CE, Munshi F, et al. 2019. *MNRAS* 482:2913–23
Bellovary JM, Governato F, Quinn TR, et al. 2010. *Ap. J. Lett.* 809:L148–52
Bentz MC, Batiste M, Seals J, et al. 2016. *Ap. J.* 831:2
Bentz MC, Denney KD, Grier CJ, et al. 2013. *Ap. J.* 767:149
Berry C, Hughes S, Sopuerta C, et al. 2019. *Bull. Am. Astron. Soc.* 51:42
Binney J, Mamon GA. 1982. *MNRAS* 200:361–75
Blagorodnova N, Gezari S, Hung T, et al. 2017. *Ap. J.* 844:46
Blanton MR, Moustakas J. 2009. *Annu. Rev. Astron. Astrophys.* 47:159–210
Böker T, van der Marel RP, Vacca WD. 1999. *Astron. J.* 118:831–42
Bond JR, Arnett WD, Carr BJ. 1984. *Ap. J.* 280:825–47
Boyce H, Lützgendorf N, van der Marel RP, et al. 2017. *Ap. J.* 846:14
Bradford JD, Geha MC, Greene JE, Reines AE, Dickey CM. 2018. *Ap. J.* 861:50
Brandt WN, Alexander DM. 2015. *Astron. Astrophys. Rev.* 23:1
Breen PG, Heggie DC. 2013. *MNRAS* 436:584–89
Brightman M, Harrison FA, Barret D, et al. 2016. *Ap. J.* 829:28
Brodie JP, Strader J. 2006. *Annu. Rev. Astron. Astrophys.* 44:193–267
Bromm V, Coppi PS, Larson RB. 2002. *Ap. J.* 564:23–51
Bromm V, Larson RB. 2004. *Annu. Rev. Astron. Astrophys.* 42:79–118
Bromm V, Loeb A. 2003. *Ap. J.* 596:34–46
Brown WR, Geller MJ, Kenyon SJ, Kurtz MJ. 2005. *Ap. J. Lett.* 809:L33–36
Brown WR, Lattanzi MG, Kenyon SJ, Geller MJ. 2018. *Ap. J.* 866:39
Buchner J, Treister E, Bauer FE, Sartori LF, Schawinski K. 2019. *Ap. J.* 874:117
Campanelli M, Lousto C, Zlochower Y, Merritt D. 2007. *Ap. J. Lett.* 809:L5–8
Cann JM, Satyapal S, Abel NP, et al. 2019. *Ap. J. Lett.* 809:L2
Caplar N, Lilly SJ, Trakhtenbrot B. 2015. *Ap. J.* 811:148
Carr B. 1994. *Annu. Rev. Astron. Astrophys.* 32:531–90
Carson DJ, Barth AJ, Seth AC, et al. 2015. *Astron. J.* 149:170
Cassano R, Fender R, Ferrari C, et al. 2018. arXiv:1807.09080
Chilingarian IV, Katkov IY, Zolotukhin IY, et al. 2018. *Ap. J.* 863:1
Civano F, Cappelluti N, Hickox R, et al. 2019. *Bull. Am. Astron. Soc.* 51:429
Colbert EJM, Mushotzky RF. 1999. *Ap. J.* 519:89–107
Conroy C. 2013. *Annu. Rev. Astron. Astrophys.* 51:393–455
Contini M. 1997. *Astron. Astrophys.* 323:71–85
Côté P, Piatek S, Ferrarese L, et al. 2006. *Ap. J. Suppl.* 165:57–94
Cresci G, Vanzi L, Telles E, et al. 2017. *Astron. Astrophys.* 604:A101
Cseh D, Kaaret P, Corbel S, et al. 2010. *MNRAS* 406:1049–54
Cseh D, Webb NA, Godet O, et al. 2015. *MNRAS* 446:3268–76
Dashyan G, Silk J, Mamon GA, Dubois Y, Hartwig T. 2018. *MNRAS* 473:5698–703
Davis SW, Narayan R, Zhu Y, et al. 2011. *Ap. J.* 734:111
de Boer TJL, Belokurov V, Beers TC, Lee YS. 2014. *MNRAS* 443:658–63
De Lorenzi F, Hartmann M, Debattista VP, Seth AC, Gerhard O. 2013. *MNRAS* 429:2974–85
den Brok M, Seth AC, Barth AJ, et al. 2015. *Ap. J.* 809:101
Desroches LB, Filippenko AV, Kaspi S, et al. 2006. *Ap. J.* 650:88–101
Desroches LB, Greene JE, Ho LC. 2009. *Ap. J.* 698:1515–22
Desroches LB, Ho LC. 2009. *Ap. J.* 690:267–78
Devecchi B, Volonteri M. 2009. *Ap. J.* 694:302–13
Dewangan GC, Mathur S, Griffiths RE, Rao AR. 2008. *Ap. J.* 689:762–74
Dickey C, Geha M, Wetzel A, El-Badry K. 2019. *Ap. J.* Submitted. arXiv:1902.01401

Annu. Rev. Astron. Astrophys. 2020.58:257-312. Downloaded from www.annualreviews.org
Access provided by National Astronomical Observatories, Chinese Academy of Sciences on 09/05/23. For personal use only.

Dijkstra M, Haiman Z, Mesinger A, Wyithe JSB. 2008. *MNRAS* 391:1961–72
Done C, Davis SW, Jin C, Blaes O, Ward M. 2012. *MNRAS* 420:1848–60
Dong R, Greene JE, Ho LC. 2012a. *Ap. J.* 761:73
Dong XB, Ho LC, Yuan W, et al. 2012b. *Ap. J.* 755:167
Drout MR, Chornock R, Soderberg AM, et al. 2014. *Ap. J.* 794:23
Dunn G, Bellovary J, Holley-Bockelmann K, Christensen C, Quinn T. 2018. *Ap. J.* 861:39
Eardley DM, Press WH. 1975. *Annu. Rev. Astron. Astrophys.* 13:381–422
Earnshaw HM, Roberts TP, Heil LM, et al. 2016. *MNRAS* 456:3840–54
Ebisuzaki T, Makino J, Tsuru TG, et al. 2001. *Ap. J. Lett.* 809:L19–22
Edelmann H, Napiwotzki R, Heber U, Christlieb N, Reimers D. 2005. *Ap. J. Lett.* 809:L181–84
Edri H, Rafter SE, Chelouche D, Kaspi S, Behar E. 2012. *Ap. J.* 756:73
El-Badry K, Quataert E, Weisz DR, Choksi N, Boylan-Kolchin M. 2019. *MNRAS* 482:4528–52
Elitzur M, Ho LC. 2009. *Ap. J. Lett.* 809:L91–94
Eracleous M, Gezari S, Sesana A, et al. 2019. *Bull. Am. Astron. Soc.* 51:10
Erkal D, Boubert D, Gualandris A, Evans NW, Antonini F. 2019. *MNRAS* 483:2007–13
Fabbiano G. 1989. *Annu. Rev. Astron. Astrophys.* 27:87–138
Falcke H, Körding E, Markoff S. 2004. *Astron. Astrophys.* 414:895–903
Fan X, Carilli CL, Keating B. 2006. *Annu. Rev. Astron. Astrophys.* 44:415–62
Farrell SA, Webb NA, Barret D, Godet O, Rodrigues JM. 2009. *Nature* 460:73–75
Feldmeier A, Neumayer N, Seth A, et al. 2014. *Astron. Astrophys.* 570:A2
Fender RP, Maccarone TJ, Heywood I. 2013. *MNRAS* 430:1538–47
Ferrarese L, Côté P, Dalla Bontà E, et al. 2006. *Ap. J. Lett.* 809:L21–24
Filippenko AV. 1989. *Astron. J.* 97:726
Filippenko AV, Ho LC. 2003. *Ap. J. Lett.* 809:L13–16
Filippenko AV, Sargent WLW. 1989. *Ap. J. Lett.* 809:L11–14
Foord A, Gallo E, Hodges-Kluck E, et al. 2017. *Ap. J.* 841:51
Fragione G, Ginsburg I, Kocsis B. 2018. *Ap. J.* 856:92
Freire PC, Kramer M, Lyne AG, et al. 2001. *Ap. J. Lett.* 809:L105–8
Freire PCC, Ridolfi A, Kramer M, et al. 2017. *MNRAS* 471:857–76
Freitag M, Gürkan MA, Rasio FA. 2006. *MNRAS* 368:141–61
Fryer CL, Woosley SE, Heger A. 2001. *Ap. J.* 550:372–82
Fürst F, Walton DJ, Harrison FA, et al. 2016. *Ap. J. Lett.* 809:L14
Gair JR, Tang C, Volonteri M. 2010. *Phys. Rev. D* 81:104014
Gallo E, Sesana A. 2019. *Ap. J. Lett.* 809:L18
Gallo E, Treu T, Jacob J, et al. 2008. *Ap. J.* 680:154–68
Gallo E, Treu T, Marshall PJ, et al. 2010. *Ap. J.* 714:25–36
Gebhardt K, Lauer TR, Kormendy J, et al. 2001. *Astron. J.* 122:2469–76
Gebhardt K, Pryor C, O'Connell RD, Williams TB, Hesser JE. 2000. *Astron. J.* 119:1268–81
Gebhardt K, Rich RM, Ho LC. 2002. *Ap. J. Lett.* 809:L41–45
Gebhardt K, Rich RM, Ho LC. 2005. *Ap. J.* 634:1093–102
Gebhardt K, Richstone D, Tremaine S, et al. 2003. *Ap. J.* 583:92–115
Gebhardt K, Thomas J. 2009. *Ap. J.* 700:1690–701
Geha M, Blanton MR, Yan R, Tinker JL. 2012. *Ap. J.* 757:85
Georgakakis A, Tsamis YG, James BL, Aloisi A. 2011. *MNRAS* 413:1729–34
Georgiev IY, Böker T. 2014. *MNRAS* 441:3570–90
Georgiev IY, Böker T, Leigh N, Lützgendorf N, Neumayer N. 2016. *MNRAS* 457:2122–38
Gerssen J, van der Marel RP, Gebhardt K, et al. 2002. *Astron. J.* 124:3270–88
Gezari S, Chornock R, Rest A, et al. 2012. *Nature* 485:217–20
Ghez AM, Duchêne G, Matthews K, et al. 2003. *Ap. J. Lett.* 809:L127–31
Ghosh H, Mathur S, Fiore F, Ferrarese L. 2008. *Ap. J.* 687:216–29
Gieles M, Balbinot E, Yaaqib RISM, et al. 2018a. *MNRAS* 473:4832–39
Gieles M, Charbonnel C, Krause MGH, et al. 2018b. *MNRAS* 478:2461–79

Giersz M, Leigh N, Hypki A, Lützgendorf N, Askar A. 2015. *MNRAS* 454:3150–65
Gliozzi M, Satyapal S, Eracleous M, Titarchuk L, Cheung CC. 2009. *Ap. J.* 700:1759–67
Godet O, Lombardi JC, Antonini F, et al. 2014. *Ap. J.* 793:105
Godet O, Plazolles B, Kawaguchi T, et al. 2012. *Ap. J.* 752:34
Goulding AD, Alexander DM, Lehmer BD, Mullaney JR. 2010. *MNRAS* 406:597–611
Governato F, Colpi M, Maraschi L. 1994. *MNRAS* 271:317–22
Graham AW, Spitler LR. 2009. *MNRAS* 397:2148–62
Greene J, Barth A, Bellini A, et al. 2019. *Bull. Am. Astron. Soc.* 51:83
Greene JE. 2012. *Nat. Commun.* 3:1304
Greene JE, Ho LC. 2004. *Ap. J.* 610:722–36
Greene JE, Ho LC. 2006. *Ap. J. Lett.* 809:L21–24
Greene JE, Ho LC. 2007a. *Ap. J.* 656:84–92
Greene JE, Ho LC. 2007b. *Ap. J.* 667:131–48
Greene JE, Ho LC. 2007c. *Ap. J.* 670:92–104
Greene JE, Ho LC, Barth AJ. 2008. *Ap. J.* 688:159–79
Greene JE, Ho LC, Ulvestad JS. 2006. *Ap. J.* 636:56–62
Greene JE, Peng CY, Kim M, et al. 2010. *Ap. J.* 721:26–45
Greene JE, Seth A, Kim M, et al. 2016. *Ap. J. Lett.* 809:L32
Grier CJ, Mathur S, Ghosh H, Ferrarese L. 2011. *Ap. J.* 731:60
Grindlay JE, Heinke C, Edmonds PD, Murray SS. 2001. *Science* 292:2290–95
Groves BA, Heckman TM, Kauffmann G. 2006. *MNRAS* 371:1559–69
Gualandris A, Portegies Zwart S. 2007. *MNRAS* 809:L29–33
Guillochon J, Ramirez-Ruiz E. 2013. *Ap. J.* 767:25
Gültekin K, King AL, Cackett EM, et al. 2019. *Ap. J.* 871:80
Gültekin K, Tremaine S, Loeb A, Richstone DO. 2011. *Ap. J.* 738:17
Gürkan MA, Freitag M, Rasio FA. 2004. *Ap. J.* 604:632–52
Habouzit M, Volonteri M, Latif M, Dubois Y, Peirani S. 2016. *MNRAS* 463:529–40
Haehnelt MG, Rees MJ. 1993. *MNRAS* 263:168–78
Haggard D, Cool AM, Heinke CO, et al. 2013. *Ap. J. Lett.* 809:L31
Haiman Z. 2004. *Ap. J.* 613:36–40
Haiman Z. 2013. In *The First Galaxies*, ed. T Wiklind, B Mobasher, V Bromm, Ap. Space Sci. Libr. 396:293–340
Haiman Z, Brandt WN, Vikhlinin A, et al. 2019. *Bull. Am. Astron. Soc.* 51:557
Haiman Z, Loeb A. 2001. *Ap. J.* 552:459–63
Hainline KN, Reines AE, Greene JE, Stern D. 2016. *Ap. J.* 832:119
Hansen BMS, Milosavljević M. 2003. *Ap. J. Lett.* 809:L77–80
Harris WE. 2016. *Astron. J.* 151:102
Hebbar PR, Heinke CO, Sivakoff GR, Shaw AW. 2019. *MNRAS* 485:5604–15
Heger A, Fryer CL, Woosley SE, Langer N, Hartmann DH. 2003. *Ap. J.* 591:288–300
Heinis S, Gezari S, Kumar S, et al. 2016. *Ap. J.* 826:62
Hénault-Brunet V, Gieles M, Strader J, et al. 2020. *MNRAS* 491:113–28
Hills JG. 1988. *Nature* 331:687–89
Hirsch HA, Heber U, O'Toole SJ, Bresolin F. 2005. *Astron. Astrophys.* 809:L61–64
Ho LC. 2008. *Annu. Rev. Astron. Astrophys.* 46:475–539
Ho LC. 2009. *Ap. J.* 699:626–37
Ho LC, Filippenko AV, Sargent WLW. 1997. *Ap. J.* 487:568–78
Ho LC, Kim M. 2014. *Ap. J.* 789:17
Ho LC, Kim M. 2016. *Ap. J.* 821:48
Holley-Bockelmann K, Gültekin K, Shoemaker D, Yunes N. 2008. *Ap. J.* 686:829–37
Holley-Bockelmann K, Micic M, Sigurdsson S, Rubbo LJ. 2010. *Ap. J.* 713:1016–25
Holoien TWS, Prieto JL, Bersier D, et al. 2014. *MNRAS* 445:3263–77
Homma D, Chiba M, Komiyama Y, et al. 2019. *Publ. Astron. Soc. Jpn.* 71(5):94
Hood CE, Barth AJ, Ho LC, Greene JE. 2017. *Ap. J.* 838:26

Annu. Rev. Astron. Astrophys. 2020.58:257-312. Downloaded from www.annualreviews.org
Access provided by National Astronomical Observatories, Chinese Academy of Sciences on 09/05/23. For personal use only.

Hopkins PF, Hernquist L, Cox TJ, Robertson B, Krause E. 2007. *Ap. J.* 669:67–73
Ibata R, Bellazzini M, Chapman SC, et al. 2009. *Ap. J. Lett.* 809:L169–73
Inayoshi K, Visbal E, Haiman Z. 2020. *Annu. Rev. Astron. Astrophys.* 58:27–97
Irwin JA, Maksym WP, Sivakoff GR, Romanowsky AJ, Lin D, et al. 2016. *Nature* 538:356–58
Islam RR, Taylor JE, Silk J. 2004. *MNRAS* 354:427–42
Israel GL, Papitto A, Esposito P, et al. 2017. *MNRAS* 809:L48–52
Izotov YI, Guseva NG, Fricke KJ, et al. 2010. *Astron. Astrophys.* 517:A90
Izotov YI, Thuan TX. 2008. *Ap. J.* 687:133–40
Izotov YI, Thuan TX, Privon G. 2012. *MNRAS* 427:1229–37
Jalali B, Baumgardt H, Kissler-Patig M, et al. 2012. *Astron. Astrophys.* 538:A19
Jardel JR, Gebhardt K. 2012. *Ap. J.* 746:89
Jarrett TH, Cohen M, Masci F, et al. 2011. *Ap. J.* 735:112
Jiang YF, Greene JE, Ho LC. 2011. *Ap. J. Lett.* 809:L45
Jiang YF, Stone JM, Davis SW. 2019. *Ap. J.* 880:67
Jin C, Done C, Ward M. 2016. *MNRAS* 455:691–702
Jin C, Ward M, Done C. 2012. *MNRAS* 425:907–29
Johnson JL, Bromm V. 2007. *MNRAS* 374:1557–68
Jonker PG, Miller-Jones JCA, Homan J, et al. 2012. *MNRAS* 423:3308–15
Jonker PG, Stone NC, Generozov A, van Velzen S, Metzger B. 2019. *Ap. J.* 889:166
Jordán A, McLaughlin DE, Côté P, et al. 2007. *Ap. J. Suppl.* 171:101–45
Kaaret P, Feng H, Gorski M. 2009. *Ap. J.* 692:653–58
Kaaret P, Feng H, Roberts TP. 2017. *Annu. Rev. Astron. Astrophys.* 55:303–41
Kacharov N, Neumayer N, Seth AC, et al. 2018. *MNRAS* 480:1973–98
Kains N, Bramich DM, Sahu KC, Calamida A. 2016. *MNRAS* 460:2025–35
Kains N, Calamida A, Sahu KC, et al. 2018. *Ap. J.* 867:37
Kamann S, Husser TO, Brinchmann J, et al. 2016. *Astron. Astrophys.* 588:A149
Kamizasa N, Terashima Y, Awaki H. 2012. *Ap. J.* 751:39
Karachentsev ID, Makarov DI, Kaisina EI. 2013. *Astron. J.* 145:101
Karlsson T, Bromm V, Bland-Hawthorn J. 2013. *Rev. Mod. Phys.* 85:809–48
Katz H, Sijacki D, Haehnelt MG. 2015. *MNRAS* 451:2352–69
Kauffmann G, Heckman TM, Tremonti C, et al. 2003. *MNRAS* 346:1055–77
Kaviraj S, Martin G, Silk J. 2019. *MNRAS* 809:L12–16
Kim M, Ho LC, Wang J, et al. 2015. *Ap. J.* 814:8
Kızıltan B, Baumgardt H, Loeb A. 2017. *Nature* 542:203–5
Klein A, Barausse E, Sesana A, et al. 2016. *Phys. Rev. D* 93:024003
Komossa S, Merritt D. 2008. *Ap. J. Lett.* 809:L21–24
Koposov SE, Douglas B, Ting SL, et al. 2019. *MNRAS* 491:2465–80
Kormendy J, Ho LC. 2013. *Annu. Rev. Astron. Astrophys.* 51:511–653
Kormendy J, Kennicutt Robert CJ. 2004. *Annu. Rev. Astron. Astrophys.* 42:603–83
Kormendy J, Richstone D. 1995. *Annu. Rev. Astron. Astrophys.* 33:581–624
Koushiappas SM, Bullock JS, Dekel A. 2004. *MNRAS* 354:292–304
Kovetz ED, Cholis I, Kamionkowski M, Silk J. 2018. *Phys. Rev. D* 97:123003
Krajnović D, Cappellari M, McDermid RM, et al. 2018. *MNRAS* 477:3030–64
Kremer K, Chatterjee S, Ye CS, Rodriguez CL, Rasio FA. 2019. *Ap. J.* 871:38
Kuin NPM, Wu K, Oates S, et al. 2019. *MNRAS* 487:2505–21
Kunth D, Sargent WLW, Bothun GD. 1987. *Astron. J.* 93:29–32
Lacey CG, Ostriker JP. 1985. *Ap. J.* 299:633–52
Lanzoni B, Mucciarelli A, Origlia L, et al. 2013. *Ap. J.* 769:107
Laporte CFP, Johnston KV, Gómez FA, Garavito-Camargo N, Besla G. 2018. *MNRAS* 481:286–306
Läsker R, Greene JE, Seth A, et al. 2016. *Ap. J.* 825:3
Lasota JP, Alexander T, Dubus G, et al. 2011. *Ap. J.* 735:89
Latimer CJ, Reines AE, Plotkin RM, Russell TD, Condon JJ. 2019. *Ap. J.* 884:78

Annu. Rev. Astron. Astrophys. 2020.58:257-312. Downloaded from www.annualreviews.org
Access provided by National Astronomical Observatories, Chinese Academy of Sciences on 09/05/23. For personal use only.

Lauer TR, Faber SM, Gebhardt K, et al. 2005. *Astron. J.* 129:2138–85
Law-Smith J, MacLeod M, Guillochon J, Macias P, Ramirez-Ruiz E. 2017. *Ap. J.* 841:132
Lee MH. 1993. *Ap. J.* 418:147–62
Lee N, Gallo E, Hodges-Kluck E, et al. 2019. *Ap. J.* 874:77
Lemons SM, Reines AE, Plotkin RM, Gallo E, Greene JE. 2015. *Ap. J.* 805:12
Lennon DJ, van der Marel RP, Ramos Lerate M, O'Mullane W, Sahlmann J. 2017. *Astron. Astrophys.* 603:A75
Lin D, Carrasco ER, Webb NA, et al. 2016. *Ap. J.* 821:25
Lin D, Godet O, Ho LC, et al. 2017. *MNRAS* 468:783–89
Lin D, Strader J, Carrasco ER, et al. 2018. *Nat. Astron.* 2:656–61
Liu C, Peng EW, Côté P, et al. 2015. *Ap. J.* 812:34
Liu HY, Yuan W, Dong XB, Zhou H, Liu WJ. 2018. *Ap. J. Suppl.* 235:40
Lodato G, King AR, Pringle JE. 2009. *MNRAS* 392:332–40
Lodato G, Natarajan P. 2006. *MNRAS* 371:1813–23
Loeb A, Rasio FA. 1994. *Ap. J.* 432:52–61
Long KS, Dodorico S, Charles PA, Dopita MA. 1981. *Ap. J.* 809:L61–64
Lora V, Sánchez-Salcedo FJ, Raga AC, Esquivel A. 2009. *Ap. J. Lett.* 809:L113–17
Lu TN, Kong AKH. 2011. *Ap. J. Lett.* 809:L25
Lu Y, Yu Q, Lin DNC. 2007. *Ap. J. Lett.* 809:L89–92
Ludlam RM, Cackett EM, Gültekin K, et al. 2015. *MNRAS* 447:2112–22
Ludwig RR, Greene JE, Barth AJ, Ho LC. 2012. *Ap. J.* 756:51
Lutz D, Spoon HWW, Rigopoulou D, Moorwood AFM, Genzel R. 1998. *Ap. J. Lett.* 809:L103–7
Lützgendorf N, Gebhardt K, Baumgardt H, et al. 2015. *Astron. Astrophys.* 581:A1
Lützgendorf N, Gualandris A, Kissler-Patig M, et al. 2012. *Astron. Astrophys.* 543:A82
Lützgendorf N, Kissler-Patig M, Gebhardt K, et al. 2013. *Astron. Astrophys.* 552:A49
Lützgendorf N, Kissler-Patig M, Noyola E, et al. 2011. *Astron. Astrophys.* 533:A36
MacArthur LA, Courteau S, Holtzman JA. 2003. *Ap. J.* 582:689–722
Maccarone TJ. 2004. *MNRAS* 351:1049–53
Maccarone TJ, Fender RP, Tzioumis AK. 2005. *MNRAS* 809:L17–22
Maccarone TJ, Servillat M. 2008. *MNRAS* 389:379–84
MacLeod CL, Brooks K, Ivezić Ž, et al. 2011. *Ap. J.* 728:26
MacLeod M, Guillochon J, Ramirez-Ruiz E, Kasen D, Rosswog S. 2016a. *Ap. J.* 819:3
MacLeod M, Trenti M, Ramirez-Ruiz E. 2016b. *Ap. J.* 819:70
Madau P, Haardt F. 2015. *Ap. J. Lett.* 809:L8
Madau P, Haardt F, Dotti M. 2014. *Ap. J. Lett.* 809:L38
Madau P, Rees MJ. 2001. *Ap. J. Lett.* 809:L27–30
Maillard JP, Paumard T, Stolovy SR, Rigaut F. 2004. *Astron. Astrophys.* 423:155–67
Maksym WP, Ulmer MP, Eracleous MC, Guennou L, Ho LC. 2013. *MNRAS* 435:1904–27
Maksym WP, Ulmer MP, Roth KC, et al. 2014. *MNRAS* 444:866–73
Mann CR, Richer H, Heyl J, et al. 2019. *Ap. J.* 875:1
Manzano-King CM, Canalizo G, Sales LV. 2019. *Ap. J.* 884:54
Mapelli M. 2016. *MNRAS* 459:3432–46
Mapelli M, Annibali F, Zampieri L, Soria R. 2013. *Astron. Astrophys.* 559:A124
Marconi A, Risaliti G, Gilli R, et al. 2004. *MNRAS* 351:169–85
Margutti R, Metzger BD, Chornock R, et al. 2019. *Ap. J.* 872:18
Marleau FR, Clancy D, Habas R, Bianconi M. 2017. *Astron. Astrophys.* 602:A28
Martín-Navarro I, Mezcua M. 2018. *Ap. J. Lett.* 809:L20
McAlpine W, Satyapal S, Gliozzi M, et al. 2011. *Ap. J.* 728:25
McLaughlin DE, Anderson J, Meylan G, et al. 2006. *Ap. J. Suppl.* 166:249–97
McNamara BJ, Harrison TE, Anderson J. 2003. *Ap. J.* 595:187–94
Méndez DI, Esteban C. 1997. *Ap. J.* 488:652–68
Merloni A, Heinz S, di Matteo T. 2003. *MNRAS* 345:1057–76
Mezcua M. 2017. *Int. J. Mod. Phys. D* 26:1730021

Annu. Rev. Astron. Astrophys. 2020.58:257-312. Downloaded from www.annualreviews.org
Access provided by National Astronomical Observatories, Chinese Academy of Sciences on 09/05/23. For personal use only.

Mezcua M, Civano F, Fabbiano G, Miyaji T, Marchesi S. 2016. *Ap. J.* 817:20
Mezcua M, Civano F, Marchesi S, et al. 2018a. *MNRAS* 478:2576–91
Mezcua M, Kim M, Ho LC, Lonsdale CJ. 2018b. *MNRAS* 809:L74–78
Mezcua M, Roberts TP, Lobanov AP, Sutton AD. 2015. *MNRAS* 448:1893–99
Mezcua M, Roberts TP, Sutton AD, Lobanov AP. 2013. *MNRAS* 436:3128–34
Mezcua M, Suh H, Civano F. 2019. *MNRAS* 488:685–95
Micic M, Holley-Bockelmann K, Sigurdsson S. 2011. *MNRAS* 414:1127–44
Miller B, Gallo E, Treu T, Woo JH. 2012. *Ap. J.* 747:57
Miller BP, Gallo E, Greene JE, et al. 2015. *Ap. J.* 799:98
Miller JM. 2005. *Ap. Space Sci.* 300:227–38
Miller MC, Davies MB. 2012. *Ap. J.* 755:81
Miller MC, Hamilton DP. 2002. *MNRAS* 330:232–40
Miller-Jones JCA, Wrobel JM, Sivakoff GR, et al. 2012. *Ap. J. Lett.* 809:L1
Milosavljević M, Couch SM, Bromm V. 2009. *Ap. J. Lett.* 809:L146–49
Milosavljević M, Merritt D, Ho LC. 2006. *Ap. J.* 652:120–25
Miniutti G, Ponti G, Greene JE, et al. 2009. *MNRAS* 394:443–53
Mockler B, Guillochon J, Ramirez-Ruiz E. 2019. *Ap. J.* 872:151
Mooley KP, Hallinan G, Bourke S, et al. 2016. *Ap. J.* 818:105
Moran EC, Eracleous M, Leighly KM, et al. 2005. *Astron. J.* 129:2108–18
Moran EC, Shahinyan K, Sugarman HR, Vélez DO, Eracleous M. 2014. *Astron. J.* 148:136
Morokuma T, Tominaga N, Tanaka M, et al. 2016. *Publ. Astron. Soc. Jpn.* 68:40
Mortlock DJ, Warren SJ, Venemans BP, et al. 2011. *Nature* 474:616–19
Naiman JP, Ramirez-Ruiz E, Debuhr J, Ma CP. 2015. *Ap. J.* 803:81
Neumayer N, Walcher CJ. 2012. *Adv. Astron.* 2012:709038
Neumayer N, Seth A, Böker T. 2020. *Astron. Astrophys. Rev.* 28:4
Nguyen DD, den Brok M, Seth AC, et al. 2019a. *Ap. J.* Submitted. arXiv:1902.03813
Nguyen DD, Seth AC, den Brok M, et al. 2017. *Ap. J.* 836:237
Nguyen DD, Seth AC, Neumayer N, et al. 2018. *Ap. J.* 858:118
Nguyen DD, Seth AC, Neumayer N, et al. 2019b. *Ap. J.* 872:104
Nguyen DD, Seth AC, Reines AE, et al. 2014. *Ap. J.* 794:34
Niederste-Ostholt M, Belokurov V, Evans NW, Peñarrubia J. 2010. *Ap. J.* 712:516–26
Noyola E, Gebhardt K, Kissler-Patig M, et al. 2010. *Ap. J. Lett.* 809:L60–64
Nyland K, Davis TA, Nguyen DD, et al. 2017. *Ap. J.* 845:50
Nyland K, Marvil J, Wrobel JM, Young LM, Zauderer BA. 2012. *Ap. J.* 753:103
Oka T, Mizuno R, Miura K, Takekawa S. 2016. *Ap. J. Lett.* 809:L7
O'Leary RM, Loeb A. 2009. *MNRAS* 395:781–86
O'Leary RM, Loeb A. 2012. *MNRAS* 421:2737–50
Omukai K. 2001. *Ap. J.* 546:635–51
Pacucci F, Loeb A, Mezcua M, Martín-Navarro I. 2018. *Ap. J. Lett.* 809:L6
Pan HW, Yuan W, Zhou XL, Dong XB, Liu B. 2015. *Ap. J.* 808:163
Pancoast A, Brewer BJ, Treu T, et al. 2014. *MNRAS* 445:3073–91
Pandya V, Mulchaey J, Greene JE. 2016. *Ap. J.* 819:162
Pardo K, Goulding AD, Greene JE, et al. 2016. *Ap. J.* 831:203
Park D, Barth AJ, Woo JH, et al. 2017. *Ap. J.* 839:93
Pasham DR, Strohmayer TE, Mushotzky RF. 2014. *Nature* 513:74–76
Pechetti R, Seth A, Cappellari M, et al. 2017. *Ap. J.* 850:15
Pellegrini S. 2005. *MNRAS* 364:169–78
Pelupessy FI, Di Matteo T, Ciardi B. 2007. *Ap. J.* 665:107–19
Penny SJ, Masters KL, Smethurst R, et al. 2018. *MNRAS* 476:979–98
Perera BBP, Stappers BW, Lyne AG, et al. 2017. *MNRAS* 468:2114–27
Perets HB, Šubr L. 2012. *Ap. J.* 751:133
Perley DA, Mazzali PA, Yan L, et al. 2019. *MNRAS* 484:1031–49

Annu. Rev. Astron. Astrophys. 2020.58:257-312. Downloaded from www.annualreviews.org
Access provided by National Astronomical Observatories, Chinese Academy of Sciences on 09/05/23. For personal use only.

Peterson BM. 2014. *Space Sci. Rev.* 183:253–75
Peterson BM, Bentz MC, Desroches LB, et al. 2005. *Ap. J.* 632:799–808
Pfahl E, Rappaport S. 2001. *Ap. J.* 550:172–76
Pfeffer J, Griffen BF, Baumgardt H, Hilker M. 2014. *MNRAS* 444:3670–83
Pfeffer J, Hilker M, Baumgardt H, Griffen BF. 2016. *MNRAS* 458:2492–508
Pfister H, Volonteri M, Dubois Y, Dotti M, Colpi M. 2019. *MNRAS* 486:101–11
Plotkin RM, Gallo E, Haardt F, et al. 2016. *Ap. J.* 825:139
Plotkin RM, Markoff S, Kelly BC, Körding E, Anderson SF. 2012. *MNRAS* 419:267–86
Pooley D, Rappaport S. 2006. *Ap. J. Lett.* 809:L45–48
Portegies Zwart SF, McMillan SLW. 2002. *Ap. J.* 576:899–907
Prestwich AH, Tsantaki M, Zezas A, et al. 2013. *Ap. J.* 769:92
Pursiainen M, Childress M, Smith M, et al. 2018. *MNRAS* 481:894–917
Quinlan GD, Shapiro SL. 1990. *Ap. J.* 356:483–500
Rafter SE, Kaspi S, Behar E, Kollatschny W, Zetzl M. 2011. *Ap. J.* 741:66
Rashkov V, Madau P. 2014. *Ap. J.* 780:187
Ravi V, Vedantham H, Phinney ES. 2018. *MNRAS* 809:L72–77
Ravindranath S, Ho LC, Peng CY, Filippenko AV, Sargent WLW. 2001. *Astron. J.* 122:653–78
Redmount IH, Rees MJ. 1989. *Comments Astrophys.* 14:165–75
Rees MJ. 1978. *Observatory* 98:210–23
Rees MJ. 1988. *Nature* 333:523–28
Reid MJ, Brunthaler A. 2004. *Ap. J.* 616:872–84
Reines A, Condon J, Darling J, Greene J. 2019. *Ap. J.* 888:36
Reines AE, Comastri A. 2016. *Publ. Astron. Soc. Aust.* 33:e054
Reines AE, Deller AT. 2012. *Ap. J. Lett.* 809:L24
Reines AE, Greene JE, Geha M. 2013. *Ap. J.* 775:116
Reines AE, Reynolds MT, Miller JM, et al. 2016. *Ap. J. Lett.* 809:L35
Reines AE, Sivakoff GR, Johnson KE, Brogan CL. 2011. *Nature* 470:66–68
Reines AE, Volonteri M. 2015. *Ap. J.* 813:82
Remillard RA, McClintock JE. 2006. *Annu. Rev. Astron. Astrophys.* 44:49–92
Ressler SM, Quataert E, Stone JM. 2019. *MNRAS* 809:L123–28
Ricarte A, Natarajan P. 2018. *MNRAS* 481:3278–92
Rix HW, de Zeeuw PT, Cretton N, van der Marel RP, Carollo CM. 1997. *Ap. J.* 488:702–19
Rodriguez CL, Amaro-Seoane P, Chatterjee S, et al. 2018. *Phys. Rev. D* 98:123005
Rodriguez CL, Zevin M, Amaro-Seoane P, et al. 2019. *Phys. Rev. D* 100:043027
Rodríguez Castillo GA, Israel GL, Belfiore A, et al. 2019. *Ap. J.* Submitted. arXiv:1906.04791
Rosswog S, Ramirez-Ruiz E, Hix WR. 2009. *Ap. J.* 695:404–19
Safonova M, Stalin CS. 2010. *New Astron.* 15:450–59
Saglia RP, Opitsch M, Erwin P, et al. 2016. *Ap. J.* 818:47
Sakurai Y, Yoshida N, Fujii MS, Hirano S. 2017. *MNRAS* 472:1677–84
Sánchez-Janssen R, Côté P, Ferrarese L, et al. 2019. *Ap. J.* 878:18
Sarajedini VL, Koo DC, Phillips AC, et al. 2006. *Ap. J. Suppl.* 166:69–88
Sartori LF, Schawinski K, Treister E, et al. 2015. *MNRAS* 454:3722–42
Satyapal S, Böker T, McAlpine W, et al. 2009. *Ap. J.* 704:439–52
Satyapal S, Secrest NJ, McAlpine W, et al. 2014. *Ap. J.* 784:113
Satyapal S, Vega D, Dudik RP, Abel NP, Heckman T. 2008. *Ap. J.* 677:926–42
Satyapal S, Vega D, Heckman T, O'Halloran B, Dudik R. 2007. *Ap. J. Lett.* 809:L9–12
Schaerer D, Fragos T, Izotov YI. 2019. *Astron. Astrophys.* 809:L10
Schaerer D, Stasińska G. 1999. *Astron. Astrophys.* 809:L17–21
Schneider R, Ferrara A, Natarajan P, Omukai K. 2002. *Ap. J.* 571:30–39
Schödel R, Eckart A, Iserlohe C, Genzel R, Ott T. 2005. *Ap. J. Lett.* 809:L111–14
Schramm M, Silverman JD, Greene JE, et al. 2013. *Ap. J.* 773:150
Schutte Z, Reines A, Greene J. 2019. *Ap. J.* 887:245

Annu. Rev. Astron. Astrophys. 2020.58:257-312. Downloaded from www.annualreviews.org
Access provided by National Astronomical Observatories, Chinese Academy of Sciences on 09/05/23. For personal use only.

Schwarzschild M. 1979. *Ap. J.* 232:236–47
Secrest NJ, Satyapal S, Gliozzi M, et al. 2012. *Ap. J.* 753:38
Servillat M, Farrell SA, Lin D, et al. 2011. *Ap. J.* 743:6
Sesana A, Gair J, Berti E, Volonteri M. 2011. *Phys. Rev. D* 83:044036
Sesana A, Haardt F, Madau P. 2007. *MNRAS* 809:L45–49
Sesana A, Madau P, Haardt F. 2009. *MNRAS* 809:L31–34
Seth AC, Blum RD, Bastian N, Caldwell N, Debattista VP. 2008. *Ap. J.* 687:997–1003
Seth AC, Dalcanton JJ, Hodge PW, Debattista VP. 2006. *Astron. J.* 132:2539–55
Seth AC, van den Bosch R, Mieske S, et al. 2014. *Nature* 513:398–400
Shankar F, Bernardi M, Sheth RK, et al. 2016. *MNRAS* 460:3119–42
She R, Ho LC, Feng H. 2017a. *Ap. J.* 835:223
She R, Ho LC, Feng H. 2017b. *Ap. J.* 842:131
Shen KJ, Boubert D, Gänsicke BT, et al. 2018. *Ap. J.* 865:15
Shi Y, Rieke G, Donley J, et al. 2008. *Ap. J.* 688:794–806
Silk J. 2017. *Ap. J.* 809:L13
Silk J, Rees MJ. 1998. *Astron. Astrophys.* 809:L1–4
Simmonds C, Bauer FE, Thuan TX, et al. 2016. *Astron. Astrophys.* 596:A64
Soria R, Musaeva A, Wu K, et al. 2017. *MNRAS* 469:886–905
Spera M, Mapelli M. 2017. *MNRAS* 470:4739–49
Stasińska G, Cid Fernandes R, Mateus A, Sodré L, Asari NV. 2006. *MNRAS* 371:972–82
Stern D, Assef RJ, Benford DJ, et al. 2012. *Ap. J.* 753:30
Stone NC, Küpper AHW, Ostriker JP. 2017. *MNRAS* 467:4180–99
Stone NC, Metzger BD. 2016. *MNRAS* 455:859–83
Strader J, Chomiuk L, Maccarone TJ, et al. 2012. *Ap. J. Lett.* 809:L27
Straub O, Godet O, Webb N, Servillat M, Barret D. 2014. *Astron. Astrophys.* 569:A116
Strubbe LE, Quataert E. 2009. *MNRAS* 400:2070–84
Swartz DA, Tennant AF, Soria R. 2009. *Ap. J.* 703:159–68
Takada M, Ellis RS, Chiba M, et al. 2014. *Publ. Astron. Soc. Jpn.* 66:R1
Takekawa S, Oka T, Iwata Y, Tsujimoto S, Nomura M. 2019. *Ap. J. Lett.* 809:L1
Tanaka K. 2018. *Ap. J.* 859:86
Tanaka M, Tominaga N, Morokuma T, et al. 2016. *Ap. J.* 819:5
Tanaka T, Haiman Z. 2009. *Ap. J.* 696:1798–822
Thater S, Krajnović D, Cappellari M, et al. 2019. *Astron. Astrophys.* 625:A62
Thornton CE, Barth AJ, Ho LC, Greene JE. 2009. *Ap. J.* 705:1196–205
Thornton CE, Barth AJ, Ho LC, Rutledge RE, Greene JE. 2008. *Ap. J.* 686:892–910
Tisserand P, Le Guillou L, Afonso C, et al. 2007. *Astron. Astrophys.* 469:387–404
Tremou E, Strader J, Chomiuk L, et al. 2018. *Ap. J.* 862:16
Trump JR, Sun M, Zeimann GR, et al. 2015. *Ap. J.* 811:26
Tsuboi M, Kitamura Y, Tsutsumi T, et al. 2017. *Ap. J. Lett.* 809:L5
Tsuboi M, Kitamura Y, Tsutsumi T, et al. 2019. *Publ. Astron. Soc. Jpn.* 71(5):105
Ulvestad JS, Greene JE, Ho LC. 2007. *Ap. J. Lett.* 809:L151–54
Urquhart R, Soria R, Johnston HM, et al. 2018. *MNRAS* 475:3561–76
Valiante R, Schneider R, Volonteri M, Omukai K. 2016. *MNRAS* 457:3356–71
Valluri M, Merritt D, Emsellem E. 2004. *Ap. J.* 602:66–92
van den Bosch RCE, de Zeeuw PT. 2010. *MNRAS* 401:1770–80
van der Marel RP, Anderson J. 2010. *Ap. J.* 710:1063–88
van der Marel RP, Kallivayalil N. 2014. *Ap. J.* 781:121
van Velzen S. 2018. *Ap. J.* 852:72
van Wassenhove S, Volonteri M, Walker MG, Gair JR. 2010. *MNRAS* 408:1139–46
Vinkó J, Yuan F, Quimby RM, et al. 2015. *Ap. J.* 798:12
Visbal E, Haiman Z, Bryan GL. 2014. *MNRAS* 445:1056–63
Voggel KT, Seth AC, Baumgardt H, et al. 2019. *Ap. J.* 871:159

Annu. Rev. Astron. Astrophys. 2020.58:257-312. Downloaded from www.annualreviews.org
Access provided by National Astronomical Observatories, Chinese Academy of Sciences on 09/05/23. For personal use only.

Volonteri M. 2010. *Astron. Astrophys. Rev.* 18:279–315
Volonteri M, Gnedin NY. 2009. *Ap. J.* 703:2113–17
Volonteri M, Haardt F, Madau P. 2003. *Ap. J.* 582:559–73
Volonteri M, Lodato G, Natarajan P. 2008. *MNRAS* 383:1079–88
Volonteri M, Natarajan P. 2009. *MNRAS* 400:1911–18
Volonteri M, Perna R. 2005. *MNRAS* 358:913–22
Volonteri M, Rees MJ. 2006. *Ap. J.* 650:669–78
Vučetić MM, Ilić D, Egorov OV, et al. 2019. *Astron. Astrophys.* 628:A87
Walcher CJ, Böker T, Charlot S, et al. 2006. *Ap. J.* 649:692–708
Walsh JL, Barth AJ, Ho LC, Sarzi M. 2013. *Ap. J.* 770:86
Webb N, Cseh D, Lenc E, et al. 2012. *Science* 337:554–56
Webb NA, Guérou A, Ciambur B, et al. 2017. *Astron. Astrophys.* 602:A103
Wevers T, Stone NC, van Velzen S, et al. 2019. *MNRAS* 487:4136–52
Wevers T, van Velzen S, Jonker PG, et al. 2017. *MNRAS* 471:1694–708
Wiersema K, Farrell SA, Webb NA, et al. 2010. *Ap. J.* 809:L102–6
Wise JH, Regan JA, O'Shea BW, et al. 2019. *Nature* 566:85–88
Wolter A, Esposito P, Mapelli M, Pizzolato F, Ripamonti E. 2015. *MNRAS* 448:781–91
Woo JH, Cho H, Gallo E, et al. 2019. *Nat. Astron.* 3:755–59
Woosley SE. 2017. *Ap. J.* 836:244
Wright AH, Robotham ASG, Driver SP, et al. 2017. *MNRAS* 470:283–302
Wrobel J, Haiman Z, Holley-Bockelmann K, et al. 2019. *Bull. Am. Astron. Soc.* 51:29
Wrobel JM, Greene JE, Ho LC, Ulvestad JS. 2008. *Ap. J.* 686:838–42
Wrobel JM, Ho LC. 2006. *Ap. J. Lett.* 809:L95–98
Wrobel JM, Miller-Jones JCA, Middleton MJ. 2016. *Astron. J.* 152:22
Xiao T, Barth AJ, Greene JE, et al. 2011. *Ap. J.* 739:28
Yalinewich A, Beniamini P. 2018. *Astron. Astrophys.* 809:L9
Yang X, Yang J, Paragi Z, et al. 2017. *MNRAS* 809:L70–74
Yoshida N, Abel T, Hernquist L, Sugiyama N. 2003. *Ap. J.* 592:645–63
Yu Q, Lu Y, Lin DNC. 2007. *Ap. J.* 666:919–33
Yu Q, Tremaine S. 2003. *Ap. J.* 599:1129–38
Yuan W, Zhou H, Dou L, et al. 2014. *Ap. J.* 782:55
Zasov AV, Cherepashchuk AM. 2013. *Astron. Rep.* 57:797–810
Zhang F, Lu Y, Yu Q. 2013. *Ap. J.* 768:153
Zhang WM, Soria R, Zhang SN, Swartz DA, Liu JF. 2009. *Ap. J.* 699:281–97
Zocchi A, Gieles M, Hénault-Brunet V. 2017. *MNRAS* 468:4429–40
Zocchi A, Gieles M, Hénault-Brunet V. 2019. *MNRAS* 482:4713–25
Zolotukhin I, Webb NA, Godet O, Bachetti M, Barret D. 2016. *Ap. J.* 817:88
Zubovas K. 2019. *MNRAS* 483:1957–69
Zumalacárregui M, Seljak U. 2018. *Phys. Rev. Lett.* 121:141101

Annu. Rev. Astron. Astrophys. 2020.58:257-312. Downloaded from www.annualreviews.org
Access provided by National Astronomical Observatories, Chinese Academy of Sciences on 09/05/23. For personal use only.

Annual Review of Astronomy and Astrophysics

Volume 58, 2020

Annu. Rev. Astron. Astrophys. 2020.58:257-312. Downloaded from www.annualreviews.org
Access provided by National Astronomical Observatories, Chinese Academy of Sciences on 09/05/23. For personal use only.

Contents

Jack of All
James E. Gunn 1

The Assembly of the First Massive Black Holes
Kohei Inayoshi, Eli Visbal, and Zoltán Haiman 27

Spatially Resolved Spectroscopic Properties of Low-Redshift Star-Forming Galaxies
Sebastián F. Sánchez 99

The Evolution of the Star-Forming Interstellar Medium Across Cosmic Time
Linda J. Tacconi, Reinhard Genzel, and Amiel Sternberg 157

Streams, Substructures, and the Early History of the Milky Way
Amina Helmi 205

Intermediate-Mass Black Holes
Jenny E. Greene, Jay Strader, and Luis C. Ho 257

Astronomers Engaging with the Education Ecosystem: A Best-Evidence Synthesis
Stephen M. Pompea and Pedro Russo 313

The Cosmic Baryon and Metal Cycles
Céline Péroux and J. Christopher Howk 363

Magnetohydrodynamics Simulations of Active Galactic Nucleus Disks and Jets
Shane W. Davis and Alexander Tchekhovskoy 407

Magnetohydrodynamic Waves in the Solar Corona
Valery M. Nakariakov and Dmitrii Y. Kolotkov 441

Observations of Protoplanetary Disk Structures
Sean M. Andrews 483

The Dust Attenuation Law in Galaxies
Samir Salim and Desika Narayanan 529

Evidence for Initial Mass Function Variation in Massive Early-Type Galaxies
Russell J. Smith 577

Observations of the Lyman-α Universe
Masami Ouchi, Yoshiaki Ono, and Takatoshi Shibuya 617

Star-Forming Galaxies at Cosmic Noon
Natascha M. Förster Schreiber and Stijn Wuyts 661

Astrochemistry During the Formation of Stars
Jes K. Jørgensen, Arnaud Belloche, and Robin T. Garrod 727

Indexes

Cumulative Index of Contributing Authors, Volumes 47–58 779

Cumulative Index of Article Titles, Volumes 47–58 782

Errata

An online log of corrections to *Annual Review of Astronomy and Astrophysics* articles may be found at http://www.annualreviews.org/errata/astro

Annu. Rev. Astron. Astrophys. 2020.58:257-312. Downloaded from www.annualreviews.org
Access provided by National Astronomical Observatories, Chinese Academy of Sciences on 09/05/23. For personal use only.